Seismic Fragility Analysis of Equipment and Structures in a Memphis Electric Substation

by

J-R. Huo[1] and H.H.M. Hwang[2]

August 10, 1995

Technical Report NCEER-95-0014

NCEER Task Numbers 93-3303 and 94-3301C

NSF Master Contract Number BCS 90-25010
and
NYSSTF Grant Number NEC-91029

1 Research Associate, Center for Earthquake Research and Information, The University of Memphis
2 Professor, Center for Earthquake Research and Information, The University of Memphis

NATIONAL CENTER FOR EARTHQUAKE ENGINEERING RESEARCH
State University of New York at Buffalo
Red Jacket Quadrangle, Buffalo, NY 14261

PREFACE

The National Center for Earthquake Engineering Research (NCEER) was established to expand and disseminate knowledge about earthquakes, improve earthquake-resistant design, and implement seismic hazard mitigation procedures to minimize loss of lives and property. The emphasis is on structures in the eastern and central United States and lifelines throughout the country that are found in zones of low, moderate, and high seismicity.

NCEER's research and implementation plan in years six through ten (1991-1996) comprises four interlocked elements, as shown in the figure below. Element I, Basic Research, is carried out to support projects in the Applied Research area. Element II, Applied Research, is the major focus of work for years six through ten. Element III, Demonstration Projects, have been planned to support Applied Research projects, and will be either case studies or regional studies. Element IV, Implementation, will result from activity in the four Applied Research projects, and from Demonstration Projects.

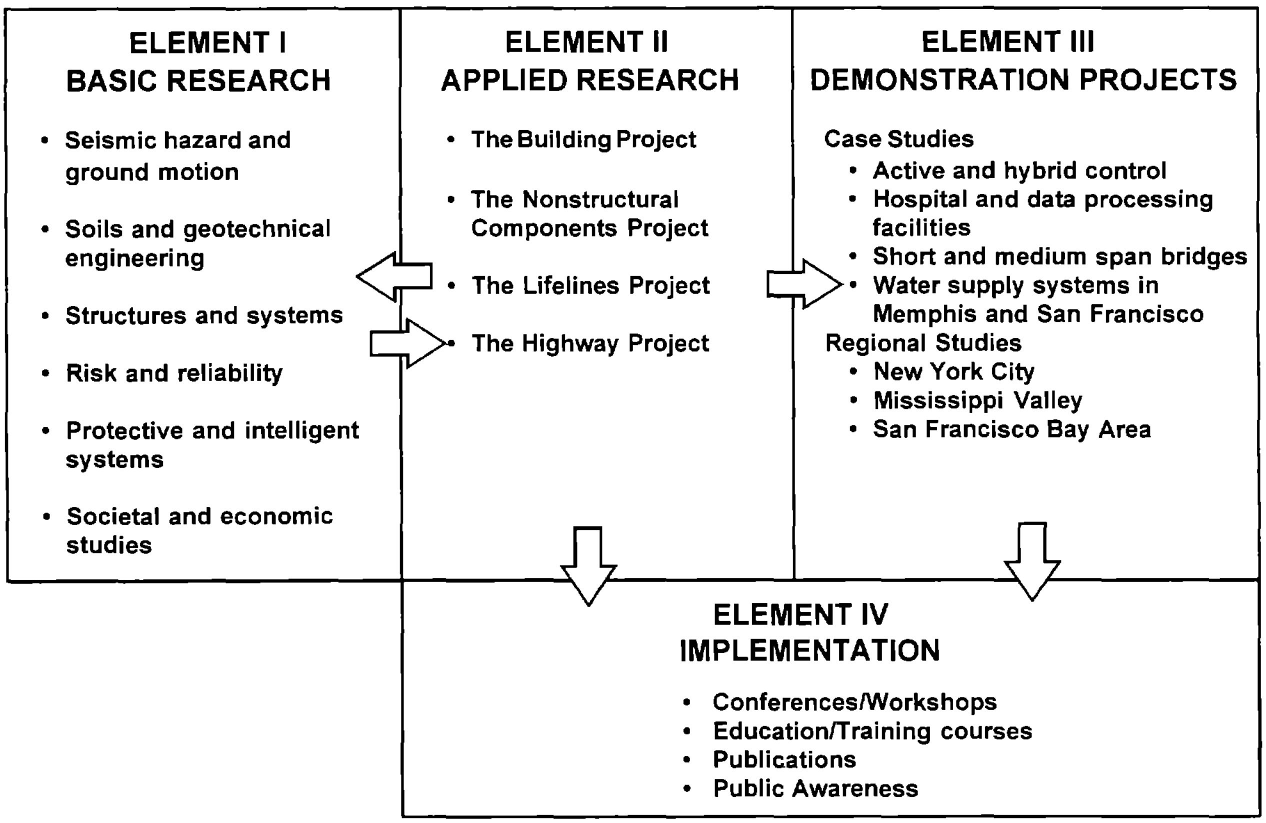

Research tasks in the **Lifeline Project** evaluate seismic performance of lifeline systems, and recommend and implement measures for mitigating the societal risk arising from their failures or disruption caused by earthquakes. Water delivery, crude oil transmission, gas pipelines, electric power and telecommunications systems are being studied. Regardless of the specific systems to be considered, research tasks focus on (1) seismic vulnerability and strengthening; (2) repair and restoration; (3) risk and reliability; (4) disaster planning; and (5) dissemination of research products.

The end products of the **Lifeline Project** will include technical reports, computer codes and manuals, design and retrofit guidelines, and recommended procedures for repair and restoration of seismically damaged systems.

This report presents a seismic fragility analysis of equipment and structures in an electric substation in Memphis, Tennessee. These include the pothead structure, 115 kv switch structure, 97 kv lightning arresters, control house, capacitor banks, 115/12 kv transformers, 12 kv regulators, 115 kv oil circuit breakers and 12 kv oil circuit breakers. The results from this fragility analysis provide the expected performance of equipment and structures in a substation. They can also be used to evaluate the seismic performance of the entire electric substation and to perform a system reliability analysis of the electric transmission system.

ABSTRACT

This report presents a seismic fragility analysis of equipment and structures in an electric substation in Memphis, Tennessee. The electric substation selected for this study is Substation 21, which is located near several major hospitals in downtown Memphis. Substation 21 consists of several major types of equipment and structures, for example, 115/12 kV transformers, oil circuit breakers, and switch structures. The failure of equipment and structures is defined as the state at which a component (an equipment or a structure) fails to perform its function. The capacity corresponding to this damage state is then established. On the other hand, the seismic response of a component is determined by either a response spectral analysis or a static analysis. The uncertainties in seismic response and capacity are quantified to determine the probabilities of failure corresponding to various levels of ground shaking. The results are displayed as fragility curves.

From the fragility analysis results, the seismic performance of equipment and structures in a substation can be revealed. For example, 115/12 kV transformers in Substation 21 are very vulnerable to earthquakes even with moderate magnitude. The fragility analysis results can also provide the necessary data for evaluating the seismic performance of the entire electric substation and for performing a reliability analysis of the electric transmission system.

ACKNOWLEDGMENTS

This report is based on research supported by the National Center for Earthquake Engineering Research under contract nos. NCEER 93-3303 and 94-3301C (NSF Grant No. BCS-9025010). Any opinions, findings, and conclusions expressed in the report are those of the writers and do not necessarily reflect the views of the NCEER, or the NSF of the United States. CERI Contribution Number 283.

The drawings of structures and equipment in Substation No. 21 were made available by Memphis Light, Gas and Water Division (MLGW). The assistance by Mr. Bill Sipe, Substation Engineer, is greatly appreciated.

TABLE OF CONTENTS

LIST OF ILLUSTRATIONS

LIST OF TABLES

SECTION 1
INTRODUCTION

The experience from many past earthquakes in California and around the world has shown that large earthquakes could cause severe damage to substations and result in major service disruption of a power system. As an example, the Loma Prieta earthquake, with a surface wave magnitude M_S measured as 7.1, struck the San Francisco Bay area of northern California in 1989. The earthquake caused extensive damage to three major substations at Moss Landing, Metcalf and San Mateo, resulting in a loss of electric service to 1.4 million customers (Tsai, 1993).

The New Madrid seismic zone (NMSZ) is considered as the most hazardous seismic zone in the eastern and central United States. The City of Memphis, Tennessee, is located close to the southwestern segment of the NMSZ (Figure 1-1); thus, Memphis is exposed to significant seismic hazards. However, most existing facilities in the Memphis area were not designed to resist earthquakes. In the event of a large New Madrid earthquake, many of these facilities might be damaged or even collapse, and this could cause human casualties, interrupt utility services and produce economic losses for a long time after the earthquake.

The electric system in the Memphis area is operated by the Memphis Light, Gas and Water Division (MLGW), City of Memphis. The MLGW electric transmission system (Figure 1-2) receives 500 kV and 161 kV electric power from the Tennessee Valley Authority (TVA) at three locations: Cordova Substation (#39), Thomas H. Allen Substation (#35), and North Shelby Substation (#65). The electric power is then transmitted to 44 substations throughout Memphis and Shelby County by means of 161 kV, 115 kV and 23 kV transmission circuits.

Substation 21 of the MLGW electric transmission system is a key electricity supplier to several major hospitals in downtown Memphis. The performance of this substation in the event of a large New Madrid earthquake is critical to the emergency operation of these hospitals after the earthquake. The objective of this study is to perform a seismic fragility analysis of equipment and structures in a Memphis electric substation, using Substation 21 to represent all the substations in the study area.

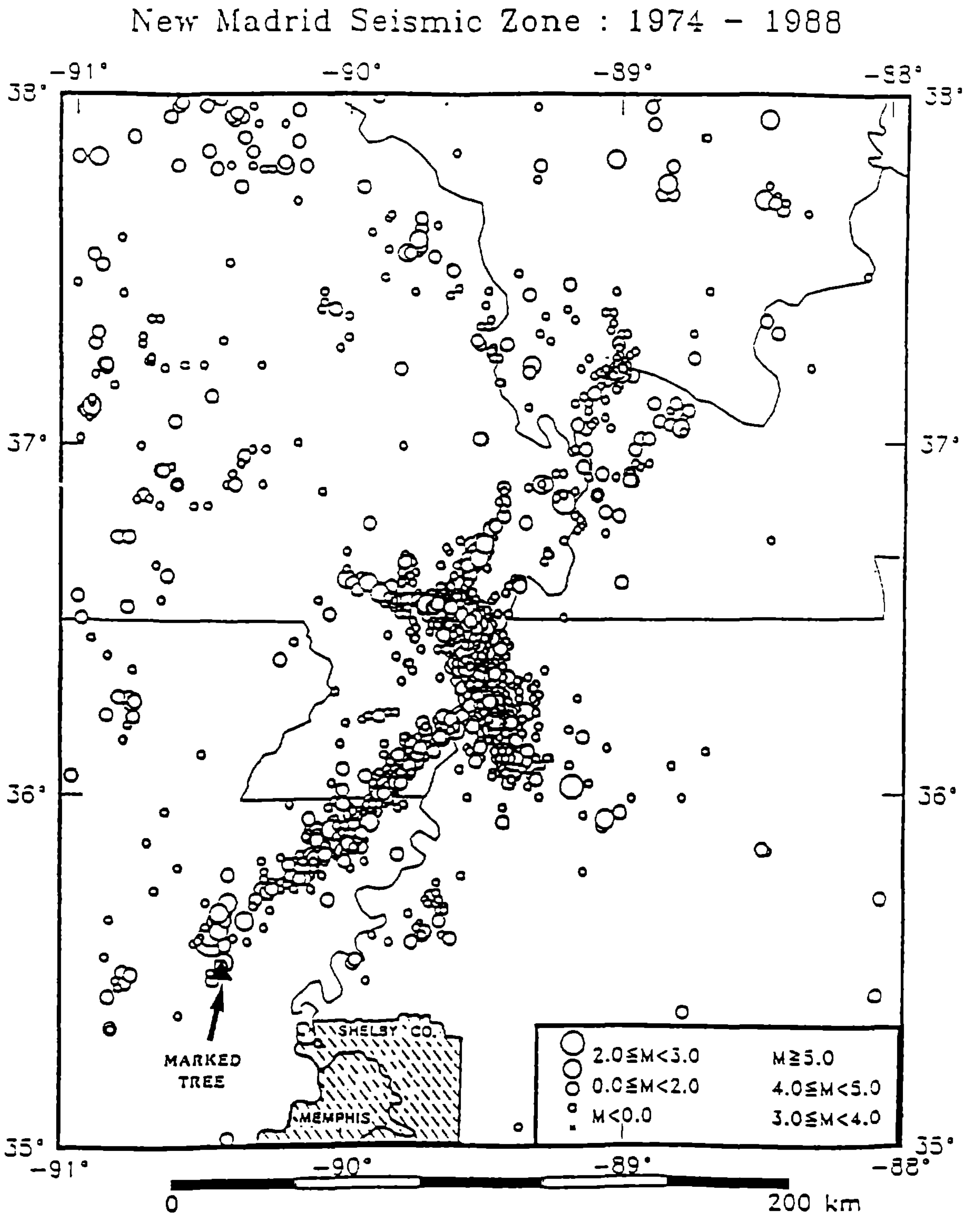

FIGURE 1-1 Epicenters of New Madrid Earthquakes

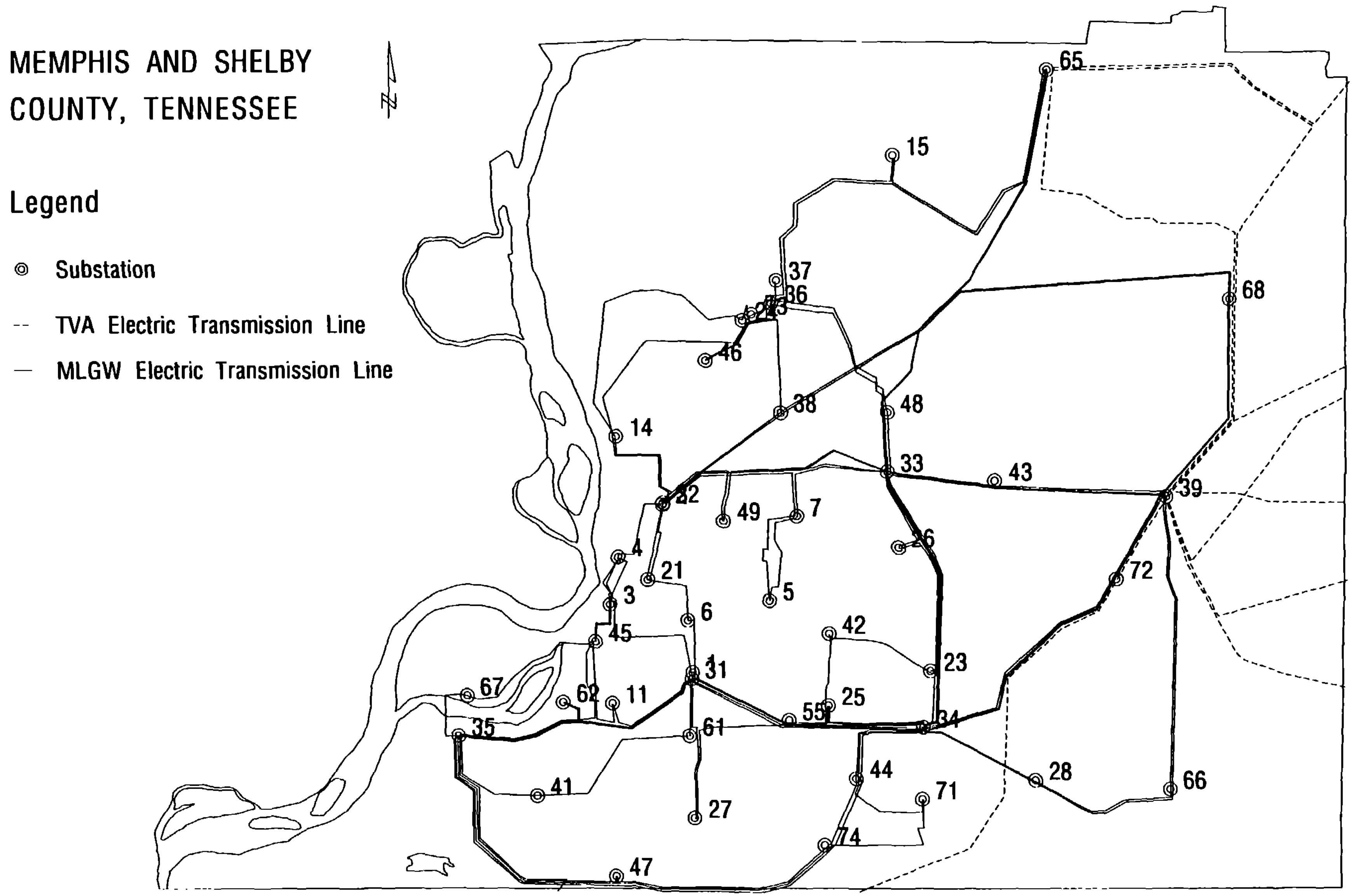

FIGURE 1-2 MLGW Electric Transmission System

The fragility data of substation equipment and structures can be generated using actual earthquake damage data, experimental data, or analytical approaches. Even though the electric substations have been damaged in several earthquakes in California, seismic damage to electric facilities in the eastern United States is rare. In the practice of the power industry, the equipment with high voltage, for example, circuit breakers with voltage 169 kV and higher, is qualified by shake-table testing, while the equipment with low voltage is qualified by dynamic or static analysis. Thus, the information on the testing of low-voltage electric equipment similar to those installed in Substation 21 is not available. From these considerations, an analytical approach is used to carry out the fragility analysis of equipment and structures in Substation 21.

SECTION 2
DESCRIPTION OF ELECTRIC SUBSTATION

The plan of MLGW Substation 21 is shown in Figure 2-1. The substation consists of the following major structures and equipment:

1. Pothead structures
2. 97 kV lightning arresters
3. 115 kV switch structure
4. 12 kV bus towers
5. 12 kV switch structures
6. Capacitor yard
7. Oil house
8. Control house
9. 115 kV oil circuit breakers
10. 115 kV/12 kV transformers
11. 12 kV oil circuit breakers
12. 12 kV regulators

Figure 2-2 shows the schematic diagram of Substation 21. Power is received or sent out from bus 215 through three 115 kV circuits. Circuit 2579, beginning from the west pothead structure, is an underground link connecting bus 215 and bus 25 of Substation 2. Circuit 6571 begins on the east pothead structure and connects bus 215 and bus 65 of Substation 6. Circuit 2573 begins at the east end of the 115 kV switch structure and connects the same buses as circuit 2579, but it is an overhead link. Note that electric power on these circuits can flow in both ways. The actual direction of power flow depends on the distribution of power sources, the network topology, and the load at that particular moment, and must be determined by means of network flow analysis.

The 115 kV switch structure supports essential parts of bus 215, the only 115 kV bus in Substation 21. The bus is sectionalized by two oil circuit breakers (OCBs). OCB 1151 is used to separate circuit 2579 and 6571, and OCB 1153 is used to separate circuit 6571 and 2573. Each section of the bus is connected to a 115/12 kV transformer, and the low voltage outputs of the transformers are connected to the 12 kV switch structures. Manually operated switches are placed on the bus to isolate any OCB that

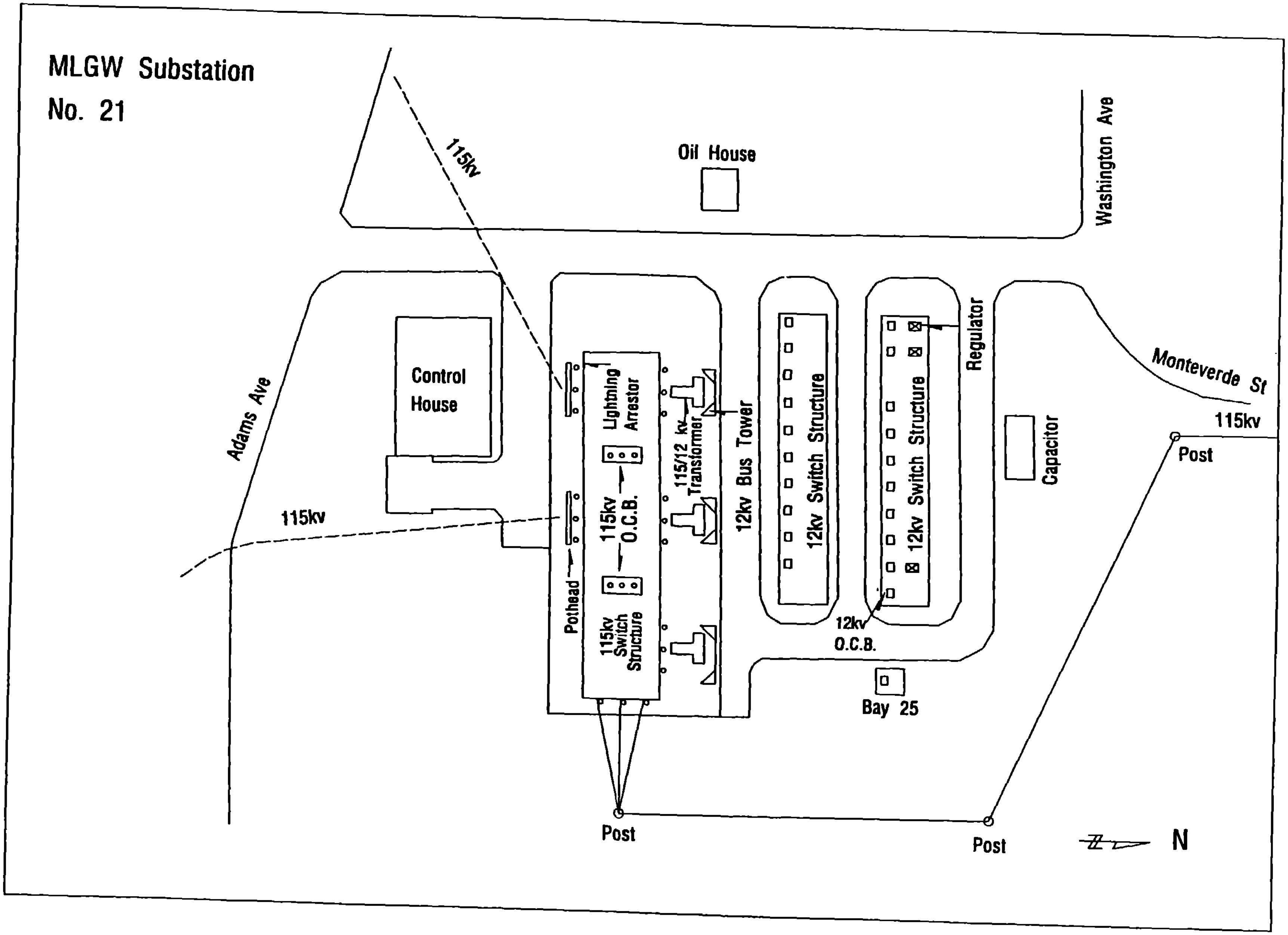

FIGURE 2-1 Plan of MLGW Substation 21

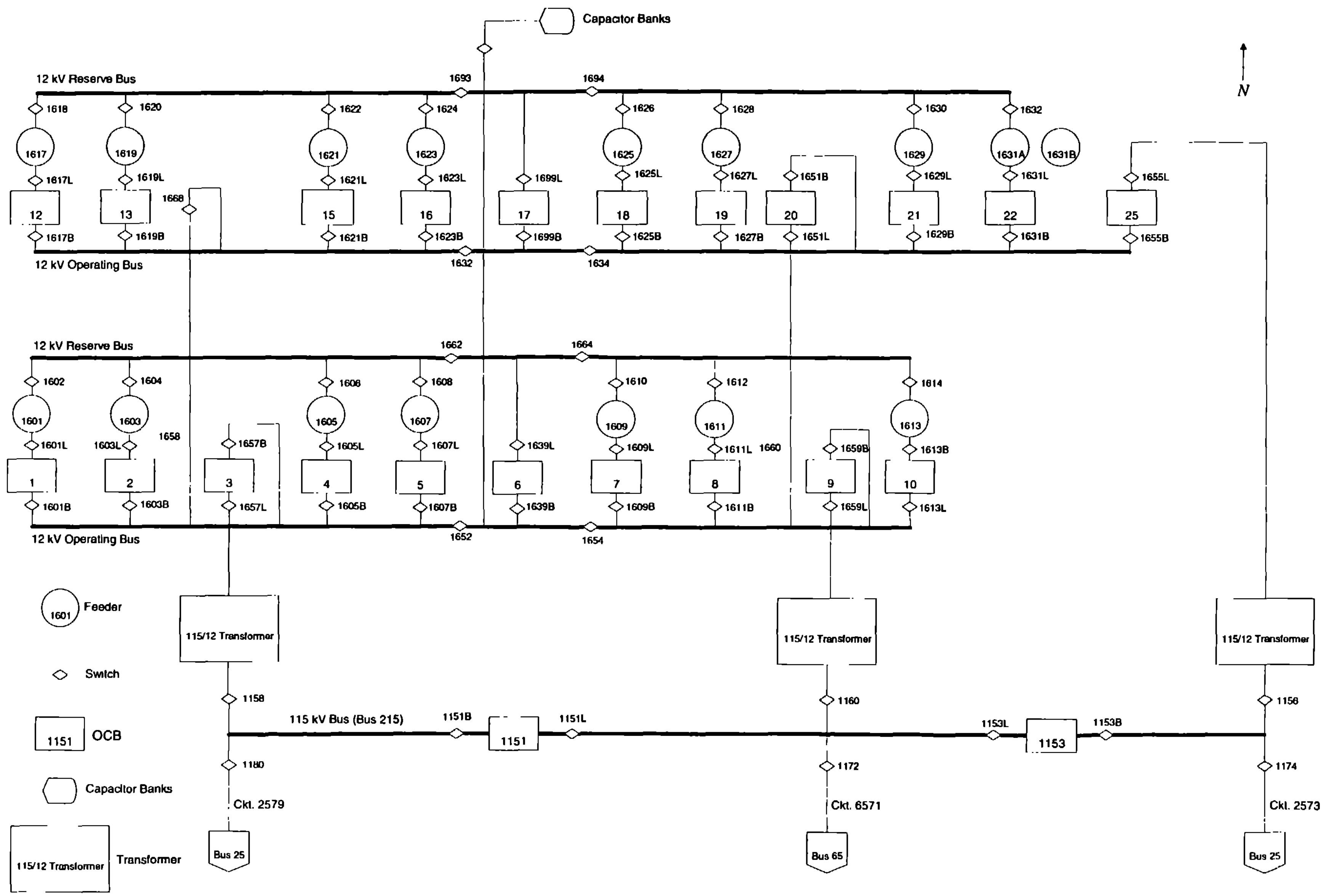

FIGURE 2-2 Schematic Diagram of MLGW Substation 21

needs to be serviced. Other switches disconnect the bus from input lines or transformers. In normal operation, all switches on the bus are closed.

The 12 kV switch structures consist of a north structure, a south structure, and a single bay tower (bay 25). Both the north and south structures are divided into 11 bays. Bay 1 through bay 11 are in the south structure and make up the south bus. Bays 12 through 22 are in the north structure and make up the north bus. Depending on the function of a bay, it may contain a 12 kV OCB, a voltage regulator, and several manually operated switches.

Each bus consists of an operating bus and a reserve bus, to provide temporary bypass for the OCBs, in case an OCB needs servicing. Four buses (north and south, operating and reserve) can be sectioned by manually operated switches into east and west sides at bay 17 and bay 6, but these two sides normally remain connected. Also, the OCBs in bay 6 and bay 17 are normally tripped (open circuit) so only the operating buses are energized.

The components can be configurated in many ways during normal operation. One of the most frequently used configurations is described here as an example. The output of the west transformer is connected to the south bus through the OCB in bay 3. The output of the middle transformer is connected to the south bus through the OCB in bay 9. The output of the east transformer is connected to the north bus through the OCB in bay 25. The north and south buses are connected by switch 1668 (in bay 14) and the OCB in bay 20. The capacitors in the capacitor yard are connected to the south operation bus at bay 6 between switch 1652 and 1654. Since the north and the south buses are connected together, the capacitors provide voltage regulation and power factor correction for the whole substation.

Power to the "hospital" network is fed through the OCBs in bays 1, 2, 4, 5, 7, 8, and 10, then to feeder 1601, 1603, 1605, 1607, 1609, 1611, and 1613. Power to the "east" network is fed through the OCBs in bays 12, 13, 21, and 22, then to feeder 1617, 1619, 1629, 1631A, and 1631B. Power to the "west" network is fed through the OCBs in bays 15, 16, 18, and 19, then by feeders 1621, 1623, 1625, 1627.

SECTION 3
SEISMIC HAZARDS AT THE SUBSTATION SITE

Memphis is in the central part of the Mississippi embayment, which is composed of mostly unconsolidated sediments. The Paleozoic rock that forms the bedrock floor of the Mississippi embayment is located about 1 km below the ground surface. For such a deep profile overlaying the bedrock, the whole profile is divided into soil layers and rock layers (Hwang and Huo, 1994). Figure 3-1 shows the detail of the soil layers. These soil layers were established from the existing boring logs around the site of Substation 21. Figure 3-2 shows the general strata of the rock layers in the Memphis area.

3.1 Seismic Hazards Potential

Estimation of seismic hazards is an essential task for a seismic fragility analysis. The seismic hazards, including ground shaking and ground failure, are affected by regional seismicity, source characteristics of earthquakes, attenuation of ground motion between the source and the site, and local soil condition.

Soil liquefaction in saturated loose cohesionless soil is caused by the buildup of excess pore pressure resulting from cyclic shear stress during an earthquake (Seed and Idriss, 1982). The liquefaction potential of a soil layer is affected by relative density, percentage of clay, grain-size distribution, effective confining pressure, and location of water table. The soil profile of the study site (Figure 3-1) mainly consists of silty clay and dense sand. Since there is no loose sand underneath the study site, liquefaction is not expected to occur during an earthquake. Thus, only ground shaking is considered as a potential seismic hazard at the study site.

3.2 Approach for Estimating Ground Shaking

The intensity of ground shaking and the characteristics of ground motion at the study site are evaluated using an approach proposed by Hwang and Huo (1994). In this approach, a probabilistic seismic hazard analysis is first performed to generate a seismic hazard curve in bedrock. From the seismic hazard curve, the peak bedrock acceleration (PBA) values corresponding to various annual probabilities of exceedance can be determined. For each PBA value, a probability-based scenario

Depth

0

Stiff Silty Clay (CL)

γ_S = 125 pcf N_{SPT} = 7 PI = 10-20 Su = 950 psf V_S = 782 fps

$\underline{\nabla}$ (water table at 14')

20'

Stiff Clayey Silt to Sandy Clay (ML-CL)

γ_S = 125 pcf N_{SPT} = 15 PI = 10-20 S_u = 1500 psf V_S = 982 fps

36'

Dense Sand (SP-GP)

γ_S = 135 pcf N_{SPT} = 45 K_o = 0.41 D_r = 0.80 ϕ' = 36° V_S = 881 fps

67'

Dense Sand with Silt Clay (SM)

γ_S = 130 pcf N_{SPT} = 35 K_o = 0.43 D_r = 0.80 ϕ' = 35° V_S = 1000 fps

98'

Very Dense Sand (SP)

γ_S = 140 pcf N_{SPT} > 50 K_o = 0.40 D_r = 0.95 ϕ' = 37° V_S = 1127 fps

150'

Hard Clay (CH)

γ_S = 130 pcf PI = 40-80 S_u = 6000 psf V_S = 1926 fps

300'

SOFT ROCK

γ_S = 145 pcf V_S = 2500 fps

FIGURE 3-1 Soil Profile at MLGW Substation 21

0 m	Ground Surface		
	Soil Layers		
91.5 m			
	Soft Rock	$\rho = 2.32\ g/cm^3$	$V_s = 1.0$ km/sec
200 m			
	Soft Rock	$\rho = 2.32\ g/cm^3$	$V_s = 1.1$ km/sec
500 m			
	Soft Rock	$\rho = 2.38\ g/cm^3$	$V_s = 1.4$ km/sec
700 m			
	Soft Rock	$\rho = 2.40\ g/cm^3$	$V_s = 1.7$ km/sec
900 m			
	Soft Rock	$\rho = 2.50\ g/cm^3$	$V_s = 2.0$ km/sec
1.0 km			
	Bedrock	$\rho = 2.70\ g/cm^3$	$V_s = 3.5$ km/sec

FIGURE 3-2 Rock Layers Underlying the Study Site

earthquake in terms of hazard-consistent magnitude and hazard-consistent distance (Ishikawa and Kameda, 1991) is then established. The scenario earthquake is classified into three categories: near-field, far-field, and long-distance earthquakes. For each category of earthquake, an analytical method is used to simulate acceleration time histories at the base of the soil profile. The ground motion at the ground surface is then determined by performing a nonlinear site response analysis. In the process of simulating ground motion, uncertainties in modeling seismic source, path attenuation, and local soil condition are taken into account.

3.3 Probabilistic Seismic Hazard Analysis

On the basis of the tectonic features and seismicity data, we establish three seismic source zones, Zones A, B, and C, within a radius of 300 km around the study site (Figure 3-3). Zone A is the same as the New Madrid seismic source zone established by Johnston and Nava (1990). It is the central part of the Reelfoot Rift where seismicity is intensive, including the epicenters of the three great New Madrid Earthquakes occurred in the winter of 1811-1812. Zone B covers part of the Reelfoot Rift Complex and is bounded by the circular boundary in the north and the Ouachita Fold Belt in the south. Zone C is the area below the Reelfoot Rift and is bounded by the Ouachita Fold Belt and the circular boundary.

The recurrence (frequency-magnitude) relationship in each source zone can be expressed as follows (Gutenberg and Richter, 1944):

$$\log N = a - b\, m_b \qquad \text{or} \qquad N(m_b) = e^{\alpha - \beta\, m_b} \tag{3.1}$$

where $\alpha = a \cdot \ln 10$, $\beta = b \cdot \ln 10$, m_b is the body-wave magnitude, and N is the cumulative number of earthquakes of magnitude m_b or greater in one year. The a-value indicates the total number of earthquakes of magnitude equal and greater than zero. The b-value is the slope of the recurrence relation and describes the relative activity of small and large earthquakes in a seismic source zone. It is noted that if the magnitude of an earthquake is limited by an upper bound m_{bu} and a lower bound m_{bo}, the frequency-magnitude relationship, Equation (3.1), needs to be modified in order to satisfy the property of the probability distribution, i.e.,

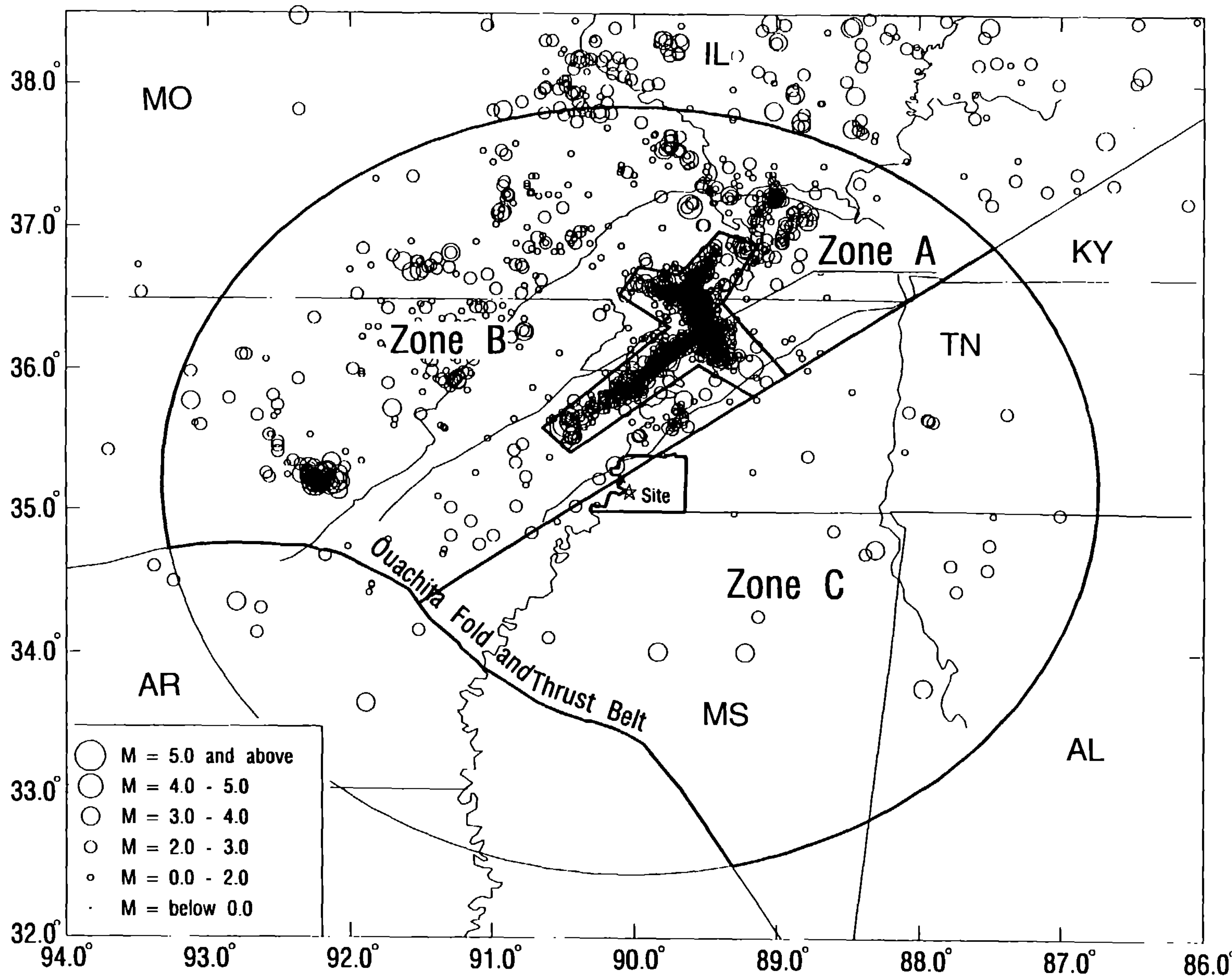

FIGURE 3-3 New Madrid Seismic Source Zones

$$N(m_b) = N_o\,[1 - F^*(m_b)] = e^{\alpha - \beta m_b} \frac{1 - e^{-\beta(m_{bu} - m_b)}}{1 - e^{-\beta(m_{bu} - m_{bo})}} \tag{3.2}$$

The values of seismic activity parameters in three source zones are summarized in Table 3-I. The determination of these parameters is given in Appendix A.

TABLE 3-I Parameter Values for Three Seismic Source Zones

Zone	a	b	m_{bo}	m_{bu}
A	3.15	0.91	4.0	7.5
B	3.17	0.91	4.0	6.5
C	2.61	1.00	4.0	6.0

Hwang and Huo (1994) developed an attenuation relation for the peak acceleration in hard-rock in the central United States.

$$\mathrm{Ln}(A) = 2.984 + 1.166\, m_b - 1.387\, \mathrm{Ln}[\sqrt{R^2+H^2} + 0.06 \exp(0.7 m_b)]$$

$$- 0.0023 \sqrt{R^2+H^2} + \varepsilon \tag{3.3}$$

where A is the horizontal PBA, R is the epicentral distance, H is the focal depth, and ε is a normal random variable expressing the variability of peak acceleration. The mean value of ε is zero and the standard deviation σ_{Lna} is 0.31. Figure 3-4 displays the attenuation relation for various magnitudes and distances. In this study, the attenuation relation established by Hwang and Huo is used to determine the seismic hazard curve.

By performing a probabilistic seismic hazard analysis for the study site, the seismic hazard curve is obtained and shown in Figure 3-5.

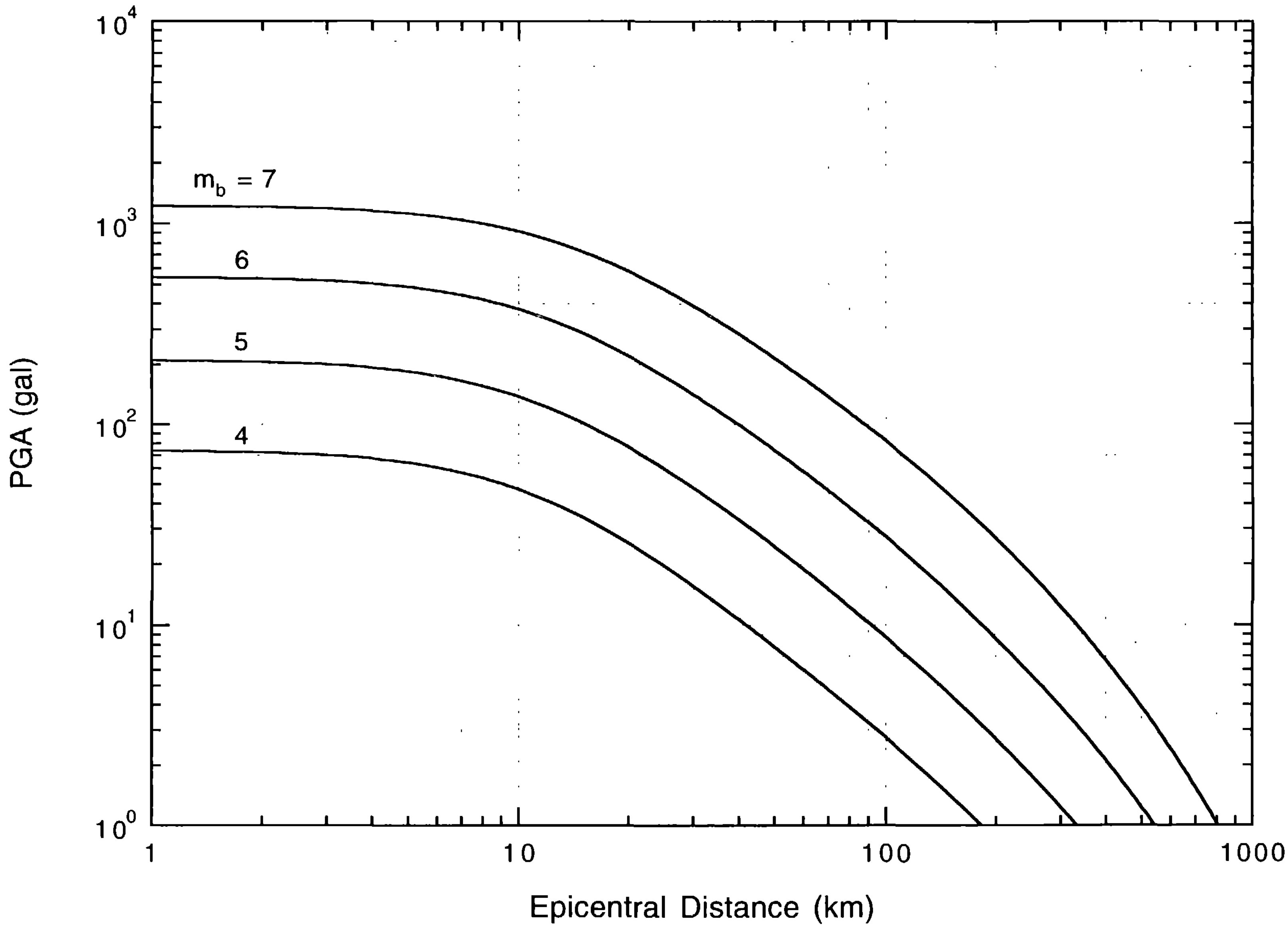

FIGURE 3-4 Attenuation of Peak Bedrock Acceleration in Central US

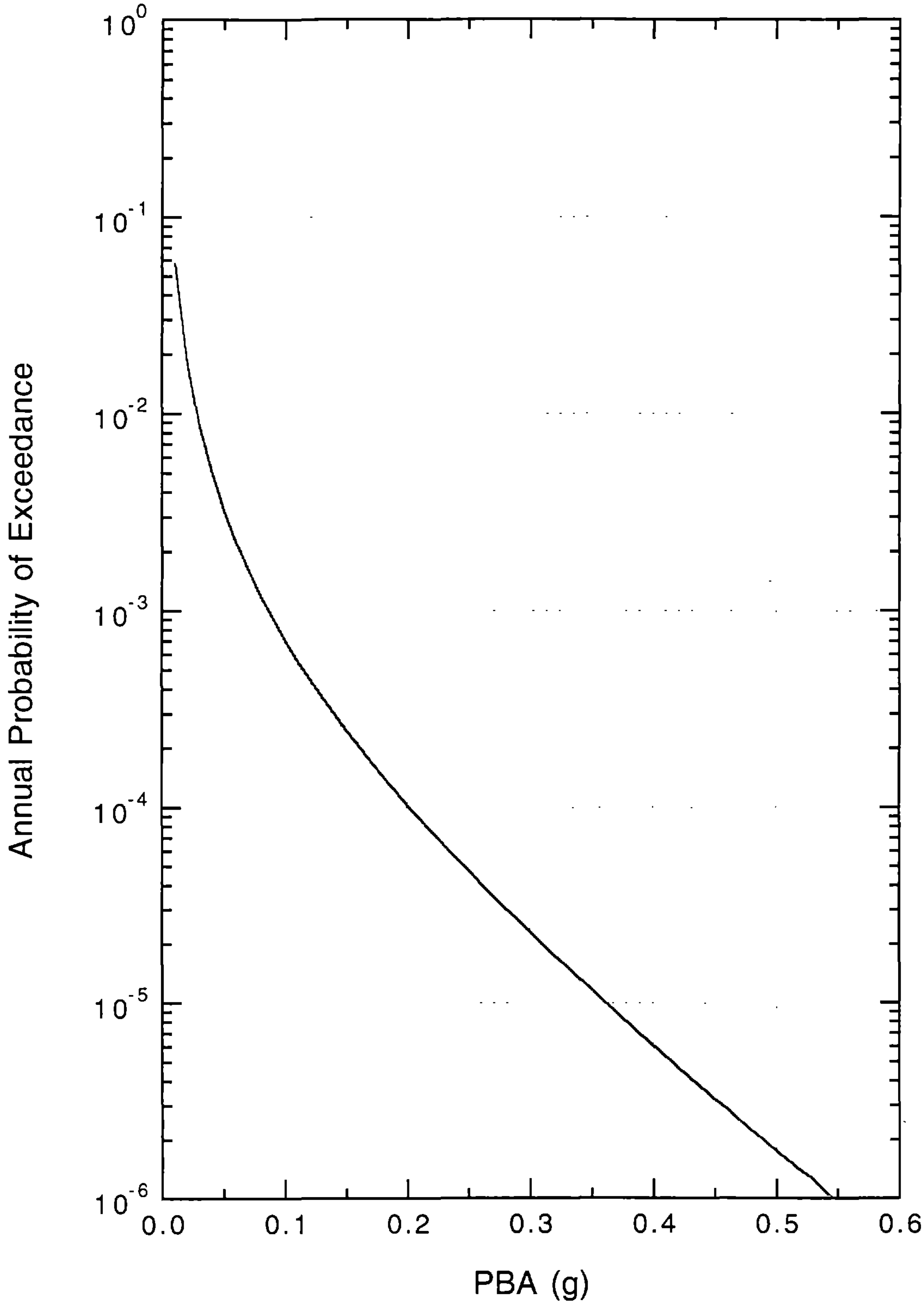

FIGURE 3-5 Seismic Hazard Curve at the Study Site (Bedrock)

3.4 Ground Motion at the Ground Surface

Table 3-II summarizes the probability-based scenario earthquakes for three zones with the PBA values ranging from 0.05g to 0.40g. In Table 3-II, the moment magnitude **M** is converted from the body-wave magnitude m_b using the formula established by Johnston (1989). The contribution factors of Zone A (about 50% or more) are much larger than those of Zone B (about 27%) and Zone C (about 23%). This implies that ground shaking from earthquakes occurring in Zone A will dominate the seismic response of facilities in Substation 21. Thus, only ground motion resulting from earthquakes occurring in Zone A is taken into consideration hereinafter.

For each scenario earthquake listed in Table 3-II (Zone A), the approach proposed by Hwang and Huo (1994) is used to generate 50 samples of acceleration time history at the ground surface and the corresponding response spectra with 2% and 5% critical damping ratios. A statistical analysis of 50 peak ground acceleration (PGA) values is performed and the mean PGA values corresponding to various scenario earthquakes are listed in Table 3-III. The response spectra from 50 simulations display significant variation. The acceleration response spectrum for each sample is normalized with the corresponding PGA. A statistical analysis is also carried out to determine the mean and standard deviation (SD) of the normalized spectral values at various periods. Figure 3-6 shows the mean and mean+SD of the normalized response spectra for a scenario earthquake (**M** = 7.5, R = 63 km).

For fragility analysis of substation structures and equipment, the mean response spectrum corresponding to a specified PGA level is constructed by multiplying the PGA value to a mean normalized response spectrum that has the average PGA value (Table 3-III) close to the specified PGA value. Figure 3-7 shows the response spectra corresponding to three PGA levels. It can be observed from Figure 3-7 that the characteristics of ground motions such as frequency content vary significantly according to the intensity of input motions.

TABLE 3-II Hazard-Consistent Magnitudes and Distances

PBA (g)	Zone A			Zone B			Zone C		
	C	$\overline{m_b}$ (M)	$\bar{R}$ (km)	C	$\overline{m_b}$	$\bar{R}$ (km)	C	$\overline{m_b}$	$\bar{R}$ (km)
0.05	0.58	6.4 (6.5)	79	0.30	5.4	40	0.12	4.8	19
0.10	0.58	6.8 (7.1)	72	0.28	5.8	32	0.15	5.0	13
0.15	0.58	7.0 (7.4)	66	0.27	5.9	28	0.16	5.2	11
0.20	0.57	7.1 (7.5)	63	0.26	6.1	26	0.17	5.4	10
0.25	0.55	7.2 (7.7)	60	0.26	6.1	24	0.19	5.5	9
0.30	0.53	7.2 (7.7)	58	0.26	6.2	22	0.21	5.5	8
0.35	0.50	7.3 (7.9)	57	0.26	6.2	21	0.24	5.6	7
0.40	0.46	7.3 (7.9)	55	0.27	6.3	19	0.27	5.7	7

TABLE 3-III Average PGAs Resulting from Scenario Earthquakes

Scenario Earthquake		PGA (g)
M	R (km)	
6.5	79	0.136
7.1	72	0.199
7.4	66	0.246
7.5	63	0.267
7.7	60	0.303
7.7	58	0.349
7.9	57	0.345
7.9	55	0.359

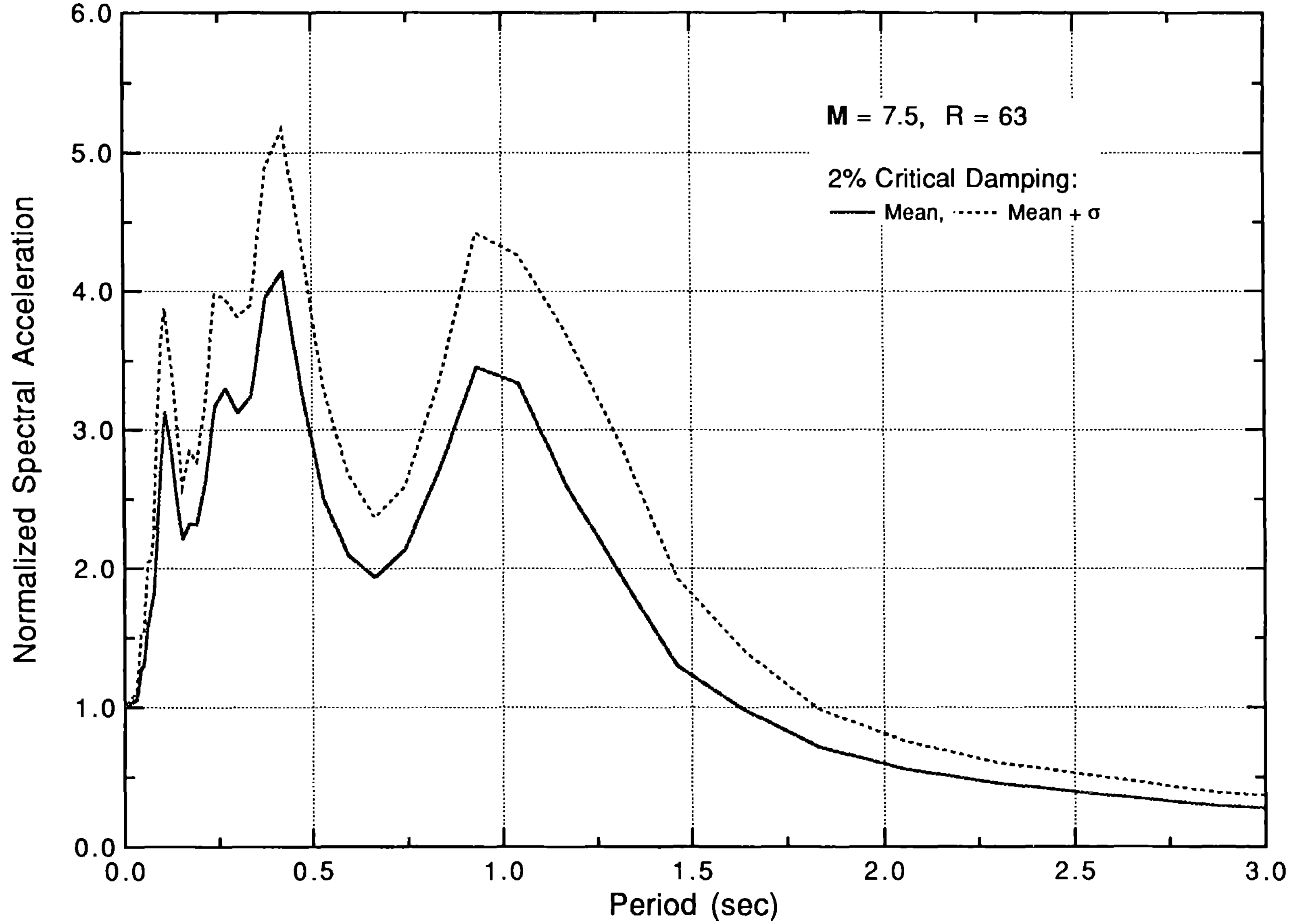

FIGURE 3-6 Normalized Acceleration Response Spectra for A Scenario Earthquake (M = 7.5, R = 63 km)

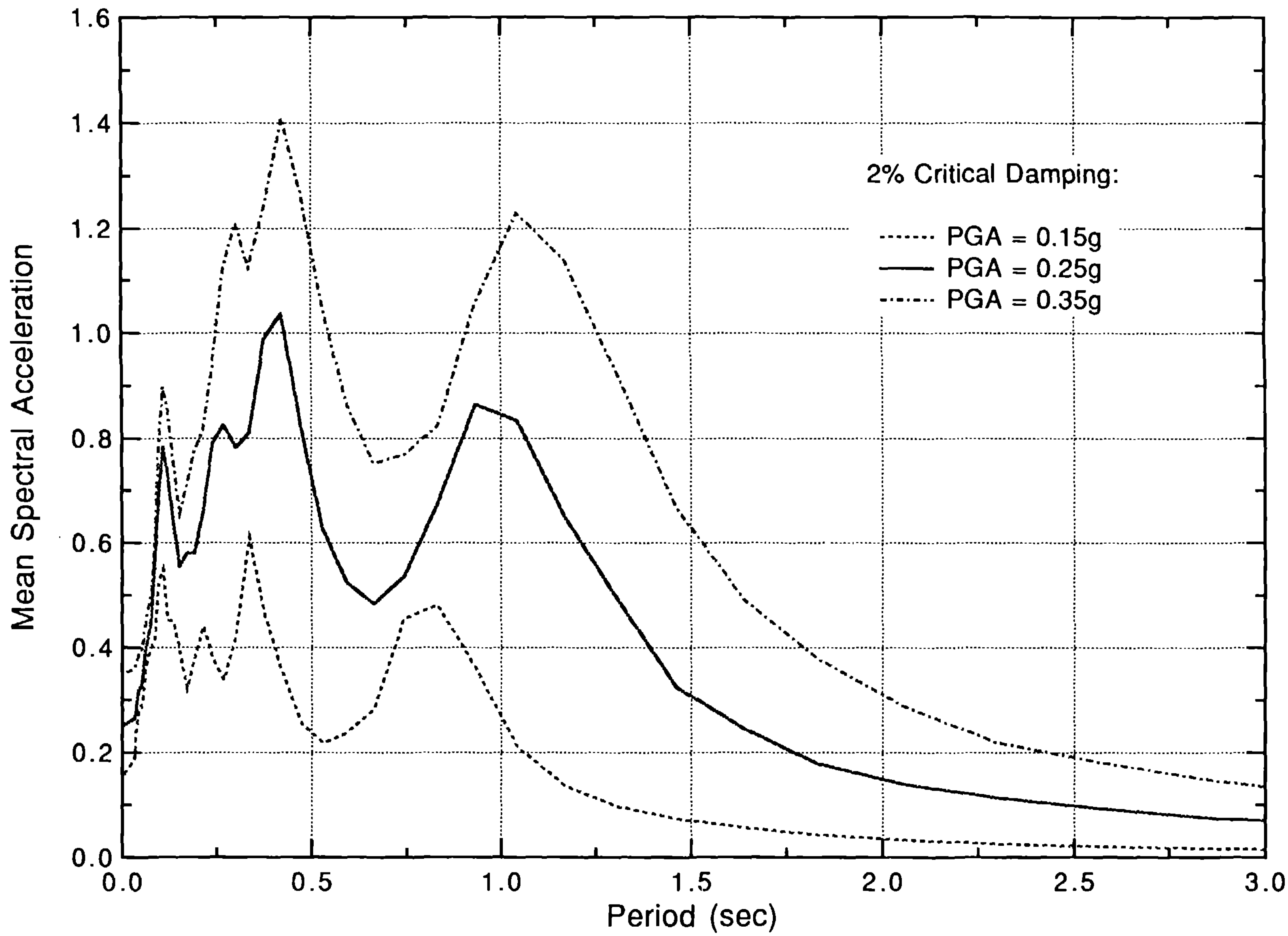

FIGURE 3-7(a) **Response Spectra Corresponding to Various PGA Levels (Damping Ratio of 2%)**

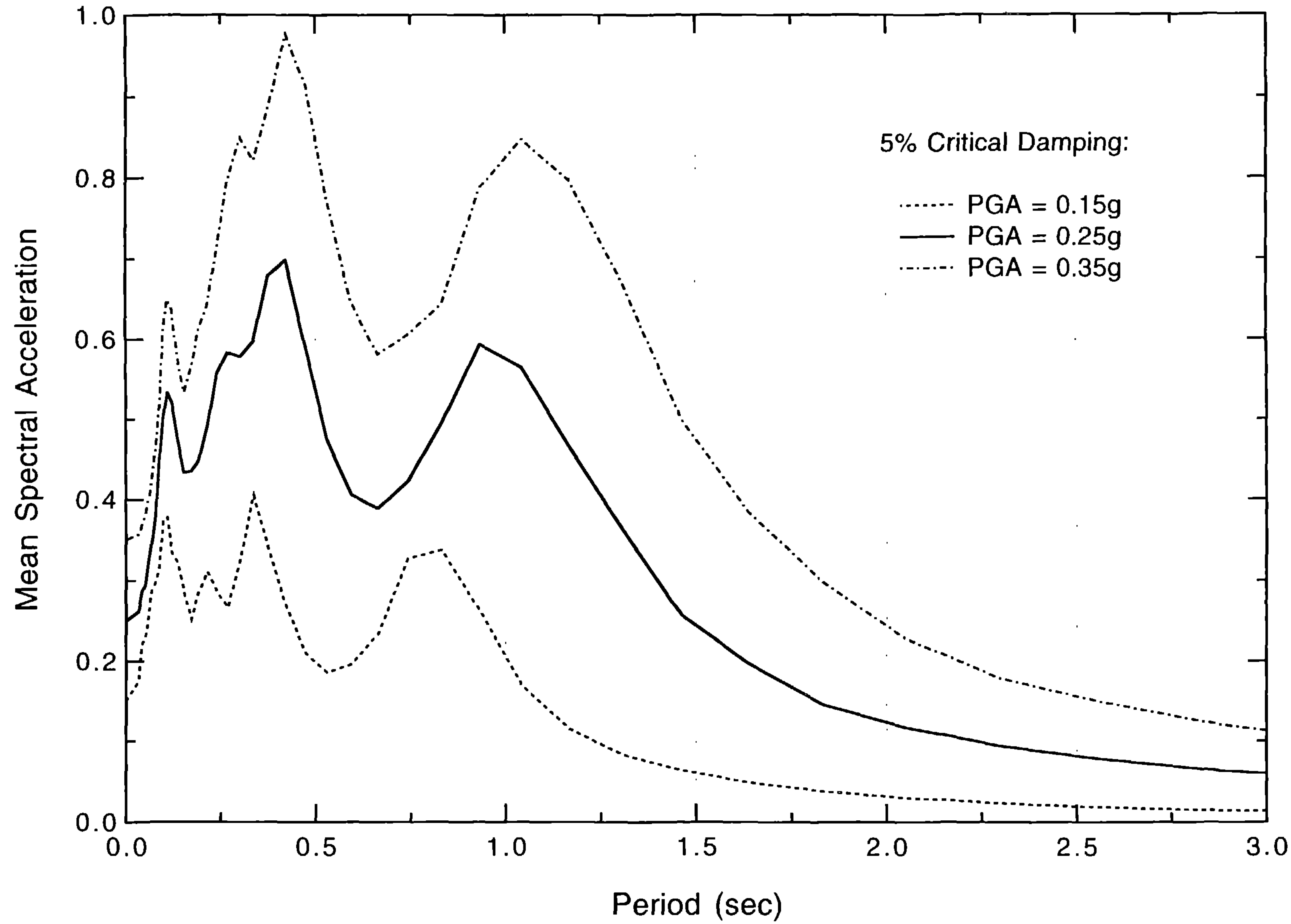

FIGURE 3-7(b) **Response Spectra Corresponding to Various PGA Levels (Damping Ratio of 5%)**

SECTION 4
POTHEAD STRUCTURE

4.1 Description of Pothead Structure

The pothead structure supports 115 kV cables between the 115 kV switch structure and the ground. It consists of a latticed steel structure and three heavy porcelain cable terminals mounted on the top of the latticed structure (Figure 4-1). The chord members of the beam and columns are made of $L3\times3\times\frac{3}{8}$ angles, while the diagonal members are made of $L1\frac{1}{2}\times1\frac{1}{2}\times\frac{1}{4}$ angles. The diagonal is connected to the chord members with a bolt at each end. At the bottom of each column, the structure is anchored to a concrete foundation by six $\frac{3}{4}$ bolts.

The detail of 115 kV cable terminal is shown in Figure 4-2. Each cable terminal consists of a porcelain cone cylinder with a ball-shaped steel container at the top and a steel base at the bottom. The height of the porcelain body is 58 inches and the minimum thickness of the cylinder shell is approximately 1 inch. The outer diameters at the top and bottom of the cylinder are 10 and 18 inches, respectively. The porcelain body contains cooling oil and electric devices. The total weight of a cable terminal, including filled cooling oil, is approximately 1400 pounds. The steel base is connected by four $\frac{3}{4}$ bolts to a square steel plate on the supporting structure. The cables linking the pothead structure and 115 kV switch structure are flexible enough so that the tensile force in the cables is negligible.

4.2 Properties of Construction Materials

Two types of materials, steel and porcelain, are used to construct the substation structures and equipment. The mechanical properties of structural steel are well established and can be found in many publications, for example, Segui (1989). The insulators are usually made of two types of porcelains, standard-strength porcelain and high-strength porcelain. In the substations located in the Memphis area, the insulators are made of standard-strength porcelain. The mechanical properties of

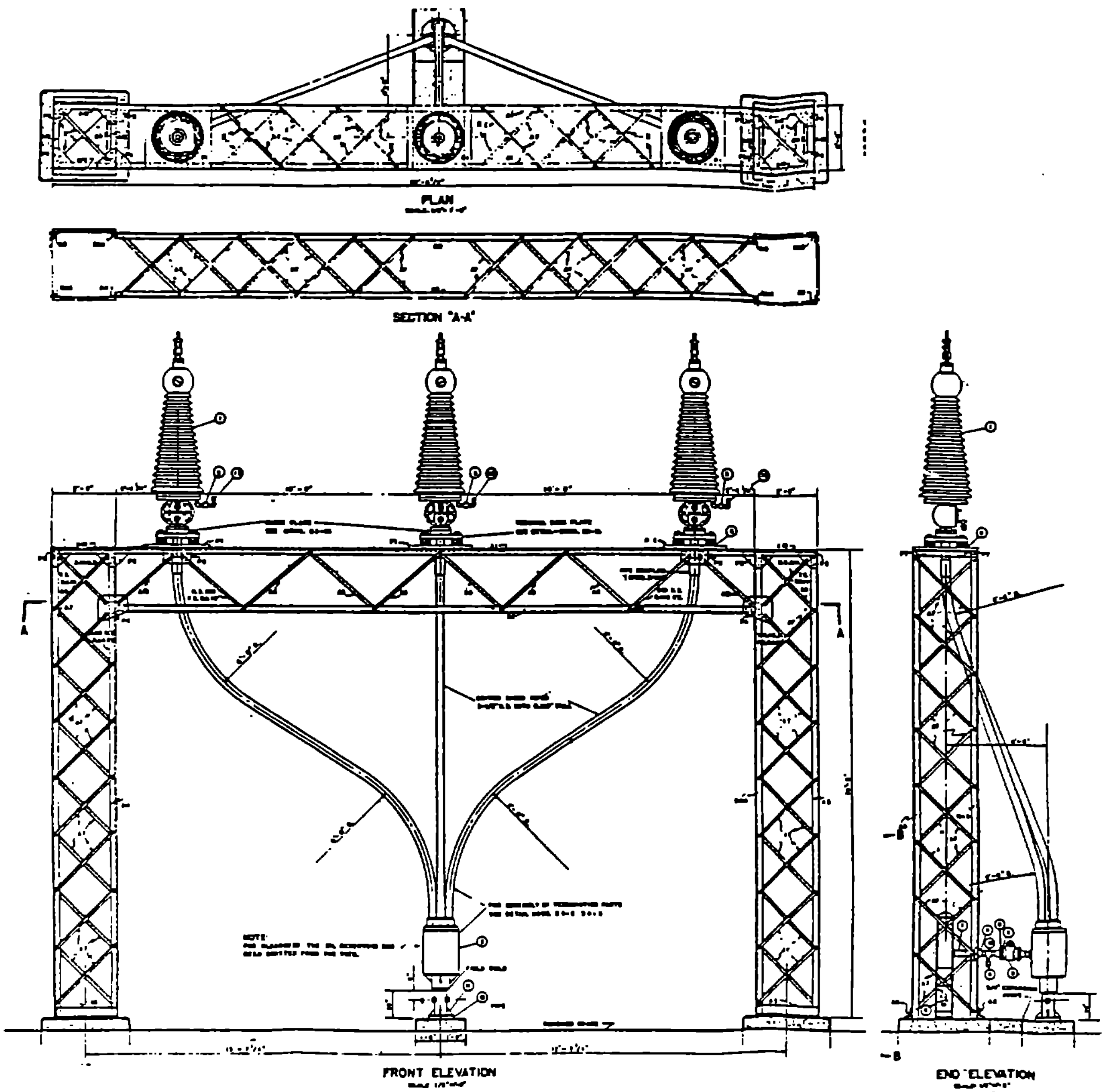

FIGURE 4-1 Plan and Elevations of Pothead Structure

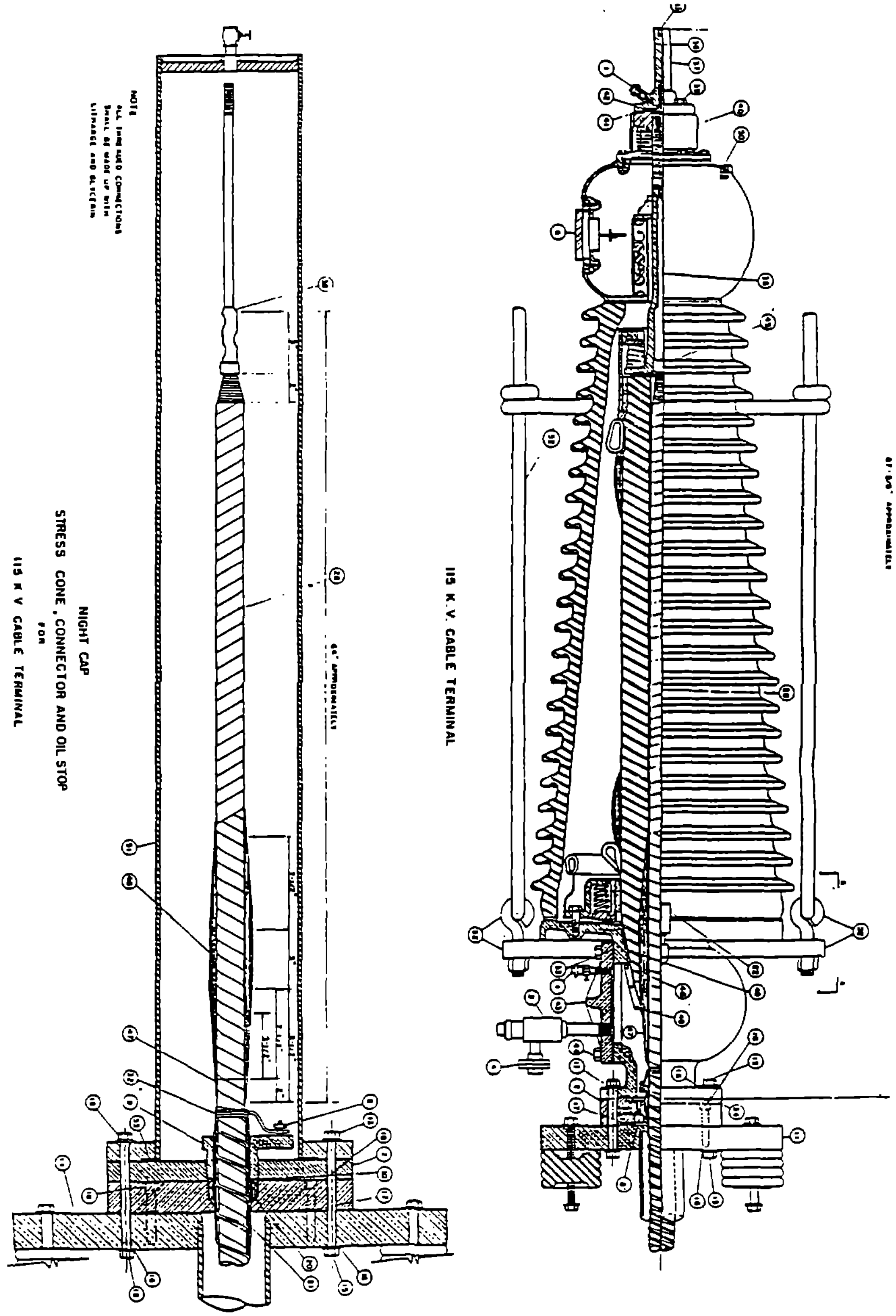

FIGURE 4-2 Detail of Cable Terminal

standard-strength porcelain such as density, modulus of elasticity, and strength are specified by the manufacturer according to the ASTM standards (LAPP, 1969).

The tensile strength of porcelain varies significantly depending on how the insulator is manufactured. Buchanan (1986) indicated that the typical value of the tensile strength of porcelain is 6.8 ksi. Based on the laboratory tests, Navias (1926) reported the tensile strength of porcelain ranging from 6 to 7 ksi. Pansini (1992) indicated that the tensile strength of porcelain may vary from 2 ksi to 9 ksi. Ang et al. (1993) indicated that the tensile strength of porcelain has a lower value of 4.26 ksi and a upper value of 12.63 ksi. On the basis of these studies, the tensile strength of porcelain is considered as a lognormal variable with the mean value of 6.8 ksi and the coefficient of variation (COV) taken as 0.3. The mean minus and plus 3 standard deviation values in logarithmic scale approximately correspond to the lower and upper bound values of the tensile strength mentioned in the above studies.

4.3 Modeling of Pothead Structure

Porcelain is a brittle material and cannot withstand large tensile stress or displacement. Thus, earthquake shaking easily causes cracks or fractures in a porcelain body. In this study, it is assumed that the latticed steel structure is strong enough to support three porcelain cable terminals, and the failure of porcelain in tension is the most dominant failure mode of the pothead structure. Since the seismic response analysis of the pothead structure is to predict the response of porcelain cable terminals, the supporting latticed structure is modeled as a steel frame as shown in Figure 4-3. The stiffness and strength of the frame members are equivalent to those of the latticed structure. The properties of the frame members are listed in Table 4-I.

The model of the cable terminal is also shown in Figure 4-3. The ball-shaped steel container, approximately 300 pounds, at the top of the porcelain body is modeled as a concentrated mass. The porcelain body is modeled as a column consisting of four finite elements. The properties of each element are computed based on a cylinder shell with a thickness of 1 inch and a constant outer diameter taken as the average of the outer diameters at the bottom and top of the element. The properties of the porcelain elements are also listed in Table 4-I. The steel base below the porcelain

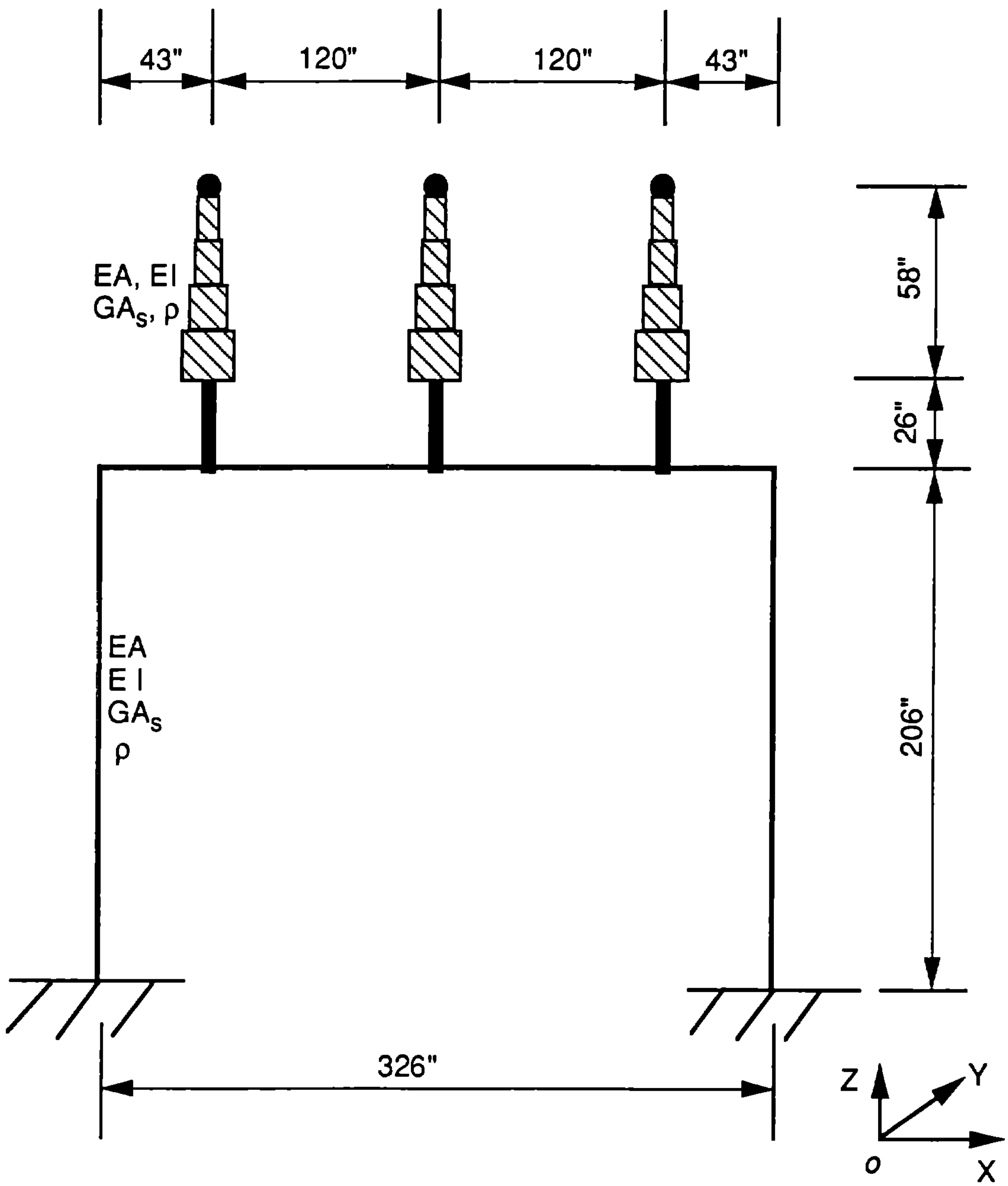

FIGURE 4-3 Model of Pothead Structure

TABLE 4-I Properties of Pothead Members

Member	Length (in)	Section Area (in^2)	Moment of Inertia (in^4)	Shear Area (in^2)	Weight (lb/in)
Column	206.0	8.44	1671.00	2.54	6.22
Beam	326.5	8.44	1671.00	2.55	4.71
Porcelain Element #1	14.5	31.42	392.70	15.71	14.91
Porcelain Element #2	14.5	37.70	678.58	18.85	17.62
Porcelain Element #3	14.5	43.98	1077.57	21.99	20.33
Porcelain Element #4	14.5	50.27	1608.50	25.13	23.04

body is modeled as a steel column with a diameter of 10 inches which has a rigid connection to the supporting structure.

4.4 Seismic Response Analysis

In this study, the seismic response analysis is performed using the SAP program (Wilson and Button, 1982). From the free vibration analysis, the natural periods and corresponding mode shapes of the structure can be obtained. Table 4-II shows the natural periods in two horizontal and vertical directions (x, y, z directions, respectively), which are the in-plan, out of plan, and vertical direction of the structure. The longest fundamental period is in the y-direction and this indicates that the stiffness of the structure is the weakest in the out of plan direction. Since the seismic response analysis of the pothead structure is mainly to determine the response of the brittle porcelain body, the response spectrum analysis is carried out to determine the linear response of the pothead structure. According to Newmark and Hall (1982), the damping ratio of a latticed steel structure is 5%, and thus the 5% damped ground response spectra in two horizontal directions determined in Section 3.4 are used as the input to the pothead structure, a latticed steel structure.

TABLE 4-II Natural Periods of Pothead Structure

Mode No.	Period (sec)		
	X-Direction	Y-Direction	Z-Direction
1	0.122	0.174	0.059
2	0.024	0.034	0.021
3	0.010	0.021	0.018

For a given PGA level in each direction of the input ground motion, the modal responses of the first three modes are combined using the complete quadratic combination (CQC) technique. From the response spectrum analysis, the bending moment M, shear force V, and axial force N at both ends of the porcelain terminal body (Figure 4-4) can be determined. These forces are then used to determine the maximum tensile stress at the most critical position of the porcelain body. For an element in the porcelain shell with an angle of θ from the x-axis and a height of z from the bottom of the porcelain body (Figure 4-5), the normal stress in the vertical direction σ_z resulting from the bending moment M and axial force N can be determined as follows:

$$\sigma_z(\theta, z) = \frac{M(z) \cdot d(\theta, z)}{I(z)} + \frac{N}{A(z)} \tag{4.1}$$

in which M(z) is the bending moment on the section caused by the ground motion in either x or y direction; I(z) and A(z) are the moment of inertia and area of the cross-section, respectively; $d(\theta, z)$ is the distance from the outer surface of the element to the x or y axis.

The shear stress τ resulting from the shear force V is

$$\tau(\theta, z) = \begin{cases} \dfrac{V_x \cdot Q(\theta, z)}{2 \cdot t \cdot I(z)} \sin(\theta) \\ \\ \dfrac{V_y \cdot Q(\theta, z)}{2 \cdot t \cdot I(z)} \cos(\theta) \end{cases} \tag{4.2}$$

where V_x and V_y are the shear forces caused by the ground motion in x and y directions, respectively, t is the thickness of the porcelain shell, and $Q(\theta, z)$ is the static moment of the cross-sectional area and can be expressed as follows:

$$Q(\theta, z) = 2\, R(z)^2\, t \sqrt{1 - \left(\frac{d(\theta, z)}{R(z)}\right)^2} \tag{4.3}$$

in which R(z) is the average of the outer and inner radii of the section where the element is located. The circumferential stress σ_θ in the element is equal to zero in this case. The maximum tensile stress in the element is then determined from the first principle stress as follows:

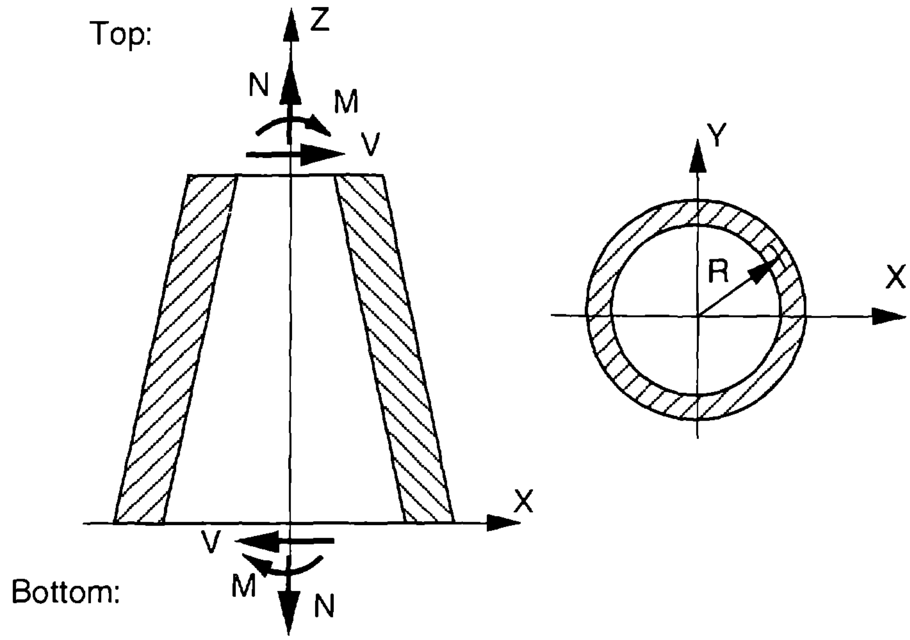

FIGURE 4-4 Forces Acting at Ends of Porcelain Body

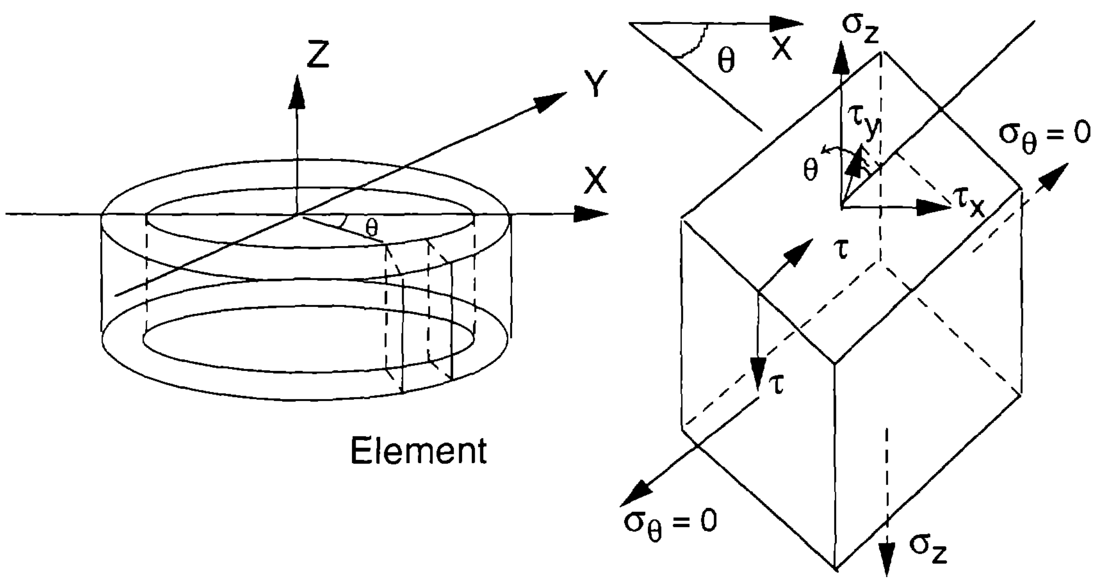

FIGURE 4-5 Stresses on A Porcelain Element

$$\sigma_1(\theta, z) = \frac{\sigma_z}{2} + \sqrt{\left(\frac{\sigma_z}{2}\right)^2 + \tau^2} \tag{4.4}$$

The total maximum tensile stress of the element caused by the ground motions in two horizontal directions is determined using the square root of the sum of the square (SRSS) method.

$$[\sigma_{max}(\theta, z)]_{total} = \sqrt{(\sigma_1)_x^2 + (\sigma_1)_y^2} \tag{4.5}$$

where $(\sigma_1)_x$ and $(\sigma_1)_y$ are the first principle stresses in the element caused by the ground motions in x and y directions, respectively. The analysis shows that the maximum tensile stress always occurs at the bottom of the porcelain body, i.e., z = 0. For the case when PGA is equal to 0.2g, the maximum tensile stress of 140 psi occurs at the bottom of the porcelain body with an angle of 4^o from the x-axis.

The structural response recorded from past earthquakes shows significant variation even under similar conditions; thus, uncertainty in structural response should be considered. Following Hwang et al. (1994), the total maximum tensile stress σ_R in the porcelain body is considered as a lognormal variable. The mean value is the value determined from Equation (4.5) and the COV is taken as 0.5.

4.5 Seismic Fragility Analysis

For the case in which both the response and capacity are lognormal variables, the probability of failure of the pothead structure subject to an earthquake with a PGA level equal to A_i can be determined as follows:

$$P_f = \text{Prob (failure} \mid \text{PGA} = A_i) = \Phi \left[\frac{\text{Ln}(\bar{\sigma}_R) - \text{Ln}(\bar{\sigma}_C)}{\sqrt{\beta_R^2 + \beta_C^2}}\right] \tag{4.6}$$

where

$\Phi[\cdot]$ = probability distribution function of the standard normal variable,

$\bar{\sigma}_R$ = median of the tensile stress in porcelain,

$\bar{\sigma}_C$ = median of the tensile strength of porcelain,
β_R = logarithmic standard deviation of response, and
β_c = logarithmic standard deviation of capacity.

For constructing the fragility curve, the probabilities of failure of the porcelain body corresponding to various PGA levels are determined (Table 4-III). On the basis of these data, the fragility curve of the pothead structure is established and displayed in Figure 4-6.

TABLE 4-III Fragility Data of Pothead Structure

PGA (g)	Probability of Failure
0.1	0.338×10^{-16}
0.2	0.602×10^{-12}
0.5	0.242×10^{-7}
1.0	0.127×10^{-4}
1.5	0.249×10^{-3}
2.0	0.151×10^{-2}
2.5	0.518×10^{-2}
3.0	0.127×10^{-1}
3.5	0.251×10^{-1}
4.0	0.428×10^{-1}
4.5	0.659×10^{-1}
5.0	0.938×10^{-1}

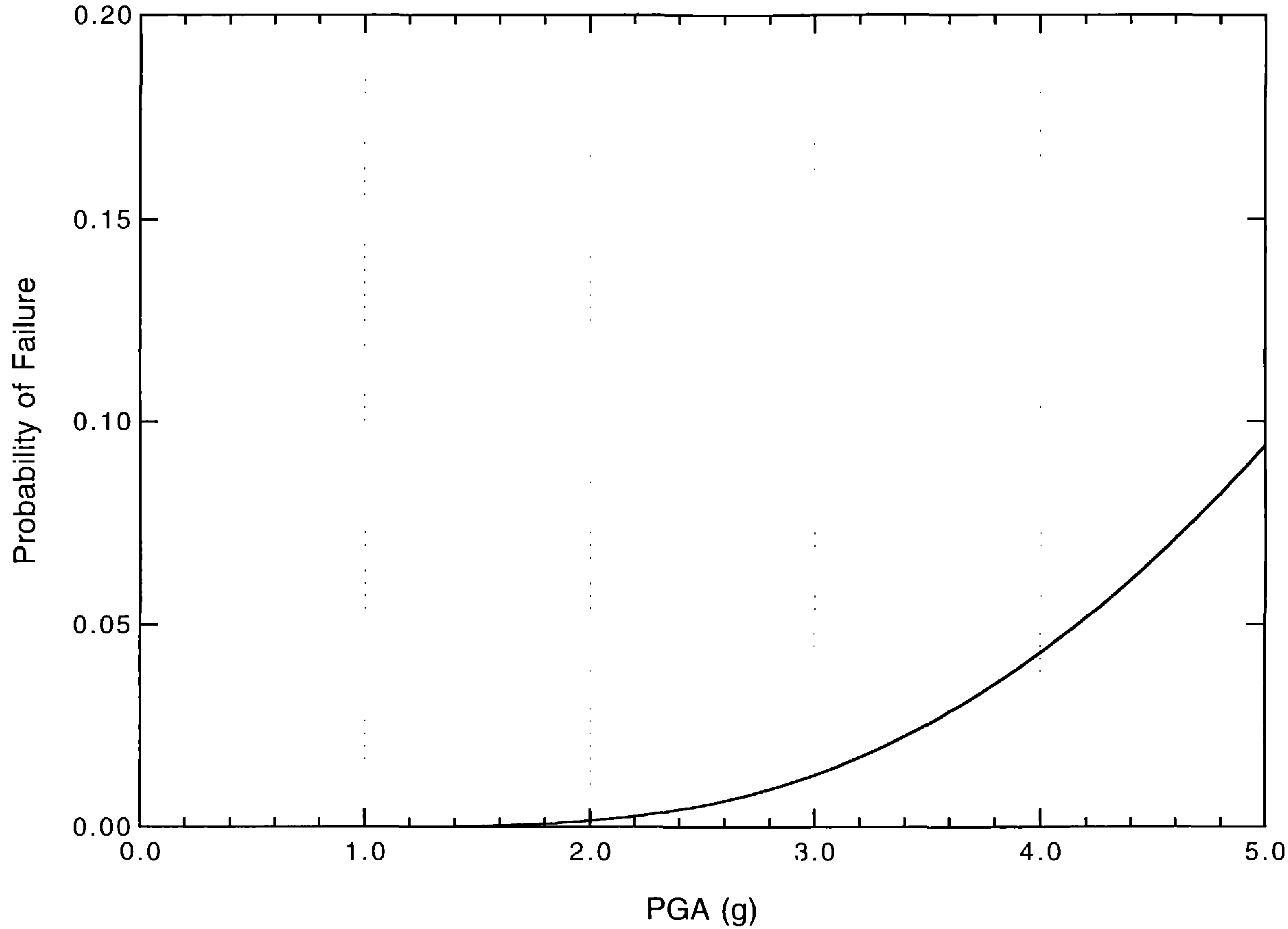

FIGURE 4-6 Fragility Curve of Pothead Structure

SECTION 5
115 KV SWITCH STRUCTURE

5.1 Description of Switch Structure

The high-pressure blade switches and 115 kV cables are supported by porcelain insulators on a 115 kV switch structure (115 kV bus), a latticed steel structure. The plan and elevation of the 115 kV switch structure are shown in Figure 5-1. The chord members of latticed beams and columns are made of $L4{\times}4{\times}\frac{1}{2}$ angles, while the diagonal members are made of $L2{\times}2{\times}\frac{5}{16}$ angles. The columns are anchored to a concrete foundation with six $\frac{7}{8}$ bolts (Figure 5-2). Three porcelain insulators as a group (Figure 5-3) support a high-pressure blade switch. These insulators are mounted on a double-channel beam, which is connected to the top or bottom of a latticed beam. The height of one insulator is 45 inches and the minimum diameter is 6.25 inches. The weight of each porcelain insulator is 183 pounds and the weight of blade switch is estimated as 50 pounds.

5.2 Modeling of Switch Structure

The latticed steel structure is modeled as a spatial frame with columns fixed to the foundation (Figure 5-4). The stiffness and strength of the frame members (Table 5-I) are calculated from the properties of the latticed members. A group of three porcelain insulators is modeled as a cantilever column with distributed mass and stiffness and the steel double-channel beam is modeled as a steel element with a rigid connection to the beams of the spatial frame (Figure 5-4). The weight of blade switch is modeled as a concentrated mass on the top of the cantilever column representing the insulators. The properties of insulators are also listed in Table 5-I.

The 115 kV switch structure does not support any heavy electric devices; thus, it is strong enough to resist the seismic effect produced from the weight of itself and porcelain insulators. In this study, the porcelain insulators are considered as the weakest part of the structure during a seismic event, because earthquake shaking may easily cause the porcelain insulator to fail in tension.

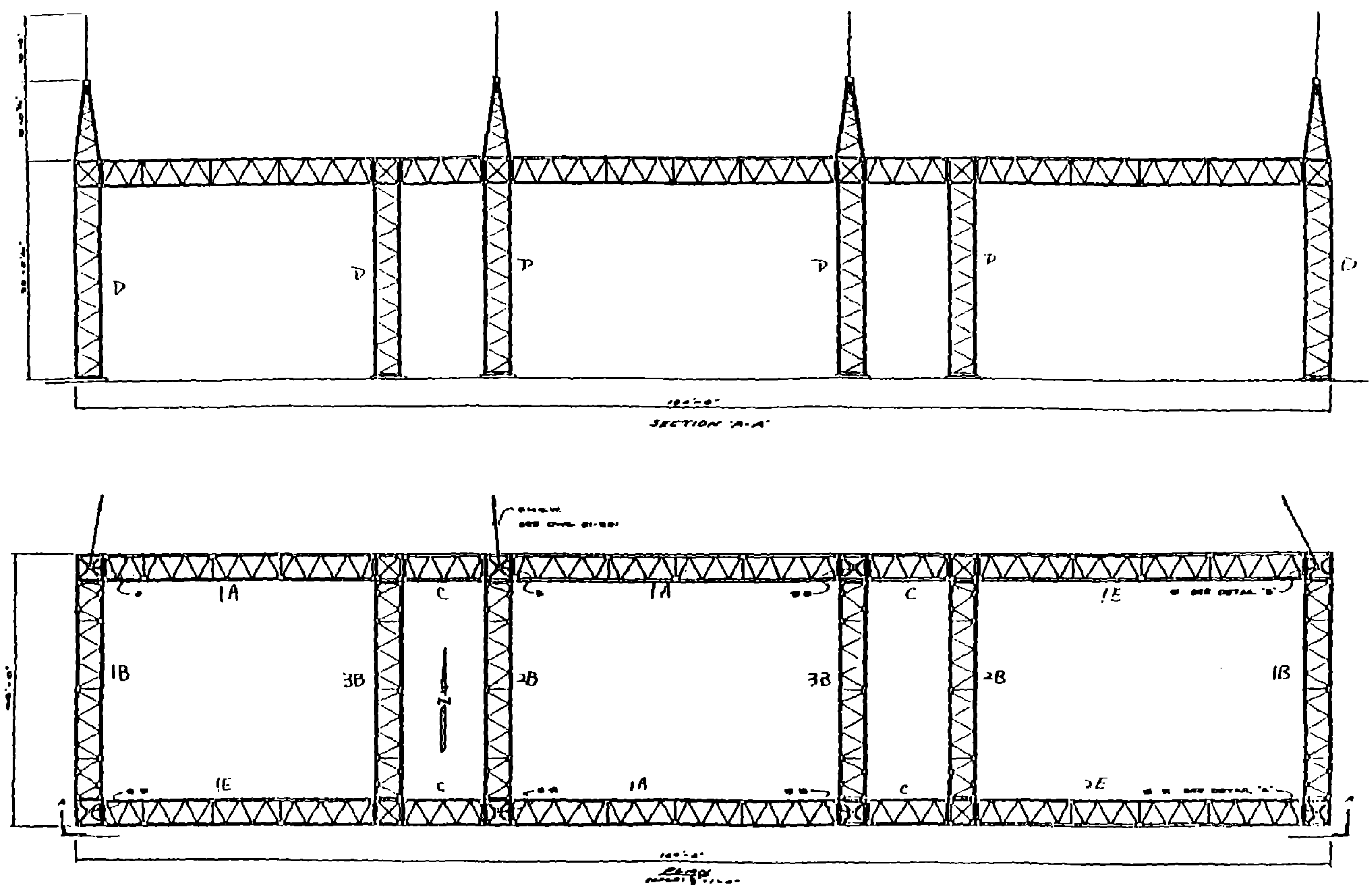

FIGURE 5-1 Plan and Elevation of 115 kV Switch Structure

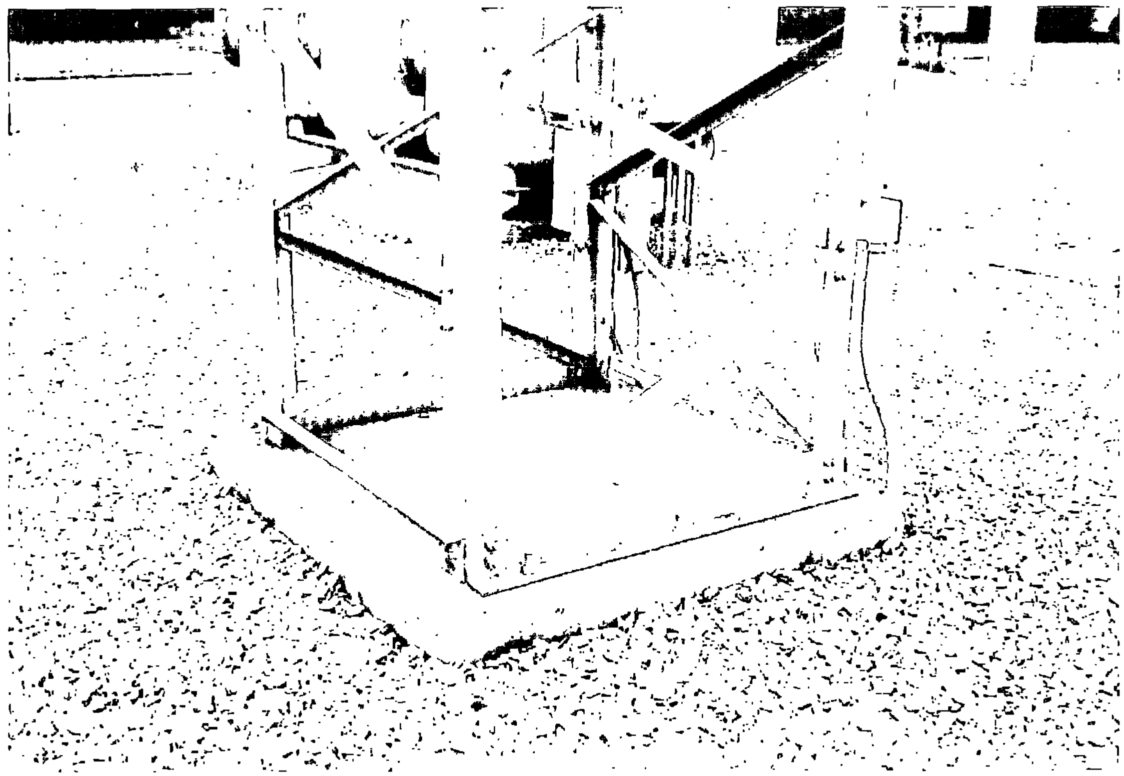

FIGURE 5-2 Column Anchors to Foundation for 115 kV Switch Structure

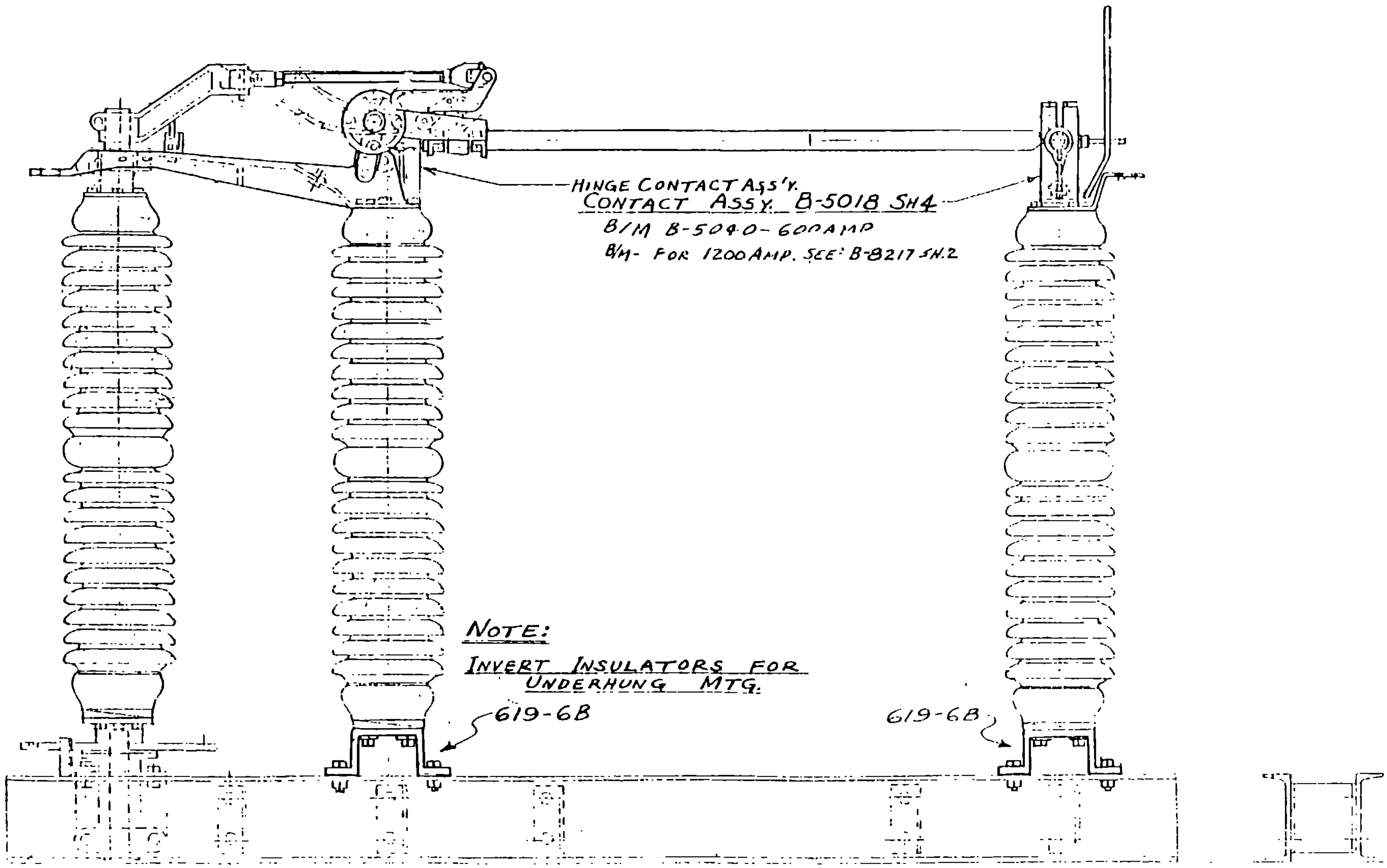

FIGURE 5-3 Detail of Porcelain Insulators on 115 kV Switch Structure

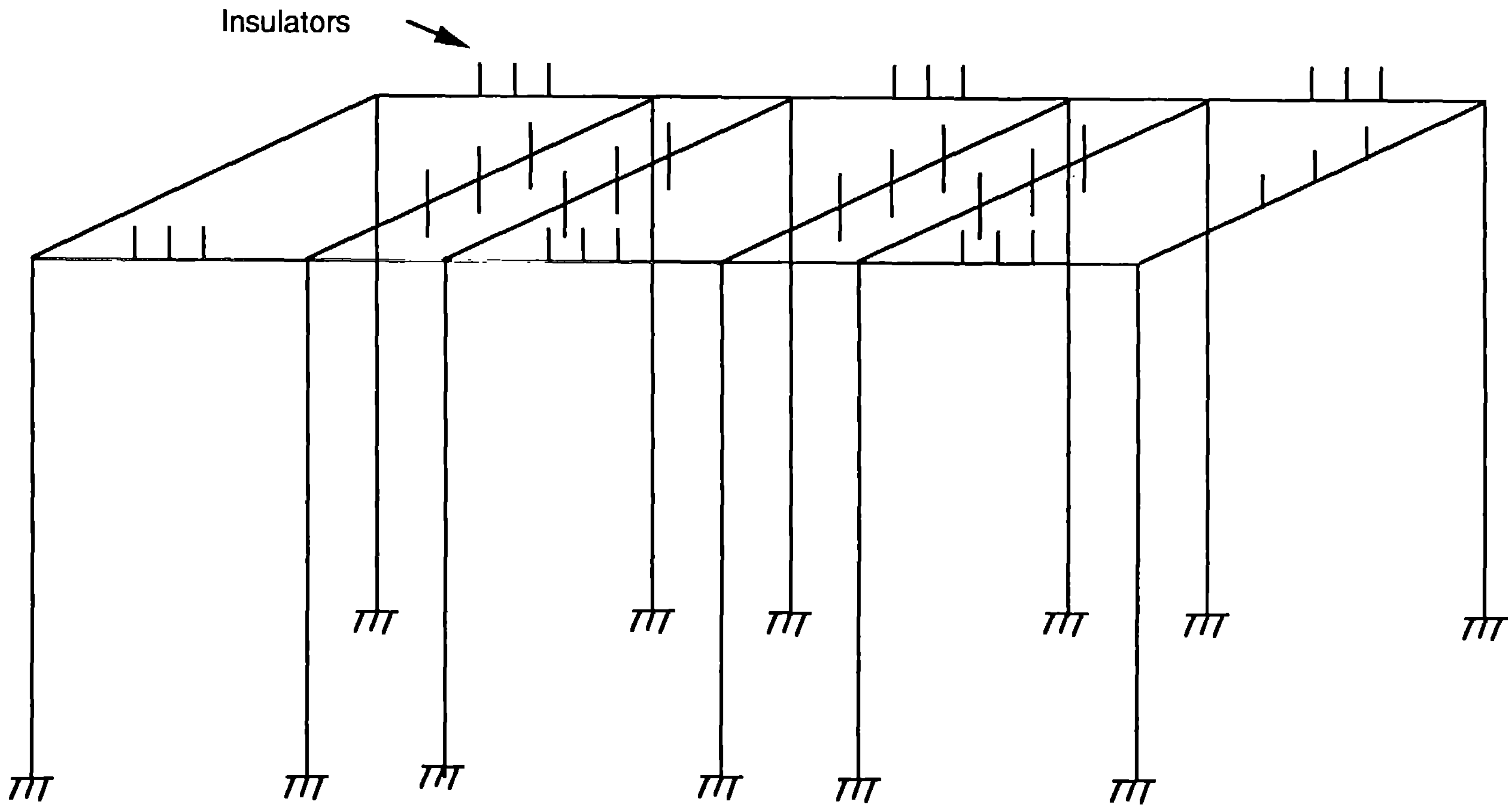

FIGURE 5-4 Model of 115 kV Switch Structure

TABLE 5-I Member Properties of 115 kV Switch Structure

Member	Section Area (in^2)	Moment of Inertia (in^4)	Shear Area (in^2)	Weight (lb/in)
Column	15	7811	4.23	10.41
Beam	15	7811	4.23	10.29
Insulator	30.7	74.9	23.01	4.07

TABLE 5-II Natural Periods of 115 kV Switch Structure

Mode No.	Period (sec)		
	X-Direction	Y-Direction	Vertical
1	0.193	0.174	0.080
2	0.067	0.139	0.076

5.3 Fragility Analysis of Switch Structure

The response of the latticed steel structure and the forces in the porcelain insulators are determined from the response spectrum analysis using the SAP program. Table 5-II shows the natural periods of the structure in three directions. The 5% damped ground response spectra in both horizontal directions are used as the input to the structure. The responses corresponding to various modes (Table 5-II) in each horizontal direction are combined using the CQC technique, and the total response caused by the ground motions in two horizontal directions is combined using the SRSS method. For a given PGA level, the bending moment M, shear force V, and axial force N at both ends of the porcelain insulators obtained from the response spectrum analysis are used to calculate the maximum tensile stress at the critical position of the porcelain according to Equations (4.4) and (4.5). As an example, the maximum tensile stress of porcelain for the case of PGA of 0.2g is about 129 psi.

The maximum tensile stress in porcelain is considered as a lognormal variable. The mean value is determined from the aforementioned analysis and the COV is taken as 0.5. As described in Section 4.2, the tensile strength of porcelain is considered as a lognormal variable with the mean value of 6.8 ksi and the COV of 0.3. On the basis of these distributions, the failure probability of porcelain can be determined using Equation (4.6). Table 5-III shows the probabilities of failure corresponding to various PGA levels, and the resulting fragility curve is displayed in Figure 5-5.

TABLE 5-III Fragility Data of 115 kV Switch Structure

PGA (g)	Probability of Failure
0.1	0.102×10^{-16}
0.2	0.216×10^{-12}
0.5	0.109×10^{-7}
1.0	0.676×10^{-5}
1.5	0.146×10^{-3}
2.0	0.951×10^{-3}
2.5	0.343×10^{-2}
3.0	0.875×10^{-2}
3.5	0.179×10^{-1}
4.0	0.315×10^{-1}
4.5	0.498×10^{-1}
5.0	0.725×10^{-1}

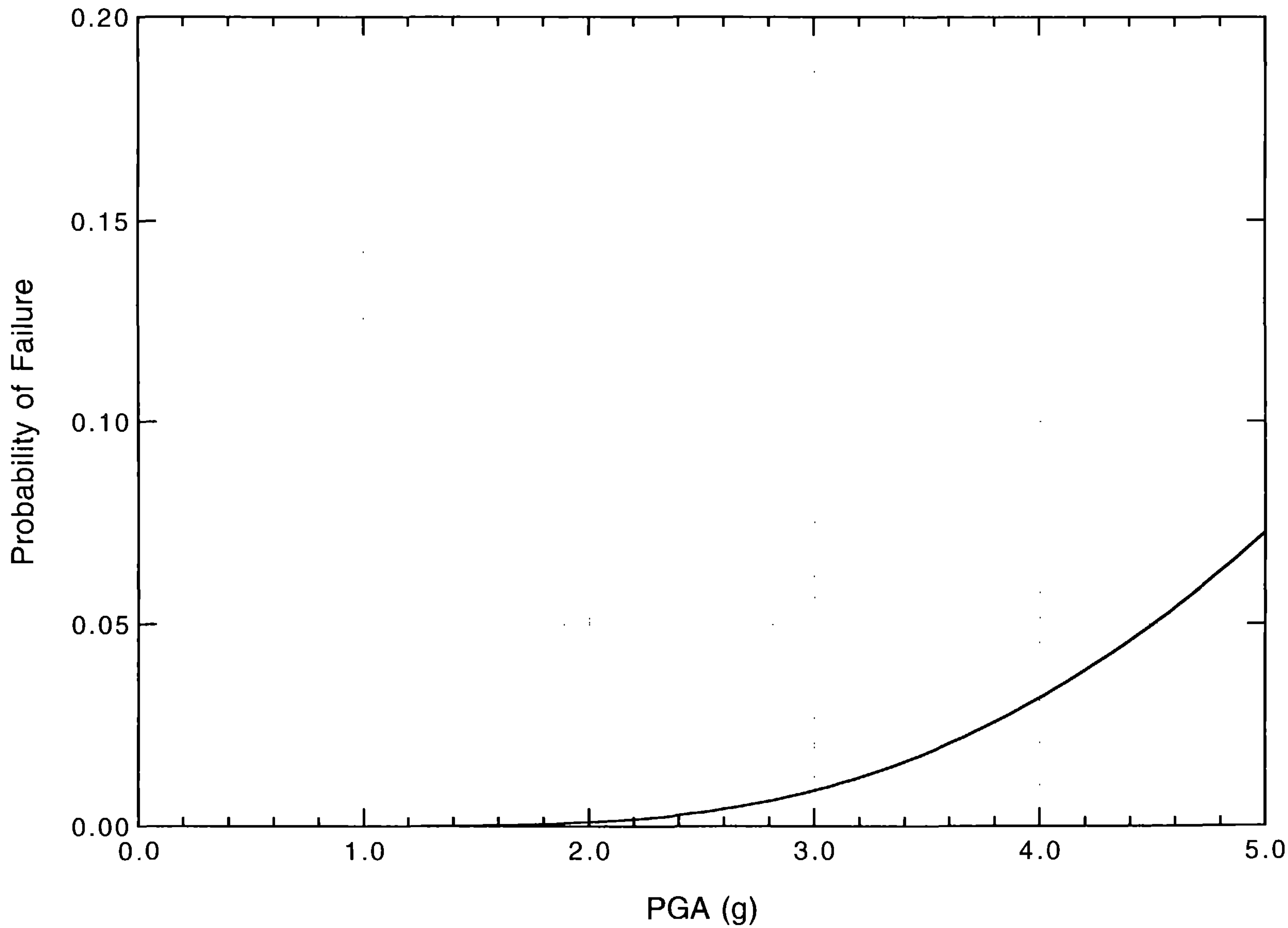

FIGURE 5-5 Fragility Curve of 115 kV Switch Structure

SECTION 6
97 KV LIGHTNING ARRESTERS

6.1 Description and Modeling of Lighting Arresters

Figure 6-1 shows a photograph of a 97 kV lightning arrester. The lightning arrester consists of a porcelain insulator supported by a reinforced concrete (RC) post. The porcelain insulator is made of three segments of porcelain placed on top of each other and connected by four $\frac{1}{2}$ bolts (Figure 6-2). The minimum diameter of the insulator is approximately 6 inches. The overall height of the insulator is 123.5 inches and the total weight is 620 pounds. The insulator is connected to the RC post by four $\frac{3}{4}$ bolts. The dimension and reinforcement of the RC post are shown in Figure 6-3. The cable on the lightning arrester is flexible enough so that the force on the insulator induced by the cable is negligible.

The lightning arrester is modeled as a cantilever column fixed at the base as shown in Figure 6-4. In the model, the porcelain insulator is divided into 15 finite elements, while the RC post is divided into 10 elements. The properties of both porcelain and concrete elements are listed in Table 6-I.

6.2 Fragility Analysis of Lightning Arresters

The failure of the porcelain insulator in tension is considered as the most probable failure mechanism of the 97 kV lightning arrester. The maximum tensile stress of porcelain in a seismic event is determined from the response spectrum analysis using the SAP program. For a given PGA level, 2% damped ground response spectra are input to the structure in two horizontal directions. For each direction, the responses from various modes (Table 6-II) are combined using the CQC technique. The total response is then determined from the combination of the responses from two horizontal directions using the SRSS method. From the analysis, the bending moment M, shear force V, and axial force N at both ends of each element can be determined. The maximum tensile stress at the most critical position of the porcelain insulator can be determined from these forces using Equations (4.4) and (4.5). As an example, for the case of PGA equal to 0.2g, the maximum total stress is determined as 1335 psi at the bottom of the porcelain insulator.

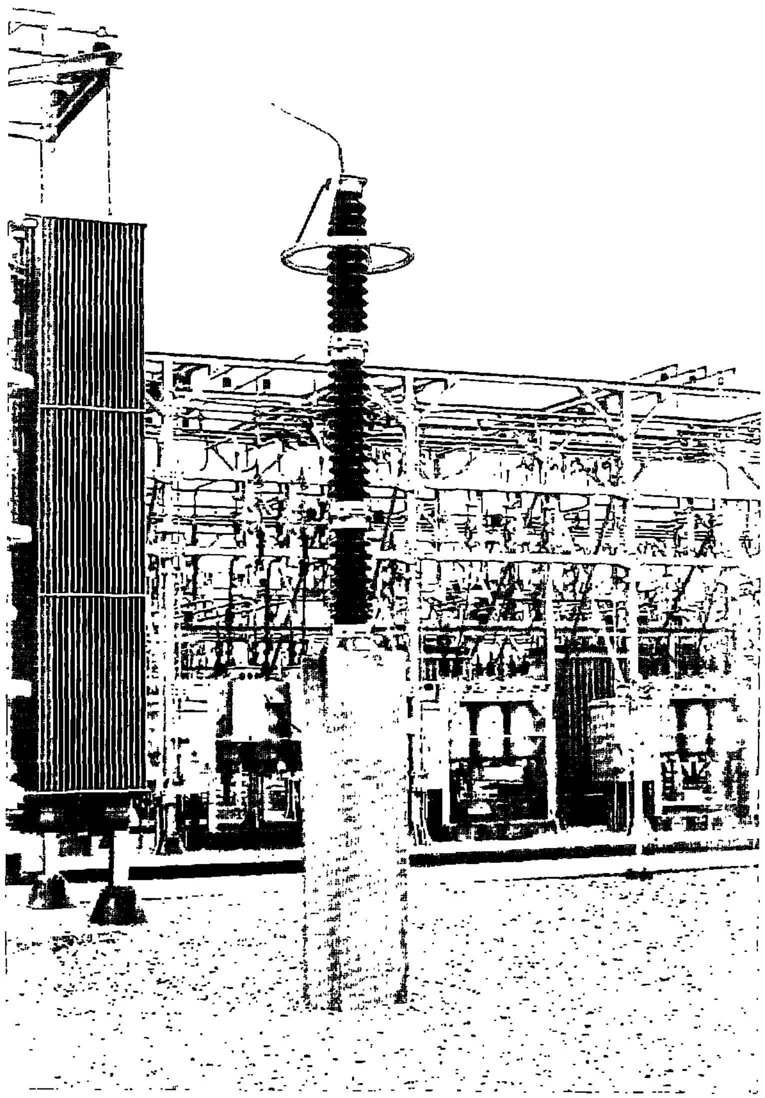

FIGURE 6-1   97 kV Lightning Arrester

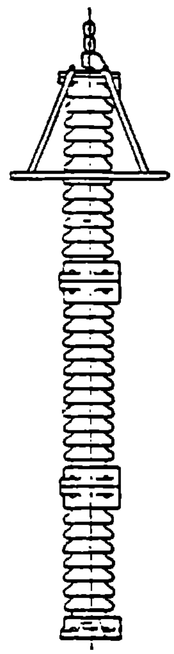

FIGURE 6-2 Porcelain Insulator of 97 kV Lightning Arrester

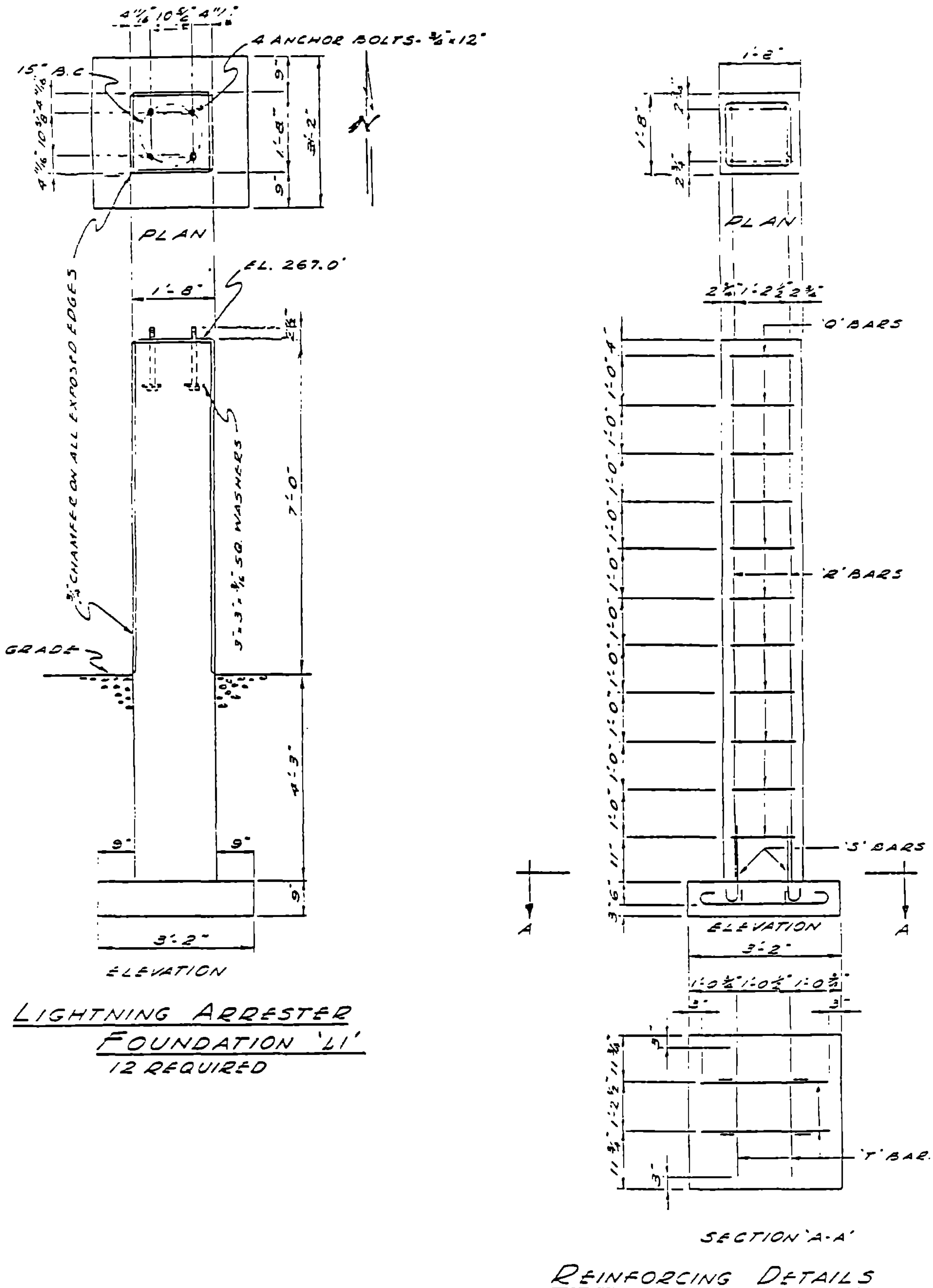

FIGURE 6-3 Foundation of 97 kV Lightning Arrester

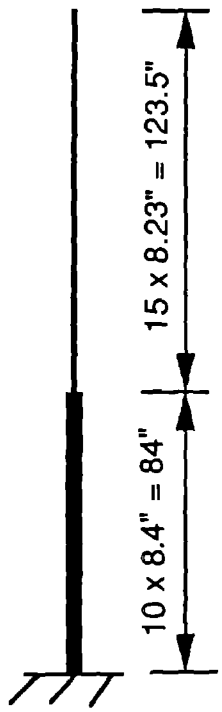

FIGURE 6-4 Model of 97 kV Lightning Arrester

TABLE 6-I Properties of 97 kV Lightning Arrester

Segment	Section Area (in^2)	Moment of Inertia (in^4)	Length (in)	Weight (lb/in)
Porcelain	28.3	63.6	123.5	5.02
RC Pole	400.0	13333.0	84.0	34.72

TABLE 6-II Natural Periods of 97 kV Lightning Arrester

Mode	Period (sec)
1	0.126
2	0.025
3	0.015

The tensile stress of the porcelain insulator is considered as a lognormal variable. The mean value is determined from the analysis, while the COV is set as 0.5. The tensile strength of porcelain is also a lognormal variable with the mean value of 6.8 ksi and the COV of 0.3 as mentioned in Section 4.2. Using Equation (4.6), the failure probabilities of the 97 kV lightning arrester for various PGA levels can be determined (Table 6-III) and displayed as a fragility curve in Figure 6-5.

TABLE 6-III Fragility Data of 97 kV Lightning Arrester

PGA (g)	Probability of Failure
0.05	0.149×10^{-7}
0.10	0.867×10^{-5}
0.20	0.114×10^{-2}
0.30	0.101×10^{-1}
0.40	0.356×10^{-1}
0.50	0.803×10^{-1}
0.60	0.141
0.70	0.212
0.80	0.288
0.90	0.365
1.00	0.438

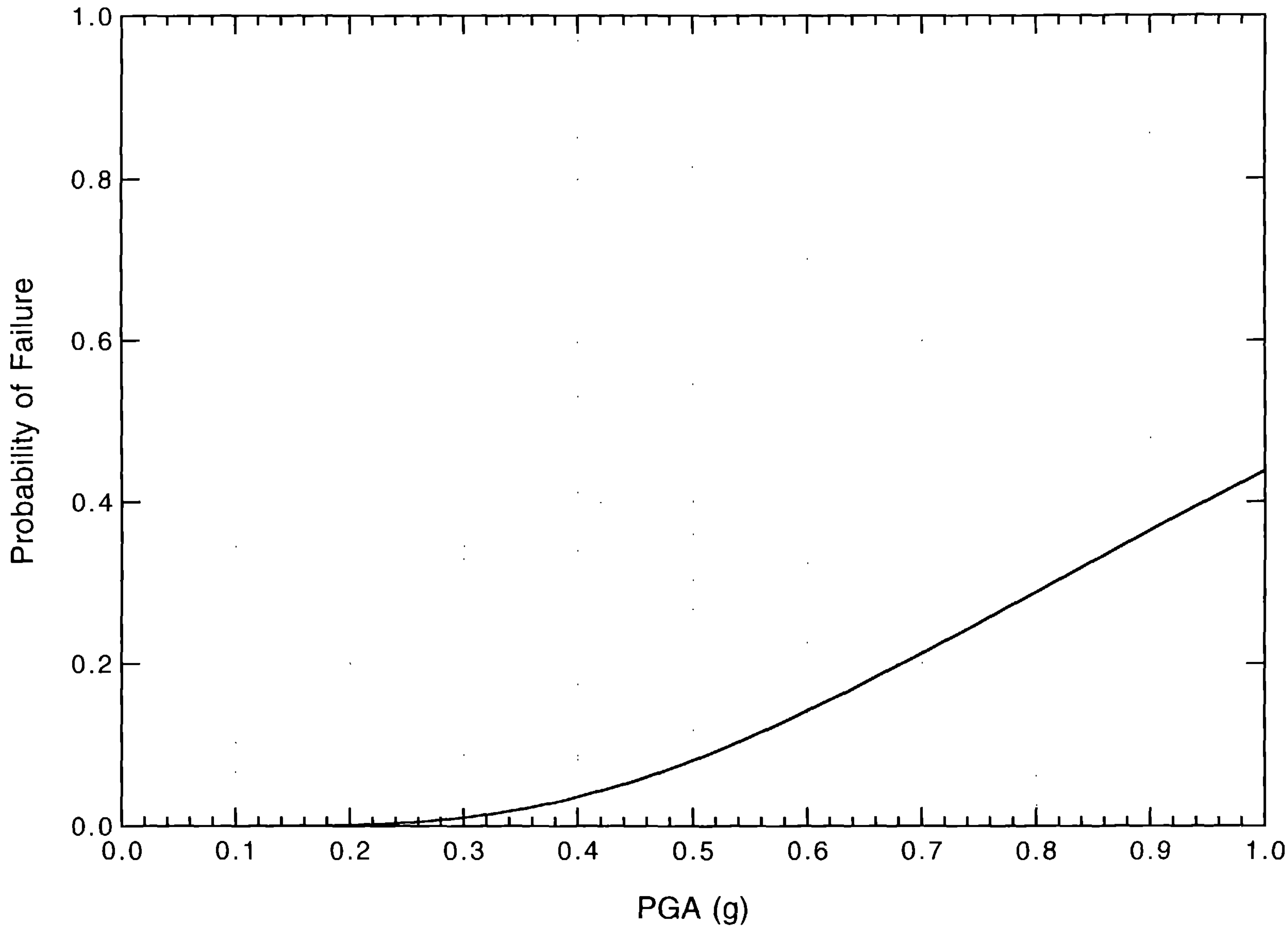

FIGURE 6-5 Fragility Curve of 97 kV Lightning Arrester

SECTION 7
CONTROL HOUSE

The control house (Figure 7-1) provides a shelter for control console, cable panel, and battery for the substation. It is a one-story unreinforced masonry (URM) building with a basement. The steel "I" beams supporting the roof are set on the masonry walls. The walls have a thickness of 18 inches and support both gravity loads and seismic loads.

The fragility analysis of the control house is focused on the damage state at which the operation of the control house is significantly affected. This damage state is defined as the moderate structural damage to the URM buildings. The relations of ground motion and seismic damage to URM buildings have been established in several studies. In a study of seismic losses for six-cities in the central United States (FEMA, 1985), the fragility curves corresponding to various damage states from non-structural damage to collapse for typical buildings commonly found in six-cities including Memphis were established from the combination of simplified analysis, engineering judgment, and damage data from past earthquakes. The fragility curve for moderate structural damage to average URM buildings is shown in Figure 7-2.

The Applied Technology Council (ATC) carried out a project (ATC-13) to establish the damage probability matrices (DPMs) for facilities in California (ATC, 1985). The DPM expresses the probabilities of damage at various Modified Mercalli Intensity (MMI) for seven damage states: no damage, slight damage, light damage, moderate damage, heavy damage, major damage, and destroyed. The estimates of the DPMs were obtained through three rounds of a questionnaire process. To establish the fragility curve of moderate structural damage to URM buildings, the fragility data is computed from the summation of the DPM values of moderate damage, heavy damage, major damage, and destroyed. The PGA is determined from the conversion of MMI with the relation used in the six-cities study. Following this procedure, the fragility curve of moderate structural damage to URM buildings from the ATC-13 study is also shown in Figure 7-2.

The DPMs for typical URM buildings in St. Louis, Missouri, were determined from the modification of the fragility data for California buildings using the expert judgment and information about buildings in the St. Louis area (FEMA, 1990). The

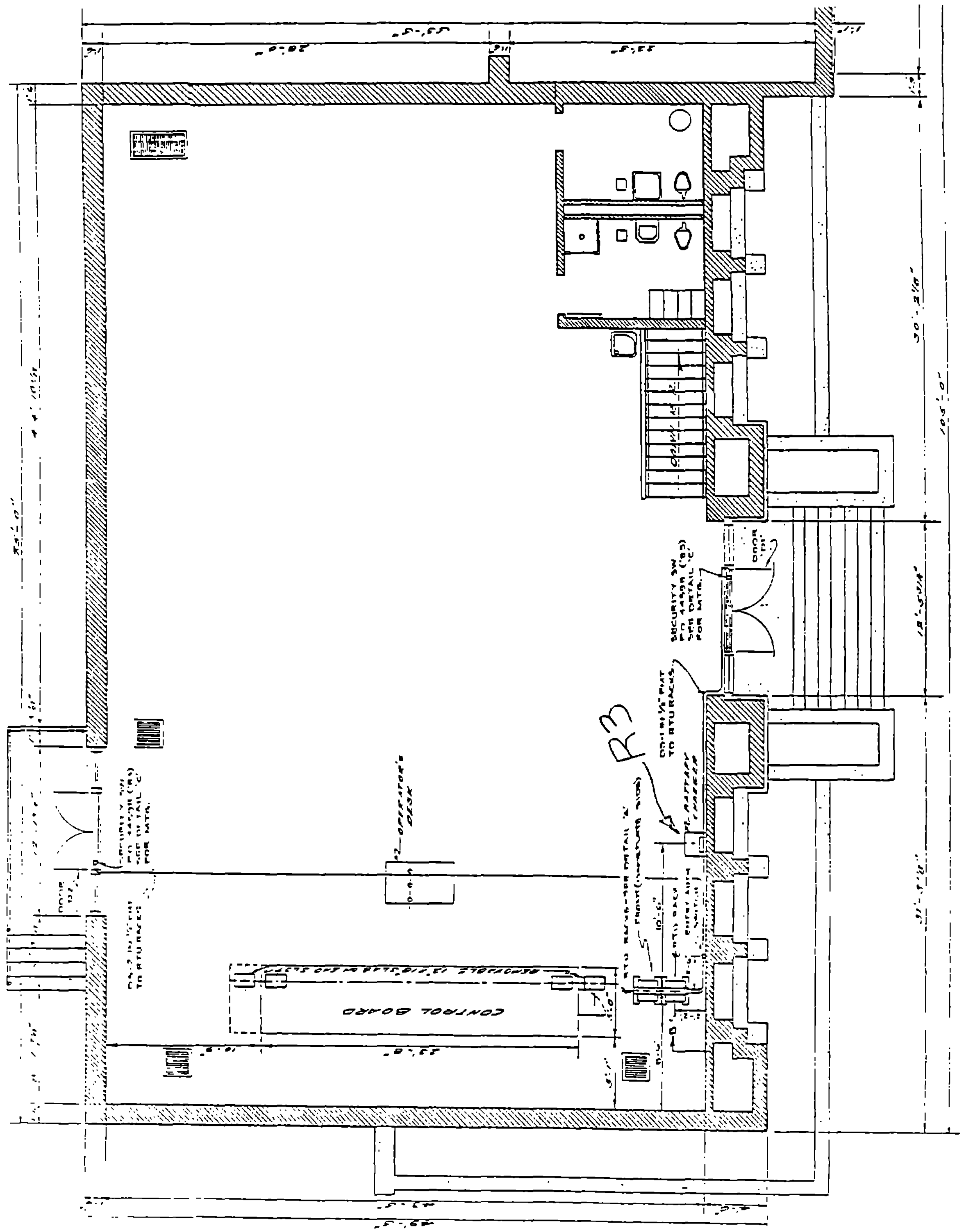

FIGURE 7-1 First Floor Plan of Control House

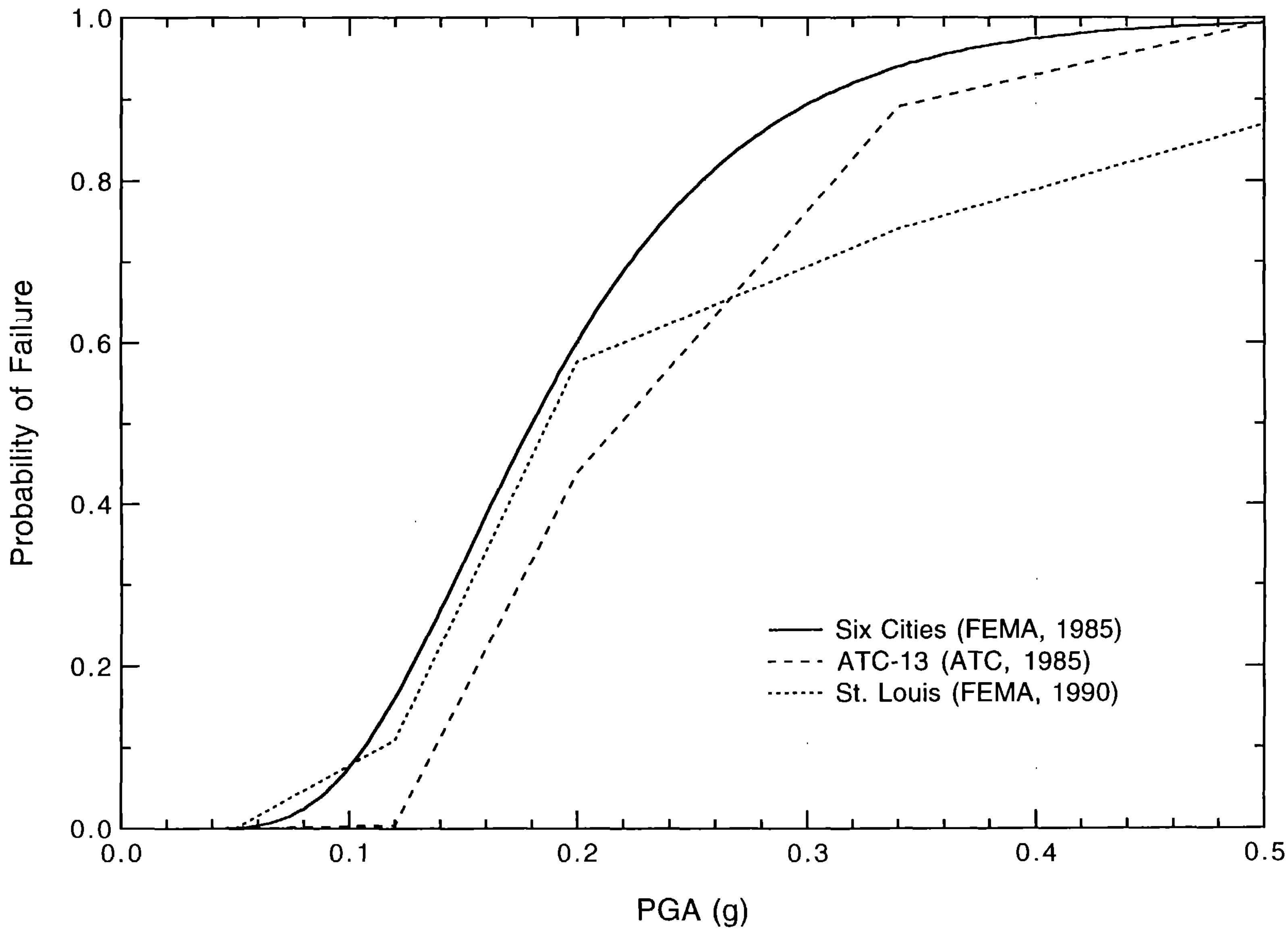

FIGURE 7-2 Comparison of Fragility Curves of Moderate Damage to Unreinforced Masonry Buildings

DPMs are converted to fragility curves using the same approach mentioned above. The fragility curve of moderate structural damage to URM buildings in the St. Louis area is also shown in Figure 7-2.

The fragility data from the ATC-13 study are for the facilities in California, while those determined in the six-cities and St. Louis studies are for typical buildings in the central United States. The fragility curves of moderate structural damage to URM buildings from these two studies are quite close up to a 60% probability of failure (see Figure 7-2). Since the fragility curves in the six-cities study were developed for typical buildings in the Mississippi Valley, where Memphis is located, the fragility curve (solid line in Figure 7-2) is adopted for the control house in this study. Table 7-I lists the fragility data of the control house corresponding to various PGA levels.

TABLE 7-I Fragility Data of Control House

PGA (g)	Probability of Failure
0.05	0.001
0.10	0.076
0.12	0.161
0.14	0.270
0.16	0.387
0.18	0.500
0.20	0.601
0.22	0.688
0.24	0.759
0.26	0.815
0.28	0.859
0.30	0.894
0.35	0.948
0.40	0.974
0.45	0.987
0.50	0.994

SECTION 8
CAPACITOR BANKS

8.1 Description of Capacitor Banks

The 12 kV capacitor yard is composed of a switch structure and two capacitor banks (Figure 8-1). The switch structure is a steel structure supporting cables from the capacitor banks to Bay 17 of the 12 kV switch structure. Since the switch structure does not support heavy electric devices and the steel members are well constructed, it is strong enough to resist the seismic load. Thus, the fragility analysis of the capacitor yard is focused on the capacitor banks.

The capacitor banks in Substation 21 were made by General Electric. An elevation of the capacitor bank is shown in Figure 8-2. The capacity bank consists of three layers of steel racks, which are placed on top of each other and are connected by four $\frac{5}{8}$ bolts at each column. At the bottom of each rack (Figure 8-3), two longitudinal and two transverse channel beams (C6×10.5) are welded to four steel angle columns ($L4\times4\times\frac{1}{2}$). Then two additional longitudinal channels are welded to the transverse beams. Eighteen capacitors in two rows are hung on four longitudinal beams at the middle of the capacitor by two bolts. The capacitor containing oil and coils has a size of $30\times5.5\times12$ in^3 and a weight of 110 pounds. On the top of each rack, two channel beams (C4×5.4) in the transverse direction are welded to two longitudinal beams made of steel angles $L4\times4\times\frac{1}{2}$ and these two longitudinal beams are then welded to four columns.

The bottom of each column is isolated from the ground by a porcelain insulator placed between the column and the foundation. Each column is connected to the insulator by four bolts. The insulator is a 15 kV heavy duty cap and pin porcelain insulator about 10 inches in height (Figure 8-4). The metal pin of the insulator has a diameter of $1\frac{1}{2}$ inches and it is bound to the porcelain body by cement sand compound. The metal pin is connected to a reinforced concrete foundation also by four bolts.

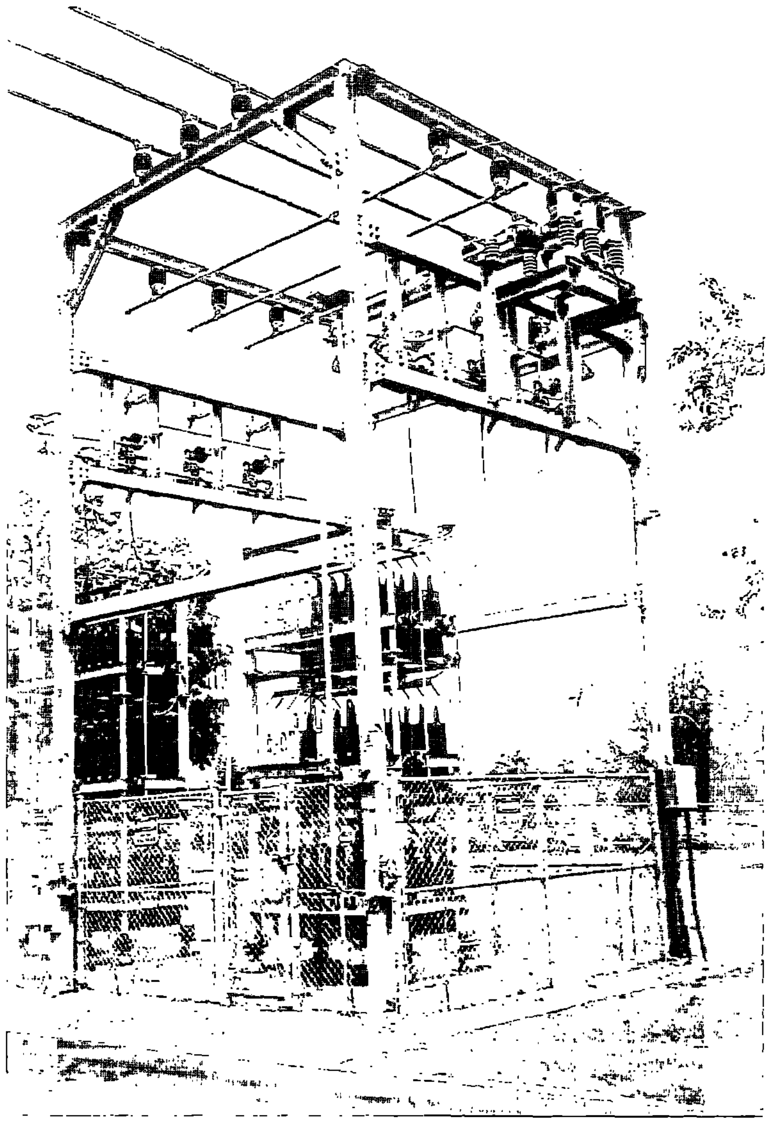

FIGURE 8-1 12 kV Capacitor Yard

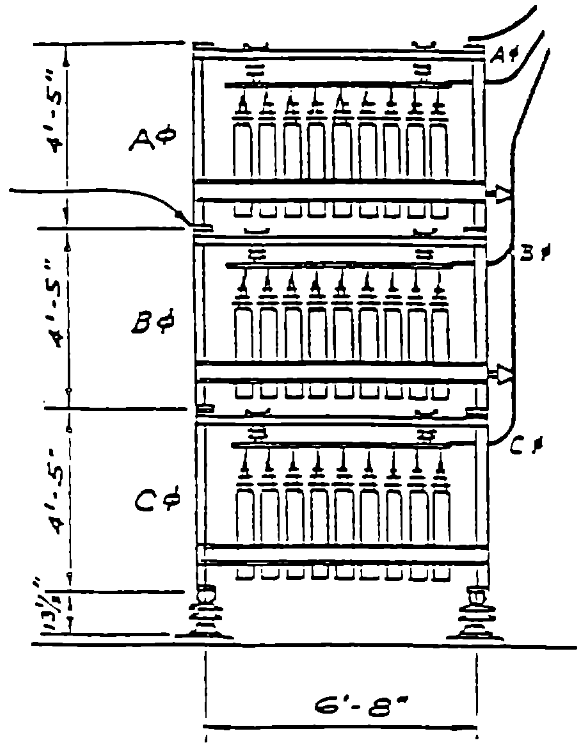

FIGURE 8-2 Elevations of Capacitor Bank

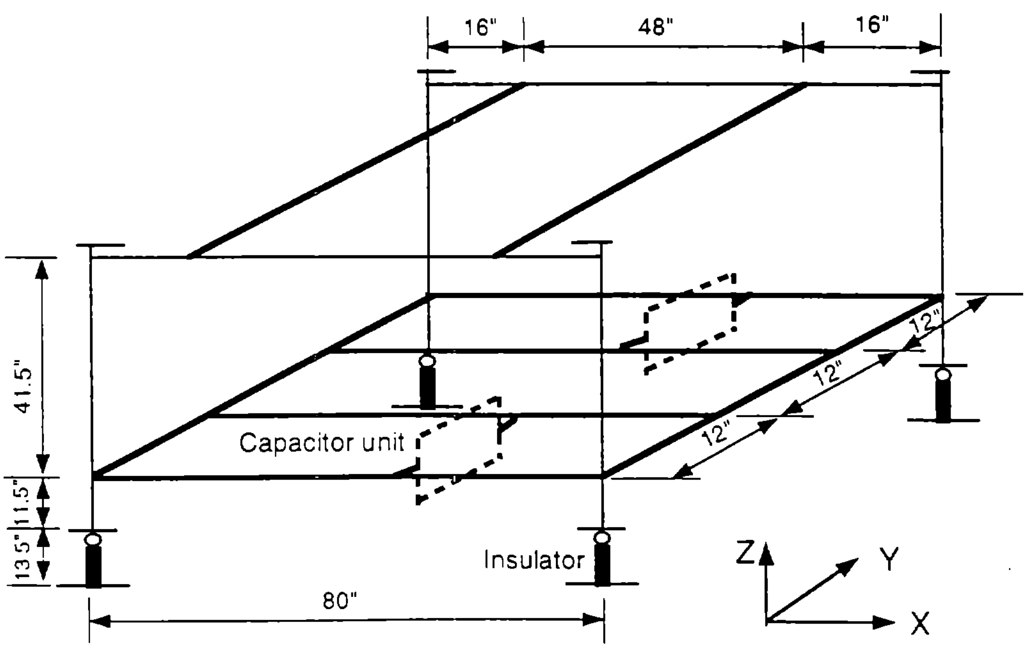

FIGURE 8-3 Model of Rack (First Layer) and Insulators

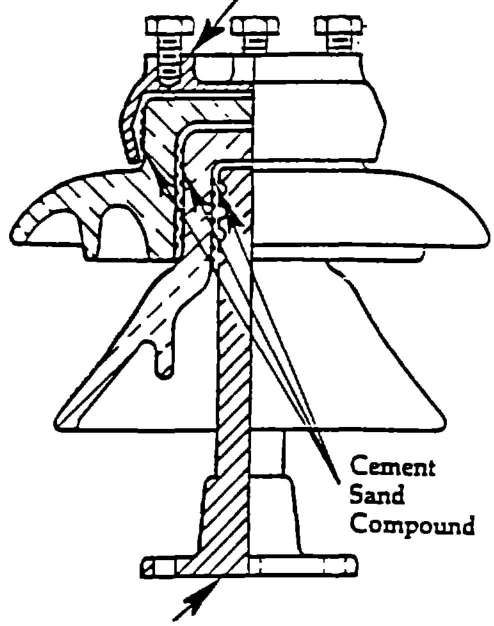

FIGURE 8-4 Cap and Pin Porcelain Insulator

8.2 Structural Modeling and Failure Mechanism

The capacitor bank is modeled as a three-dimensional steel frame consisting of three layers of racks. A model of the capacitor bank (first layer) is shown in Figure 8-3. In the figure, the thick solid lines indicate steel channels and the fine lines indicate steel angles. Two typical capacitors indicated by dash lines are also shown in Figure 8-3. The capacitor is considered as the distributed mass on the longitudinal beams. The racks are connected to each other by a bolt at each column. Such a connection cannot transfer bending moment well and thus the connection is modeled as a hinge. The insulator is connected to a metal pin by cement sand compound. Such a connection also cannot sustain large bending moment. Thus, the connection of the porcelain body to the metal pin is also considered as a hinge.

The metal pin and porcelain body of the insulator are bound together using cement sand compound. The pin may easily separate from the porcelain body by the tensile force or bending moment acting on the insulator. The insulators are thus considered as the weakest part of the capacitor bank, and the tensile strength of the insulator controls the failure of the structure.

8.3 Seismic Response Analysis of Capacitor Bank

Since the insulator is made of brittle material, the response spectrum analysis of the SAP program is used to determine the maximum seismic response of the insulator. From the free vibration analysis, the natural periods and modal shapes of the structure can be determined. The first three natural periods in two horizontal directions are shown in Table 8-I. In the table, the x and y directions, respectively, represent the longitudinal and transverse directions of the structure.

For each PGA level, the seismic input to the structure is the ground response spectra with 2% damping ratio in two horizontal directions. The response spectrum analysis is carried out using the first three modes in each horizontal direction to determine the modal responses of structure. The modal responses in each direction are combined using the CQC technique, and the seismic responses in different directions are then combined by the SRSS method. Finally, the seismic responses are combined with the result of a dead load analysis to determine the maximum tensile force on the insulator. As an example, assuming the capacitor bank is subject to an earthquake with a PGA of 0.2g , the maximum tensile force on the insulator due to the earthquake and dead load is 3,557 pounds.

TABLE 8-I Natural Periods of Capacitor Bank

Mode No.	Natural Period (sec)	
	X-Direction	Y-Direction
1	0.240	0.213
2	0.081	0.073
3	0.045	0.039

8.4 Fragility Analysis of Capacitor Bank

For constructing fragility curves, the maximum tensile forces on the insulator corresponding to various PGA levels are computed and summarized in Table 8-II. It is noted that the tensile axial force is taken as positive in the table. The tensile force on the insulator is considered as a lognormal variable with the mean value taken as the value determined from the analysis (Table 8-II), and the COV is set as 0.5.

In this study, the tensile strength of insulators is also assumed as a lognormal variable with the COV set as 0.3. The cap and pin insulators used in Substation 21 have a tensile strength of 5000 pounds as specified by the manufacturer. Following the similar consideration as indicated in Section 4.2, the mean value of tensile strength is determined as 6800 pounds. Since both response and capacity are lognormal variables, the failure probabilities of the capacitor bank corresponding to various PGA levels can be determined using Equation (4.6) and shown in Table 8-III. The resulting fragility curve of the capacitor bank is displayed in Figure 8-5.

TABLE 8-II Maximum Response of Capacitor Bank Insulator

PGA (g)	Axial Force (lb)		
	Seismic Load	Dead Load	Combined
0.05	1250	-2010	-760
0.10	2764	-2010	754
0.15	4233	-2010	2223
0.20	5567	-2010	3557
0.25	6490	-2010	4480
0.30	7495	-2010	5485
0.35	8631	-2010	6621
0.40	9824	-2010	7814
0.50	12330	-2010	10320
0.60	14796	-2010	12786
0.70	17262	-2010	15252
0.80	19728	-2010	17718
0.90	22194	-2010	20184
1.00	24660	-2010	22650

TABLE 8-III Fragility Data of Capacitor Bank

PGA (g)	Probability of Failure
0.10	0.210×10^{-4}
0.15	0.164×10^{-1}
0.20	0.988×10^{-1}
0.25	0.191
0.30	0.305
0.35	0.432
0.40	0.554
0.50	0.735
0.60	0.844
0.70	0.908
0.80	0.945
0.90	0.967
1.00	0.979

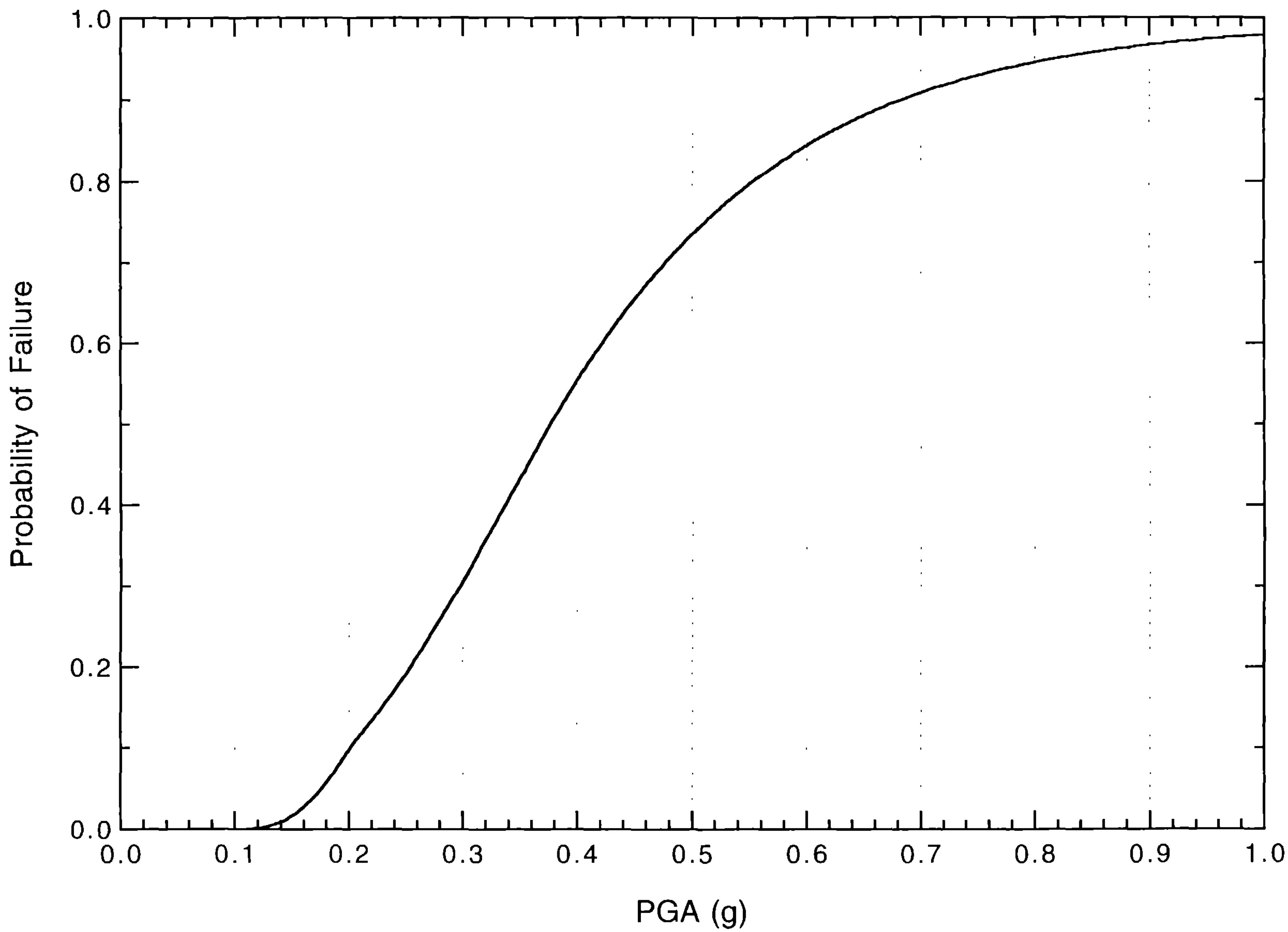

FIGURE 8-5 Fragility Curve of Capacitor Bank

SECTION 9
115/12 KV TRANSFORMERS

9.1 Description of Transformers

There are three 115/12 kV transformers in Substation 21. Two of them (Type I) were installed in the 1950s, when the substation was originally constructed. The third one (Type II) was installed in the 1960s, when the substation was expanded. The basic information about these two types of transformers is summarized in Table 9-I.

Figure 9-1 shows a photograph of Type I transformer. The box-shaped body with four wheels is seated on two rails. The transformer is restrained from moving in the horizontal direction by two wheel stops at each side of the transformer (Figure 9-2). The wheel stops consist of two L6×$3\frac{1}{2}$×$\frac{1}{2}$ angles clamped to the rail by two $\frac{5}{8}$ bolts (Figure 9-3). Type II transformer is similar to Type I transformer (Figure 9-4). From a field inspection, it is noted that only one wheel stop is installed at each side of the Type II transformer (Figure 9-5).

9.2 Failure Mode of Transformers

Failure of transformers is one of the most common types of damage to electric power systems in past earthquakes. In the event of an earthquake, inadequately secured transformers will sliding or overturning. As a result, it can easily cause major damage to bushings, radiators, internal parts, and interconnecting bus. The body of a transformer is very stiff and it is usually modeled as a rigid block (Ishiyama, 1982). For a transformer considered as a rigid block, there are two possible modes of failure. One is sliding, the excessive horizontal movement of the transformers along the rails after the failure of the wheel stops. The other is overturning, that is, the transformers fall down from the rails.

9.3 Fragility Analysis of Type II Transformer

9.3.1 Overturning

For a transformer modeled as a rectangular rigid body (Figure 9-6), the transformer

TABLE 9-I Basic Information of 115/12 kV Transformers

Transformer	Type I	Type II
Manufacturer	Wagner Electric Corporation	Wagner Electric Corporation
Installed Date	1950s	1960s
Quantity installed	2	1
Phases	3	3
High Voltage (kV)	115	115
Low Voltage (kV)	12	12
Height (in)	229	202
Wheelbase (in)	84	78
Track Gauge (in)	56.5	56.5
Total Weight (lb)	225,500	205,500

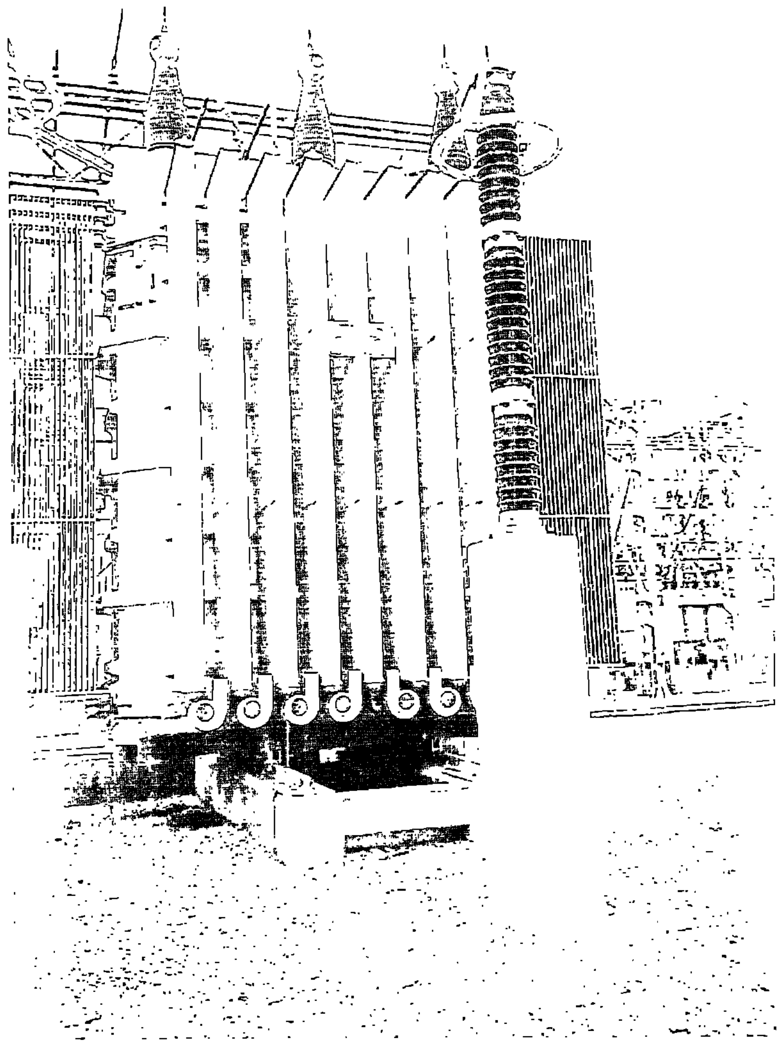

FIGURE 9-1 Type I Transformer

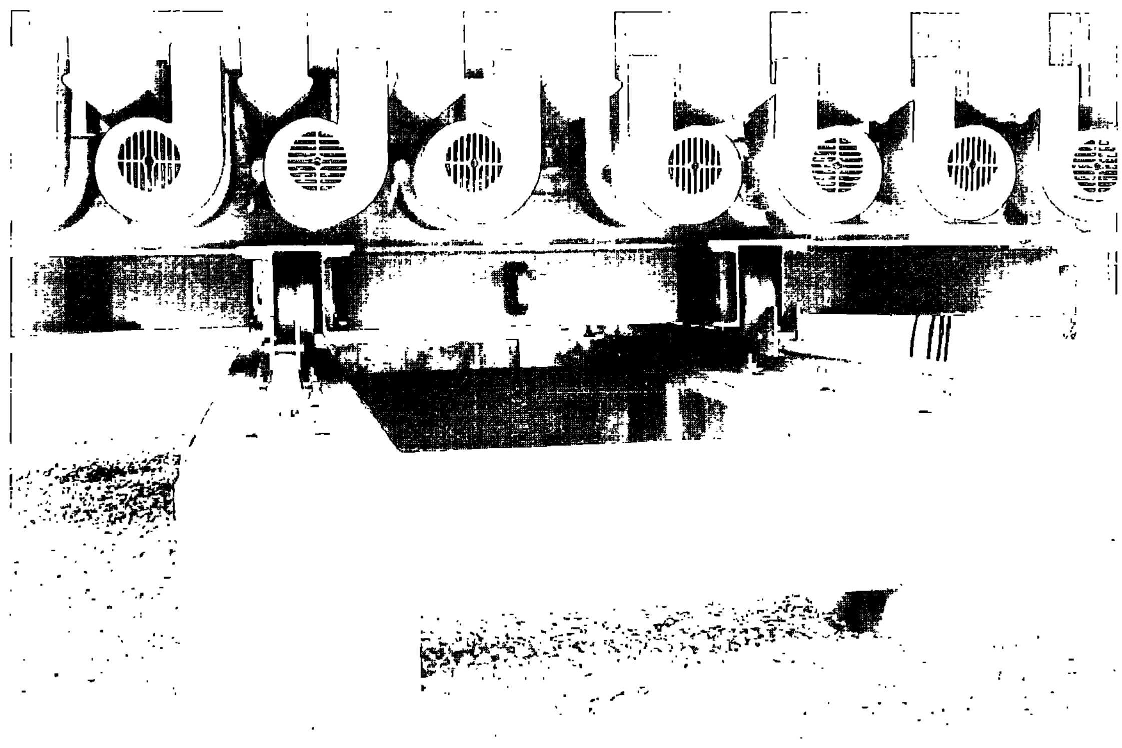

FIGURE 9-2 Wheel Stops of Type I Transformer

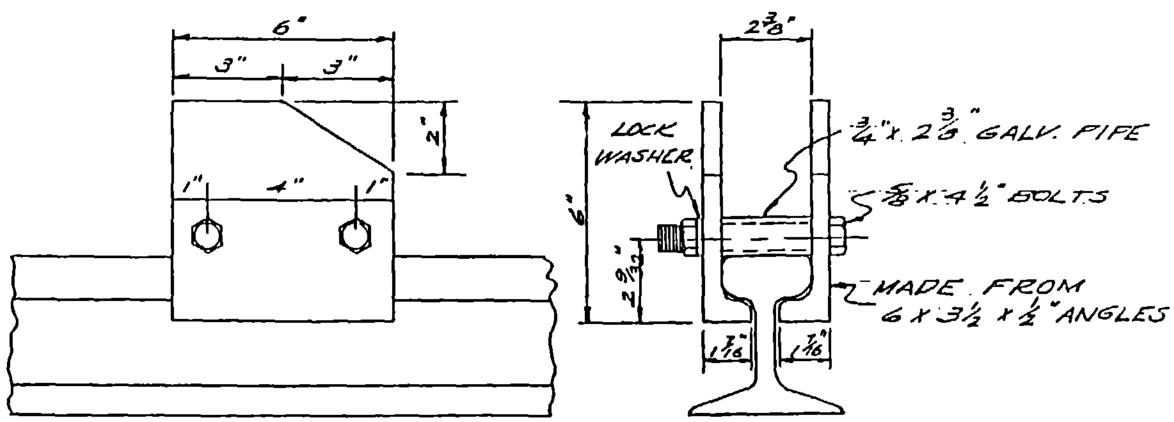

FIGURE 9-3 Detail of Wheel Stop Construction

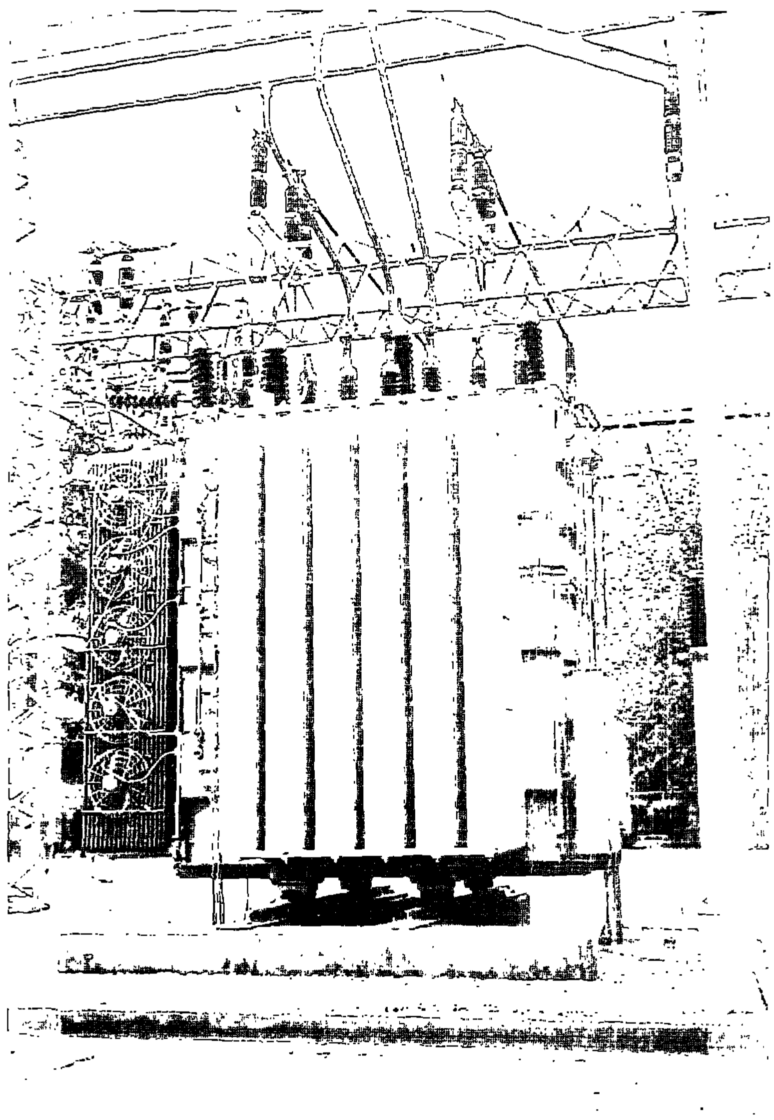

FIGURE 9-4 Type II Transformer

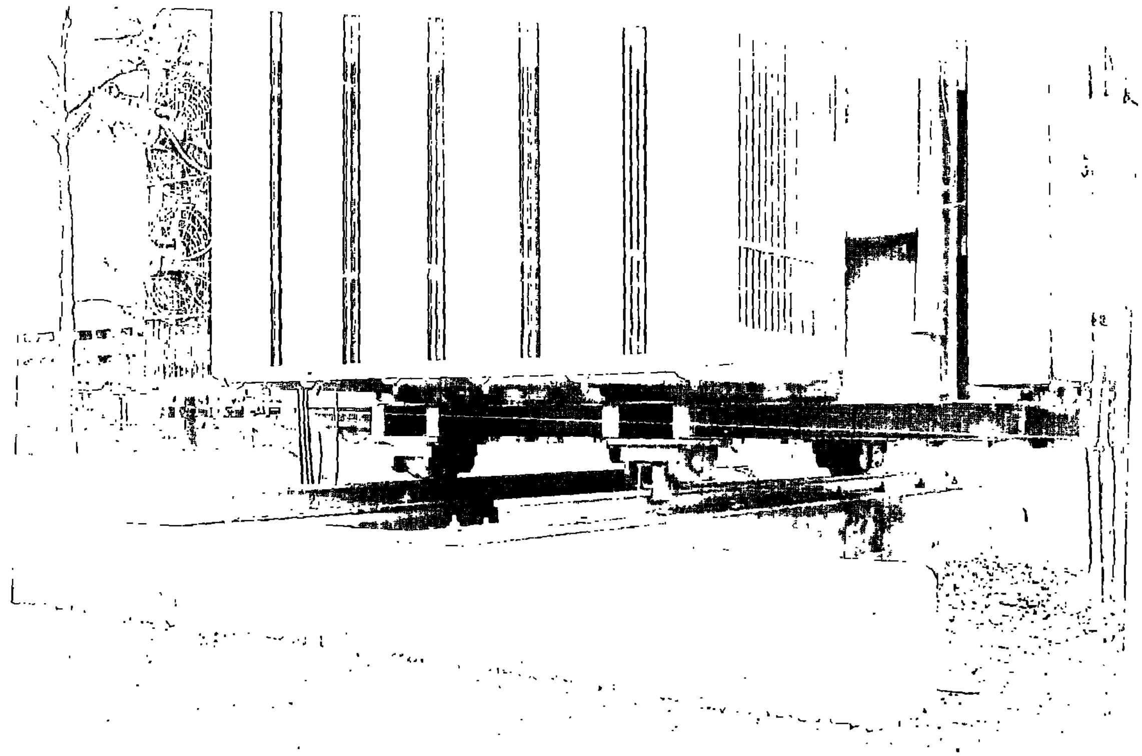

FIGURE 9-5 One Wheel Stop Used for Type II Transformer

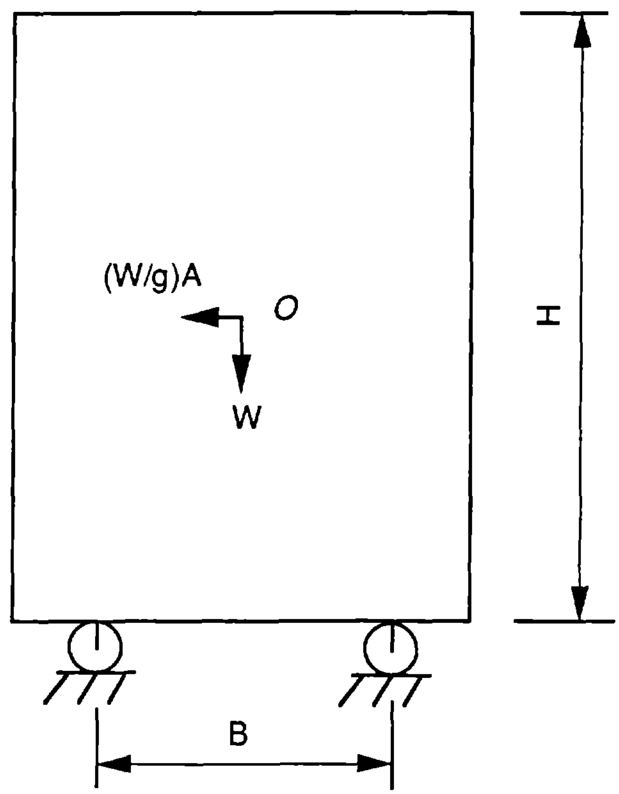

FIGURE 9-6 Model of Transformer for Overturning Analysis

will overturn when the moment induced by the horizontal ground shaking exceeds the moment resulting from the weight of the transformer,

$$\frac{H}{2}\frac{W}{g}\,A > \frac{B}{2}\,W \tag{9.1}$$

where A is horizontal PGA, B and H are the track gauge and height of the transformer, respectively, W is the weight of the transformer, and g is the gravity acceleration. From Equation (9.1), the critical acceleration A_C at which the transformer is overturned can be determined as follows:

$$A_C = \left(\frac{B}{H}\right) g \tag{9.2}$$

For Type II transformer, H is 202 inches and B is 56.5 inches (Table 9-I). Substituting the values of H and B into Equation (9.2), we obtain

$$A_C = \frac{56.5}{202}\,g = 0.28\,g \tag{9.3}$$

The overturning capacity of the transformer A_C is determined based on the dimensions of the transformer; thus, the overturning capacity is considered as a deterministic variable.

The ground motions recorded from past earthquakes show significant variation even under the similar conditions. Thus, the PGA value is considered as a lognormal variable with the COV of 0.5. For a given PGA level, the probability of overturning of a type II transformer can be computed from Equation (4.6). Table 9-II shows the fragility data corresponding to various PGA levels and the resulting fragility curve for the overturning of Type II transformer is displayed in Figure 9-9.

9.3.2 Sliding

The sliding failure of a transformer may be caused by the loosening of bolts clamping the wheel stop onto the rail. As shown in Figure 9-2, the transformer contacts only one of two plates of the wheel stop. During the horizontal ground shaking, the transformer will exert a horizontal force P pushing the plate. Since

TABLE 9-II Fragility Data of Type II Transformer

PGA (g)	Probability of Failure	
	Sliding	Overturning
0.025	0.319×10^{-2}	0.439×10^{-7}
0.050	0.930×10^{-1}	0.516×10^{-4}
0.075	0.374	0.124×10^{-2}
0.100	0.652	0.785×10^{-2}
0.125	0.823	0.260×10^{-1}
0.150	0.913	0.597×10^{-1}
0.175	0.957	0.109
0.200	0.978	0.171
0.225	0.989	0.242
0.250	0.994	0.317
0.300	0.998	0.464
0.350	0.999	0.593
0.400	1.000	0.698
0.500	1.000	0.839
0.600	1.000	0.916
0.700	1.000	0.956
0.800	1.000	0.976
0.900	1.000	0.987
1.000	1.000	0.993

Type II transformer has only one wheel stop installed at each side of the transformer, the wheel stop will receive the total pushing force from the transformer. The pushing force P from the horizontal peak ground acceleration A can be determined as follows:

$$P = \frac{W}{g} A \tag{9.4}$$

Given the horizontal pushing force P, there are several forces acting on the plate as shown in Figure 9-7. F_A and F_C are the vertical forces, which form a couple to balance the moment produced by force P. H_A and H_B are the horizontal forces acting on bolts A and B. F_S is the static horizontal friction force on one plate resulting from the clamping of the wheel stop onto the rail. As shown in Figure 9-8, the wheel stop has a steel pipe sleeved on the bolt to prevent two plates from moving towards each other. The tightening of the nut will produce an axial force F_b in the bolt. In general, F_b is approximately equal to the tensile yielding strength of the bolt (ASCE, 1991). For an A36 bolt with a diameter of $\frac{5}{8}$ inches, the area at thread stress area is 0.226 in^2 and the specified tensile yielding strength F_y is

$$F_y = 0.226 \times 36000 = 8136 \text{ lb} \tag{9.5}$$

The mean value of tensile yielding strength of the bolt is taken as $1.1F_y$ (Ellingwood, 1983). Thus, the mean value of F_b can be determined as

$$F_b = 1.1 \times 8136 = 8949.6 \text{ lb} \tag{9.6}$$

The axial force of the bolt will be transmitted into a normal force F_2 acting on the contacting area between the plate and the side surface of the rail (Figure 9-8). Since the thickness of the pipe is only $\frac{1}{16}$ inch and its stiffness is much less than that of the rail, the pressure from the plate will reduce the length of the pipe. When the nut is tightened, there will be two contacting points (A and B in Figure 9-8) to resist the axial force F_b. The normal force F_2 can be determined as

$$F_2 = \frac{L_a}{L_a + L_b} F_b \tag{9.7}$$

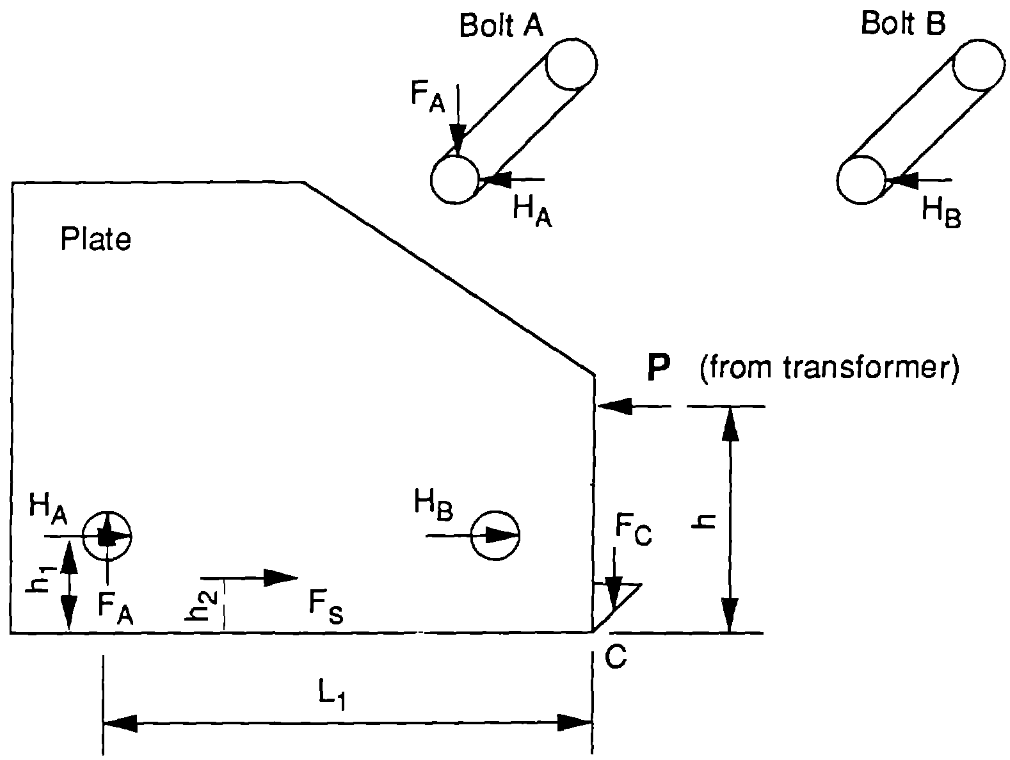

FIGURE 9-7 Forces on Wheel Stop Caused by Pushing from Transformer

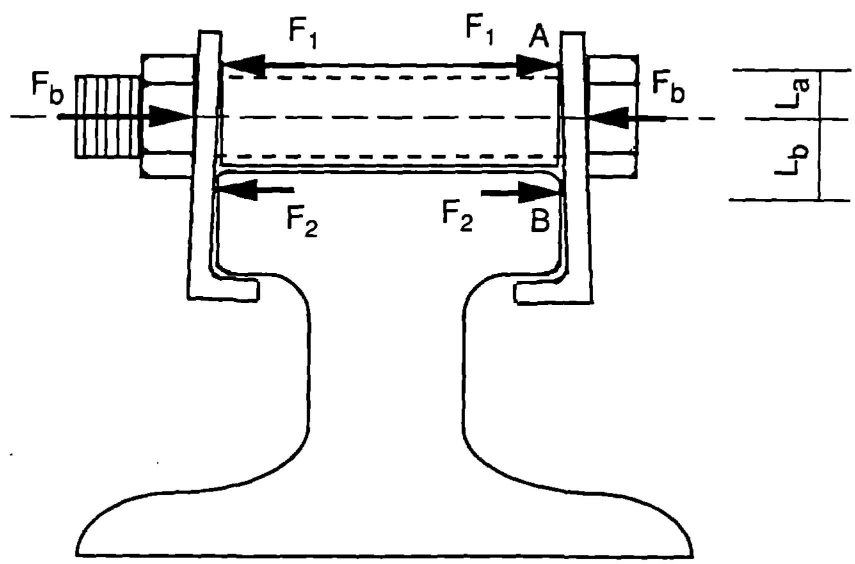

FIGURE 9-8 Forces on Wheel Stop Caused by Tightening Bolt

L_a and L_b are 0.375 and 0.6 inches, respectively. Substituting the values of L_a, L_b, and F_b into Equation (9.7), we have

$$F_2 = \frac{0.375}{0.375 + 0.6} \times 8949.6 = 3442.2 \text{ lb} \tag{9.8}$$

The static friction force F_S acting on each plate from two bolts can be expressed as follows:

$$F_S = 2\,F_2\,f \tag{9.9}$$

where f is the coefficient of friction between clean and dry metals, which ranges from 0.5 to 1.5 (Moore, 1975). In this study, f is taken as an average value, 1.0. The static friction force on each plate is then determined as

$$F_S = 2 \times 3442.2 \times 1.0 = 6884.4 \text{ lb} \tag{9.10}$$

The horizontal forces on the bolts H_A and H_B occur only after the pushing force P exceeds the static friction force Fs, i.e.,

$$\frac{W}{g} A > F_S \qquad \text{or} \qquad \frac{A}{g} > \frac{F_S}{W} = 0.03 \tag{9.11}$$

From the equilibrium of the horizontal forces in Figure 9-7, H_A and H_B (with the assumption of H_A equal to H_B) can be expressed as

$$H_A = H_B = \frac{P - F_S}{2} \tag{9.12}$$

From the equilibrium of the moment about the contacting point C in Figure 9-7, we obtain

$$P \times h - F_A \times L_1 - (H_A + H_B) \times h_1 - F_S \times h_2 = 0 \tag{9.13}$$

Substituting Equation (9.12) into (9.13), the vertical shear force acting on bolt A can be expressed as

$$F_A = \frac{P(h - h_1) + F_S(h_1 - h_2)}{L_1} \tag{9.14}$$

Bolt A is subject to both vertical and horizontal shear forces F_A and H_A, while bolt B is only subject to the horizontal shear force H_B. Thus, bolt A is the most critical part of the wheel stop and the shear strength of bolt A will control the capacity of the transformer from sliding. The total shear force V acting on bolt A can be obtained as

$$V = \sqrt{H_A^2 + F_A^2} = \sqrt{\left(\frac{P - F_S}{2}\right)^2 + \left[\frac{P(h - h_1) + F_S(h_1 - h_2)}{L_1}\right]^2} \tag{9.15}$$

From measuring the dimensions of the wheel stop, h is 3 inches, h_1 is 1.5 inches, h_2 is 0.9 inches, and L_1 is 5 inches. Substituting the values of h, h_1, h_2, L_1, F_S, and W into Equation (9.15), we can determine the total shear force in bolt A for a given level of PGA as follows:

$$V = \sqrt{96267A^2 - 1567914\,A + 12531228} \qquad (A > 0.03g) \tag{9.16}$$

in which A is in the unit of in/sec^2. The shear force in the bolt is considered as a lognormal variable with the mean taken from Equation (9.16) and the COV of 0.5.

In this study, the capacity of the bolt is taken as its shear yielding strength because a permanent stretch of the bolt will occur and the wheel stop will loosen if the yielding strength of the bolt is exceeded. The shear yielding stress is usually taken as 60% of the value for tension in practice (Segui, 1994). For an A36 bolt with a diameter of $\frac{5}{8}$ inches, the specified shear yielding strength through body is 6626.8 pounds. The mean value of the shear yielding strength is then determined as

$$V_y = 1.1 \times 6626.8 = 7289.5 \text{ lb} \tag{9.17}$$

The capacity of the bolt is also considered as a lognormal variable with the mean value taken from Equation (9.17) and the COV of 0.11 (Ellingwood, 1983). Using Equations (4.6), the probabilities of a sliding failure of Type II transformer corresponding to various PGA levels are determined (Table 9-II), and the resulting fragility curve is shown in Figure 9-9. From the comparison of fragility curves for overturning and sliding, the Type II transformer will most probably fail in sliding.

9.4 Fragility Analysis of Type I Transformer

Since Type I transformer is similar to Type II transformer in construction, the failure mechanism is similar. The major difference between these two types of transformers is that there are two wheel stops at each side of the Type I transformer. The procedure and the formula for determining shear force in bolt A for the Type II transformer can be used directly for the Type I transformer with the pushing force P expressed below.

$$P = \frac{1}{2}\,\frac{W}{g}\,A \tag{9.18}$$

The failure of bolt A in shear controls the sliding failure of Type I transformer. The total shear force in bolt A can be determined from Equation (9.15) as follows:

$$V = \sqrt{28979\,A^2 - 860229\,A + 12531228} \qquad (A > 0.06g) \tag{9.19}$$

The probabilities of the Type I transformer failure in sliding corresponding to various PGA levels are determined and summarized in Table 9-III. The resulting fragility curve is shown in Figure 9-10.

The critical value of PGA at which the Type I transformer fails in overturning can be determined by substituting H of 229 inches and B of 56.5 inches (Table 9-I) into Equation (9.2),

$$A_c = \frac{56.5}{229}\,g = 0.25\,g \tag{9.20}$$

The resulting fragility data and fragility curve of failure in overturning are shown in Table 9-III and Figure 9-10, respectively. Similar to the Type II transformer, the Type I transformer will fail probably in sliding rather than in overturning.

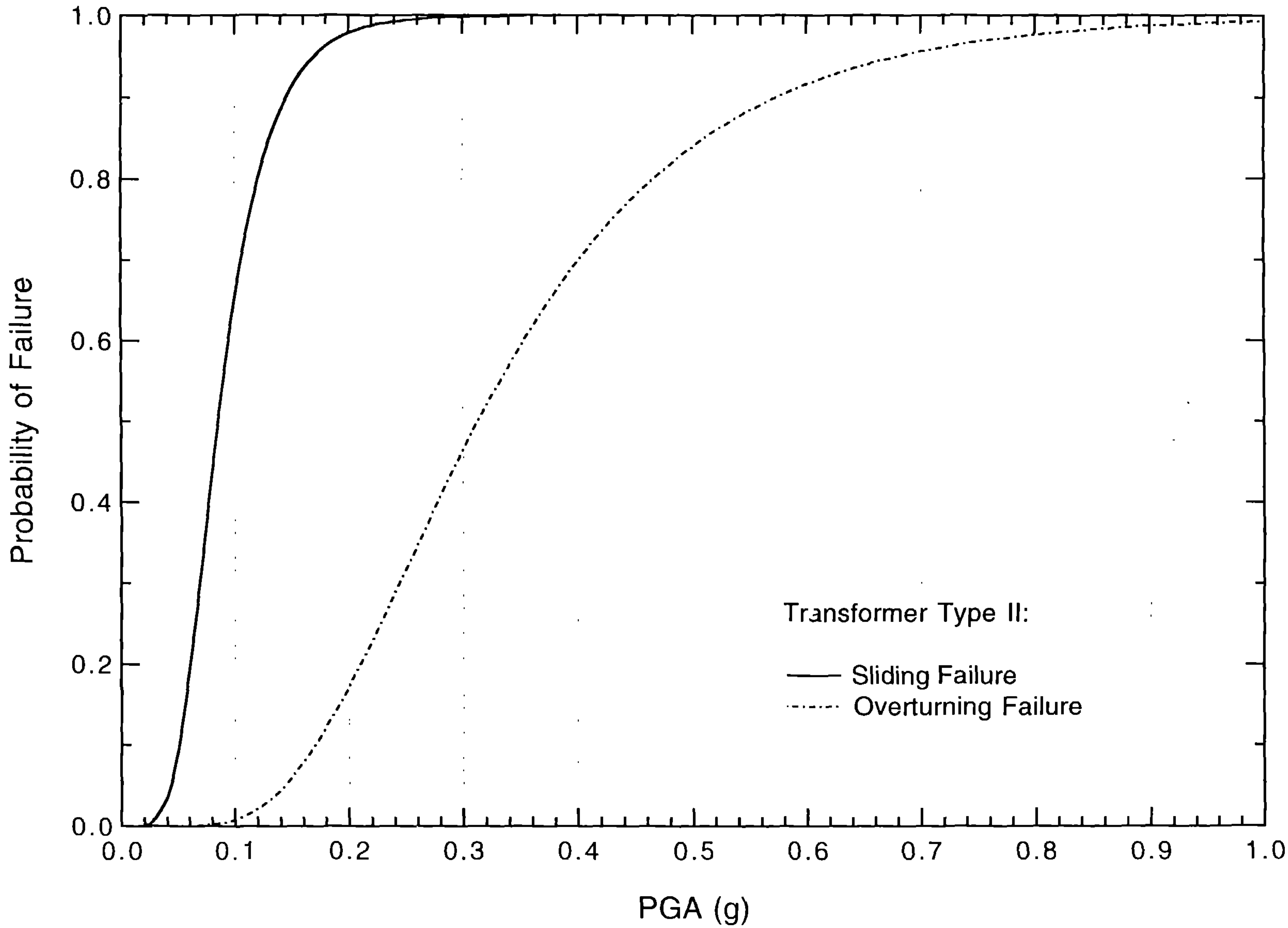

FIGURE 9-9 Fragility Curves of Type II Transformer

TABLE 9-III Fragility Data of Type I Transformer

PGA (g)	Probability of Failure	
	Sliding	Overturning
0.025	0.367×10^{-4}	0.161×10^{-6}
0.050	0.561×10^{-2}	0.135×10^{-3}
0.075	0.394×10^{-1}	0.268×10^{-2}
0.100	0.136	0.148×10^{-1}
0.125	0.292	0.442×10^{-1}
0.150	0.464	0.938×10^{-1}
0.175	0.614	0.161
0.200	0.731	0.239
0.225	0.816	0.323
0.250	0.875	0.407
0.300	0.942	0.560
0.350	0.973	0.683
0.400	0.987	0.776
0.500	0.997	0.891
0.600	0.999	0.947
0.700	1.000	0.974
0.800	1.000	0.987
0.900	1.000	0.993
1.000	1.000	0.997

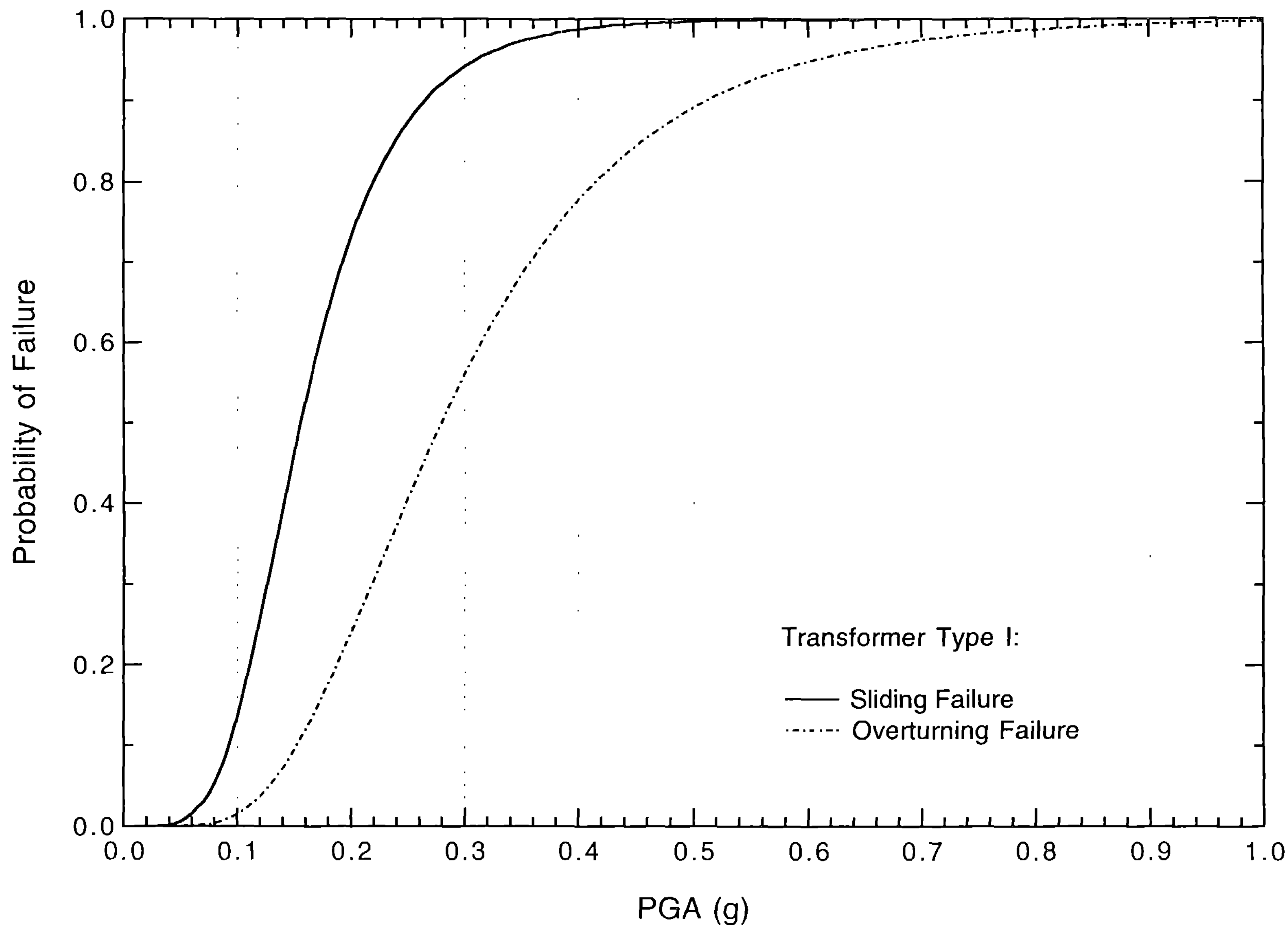

FIGURE 9-10 Fragility Curves of Type I Transformer

SECTION 10
12 KV REGULATORS

10.1 Description of 12 kV Regulator

In Substation 21, three 12 kV regulators are in operation and another four are stored for spare use. The basic information of the regulators is summarized in Table 10-I. The regulator with four wheels is supported on two rails as shown in Figure 10-1. The regulator is restrained from moving in the horizontal direction by a wheel stop installed at each side of the regulator. The wheel stop is composed of two $L6\times3\frac{1}{2}\times\frac{1}{2}$ angles clamping on the rail by two $\frac{5}{8}$ bolts. The wheel stop is the same as that used for the 115/12 kV transformers as shown in Figure 9-3.

10.2 Fragility Analysis of 12 kV Regulator

If the regulator is moving during earthquakes, the bushing, oil pipe, control cable, and lightening arresters may be damaged. The possible failure modes of the regulator are overturning and sliding. The physical appearance of the 12 kV regulator is similar to that of the 115/12 kV transformers, except the weight of the regulator is less and the ratio of track gauge to height is large. Thus, the fragility analysis of the regulator can follow the approach similar to those used for the 115/12 kV transformer.

The critical value of PGA at which the regulator fails in overturning can be determined by substituting H of 115 inches and B of 56.5 inches (Table 10-I) into Equation (9.2),

$$A_C = \frac{B}{H}\, g = \frac{56.5}{115}\, g = 0.49\, g \tag{10.1}$$

The overturning capacity of the regulators A_C is taken as a deterministic variable, while the PGA value is considered as a lognormal variable with the COV taken as 0.5. The probability of the regulators failure in overturning can be computed from Equation (4.6). Table 10-II shows the fragility data corresponding to various PGA levels and the resulting fragility curve in overturning is shown in Figure 10-2.

TABLE 10-I Basic Information of 12 kV Regulator

Manufacturer	General Electric
Type	MLT-32
Installed Date	1950s
Quantity	7
Phases	3
Max. Volume (kVA)	750
Height (in)	115
Track Gauge (in)	$56\frac{1}{2}$
Total Weight (lb)	26,200

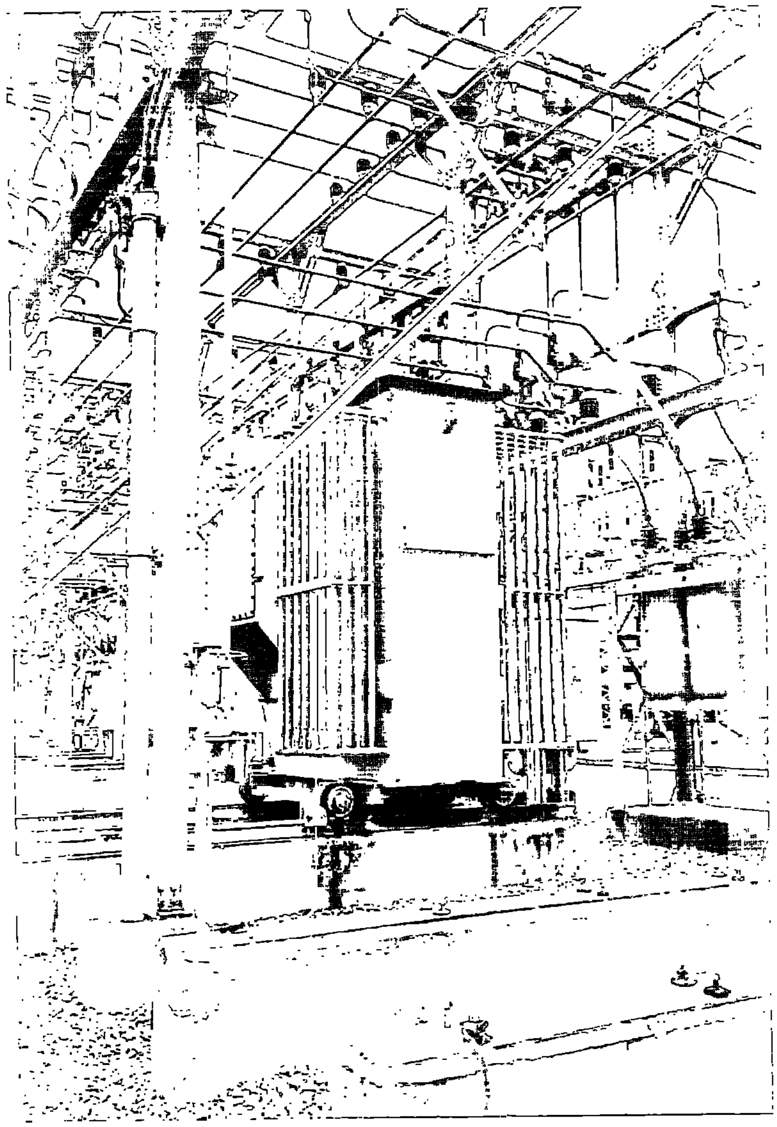

FIGURE 10-1 12 kV Regulator

TABLE 10-II Fragility Data of 12 kV Regulator

PGA (g)	Probability of Failure	
	Sliding	Overturning
0.05	0.147×10^{-7}	0.201×10^{-6}
0.10	0.193×10^{-4}	0.159×10^{-3}
0.15	0.519×10^{-3}	0.305×10^{-2}
0.20	0.361×10^{-2}	0.165×10^{-1}
0.25	0.130×10^{-1}	0.484×10^{-1}
0.30	0.286×10^{-1}	0.101
0.35	0.565×10^{-1}	0.171
0.40	0.101	0.253
0.45	0.160	0.339
0.50	0.232	0.423
0.55	0.311	0.503
0.60	0.392	0.576
0.65	0.470	0.641
0.70	0.543	0.698
0.75	0.609	0.747
0.80	0.669	0.789
0.85	0.720	0.824
0.90	0.765	0.853
0.95	0.803	0.878
1.00	0.835	0.899

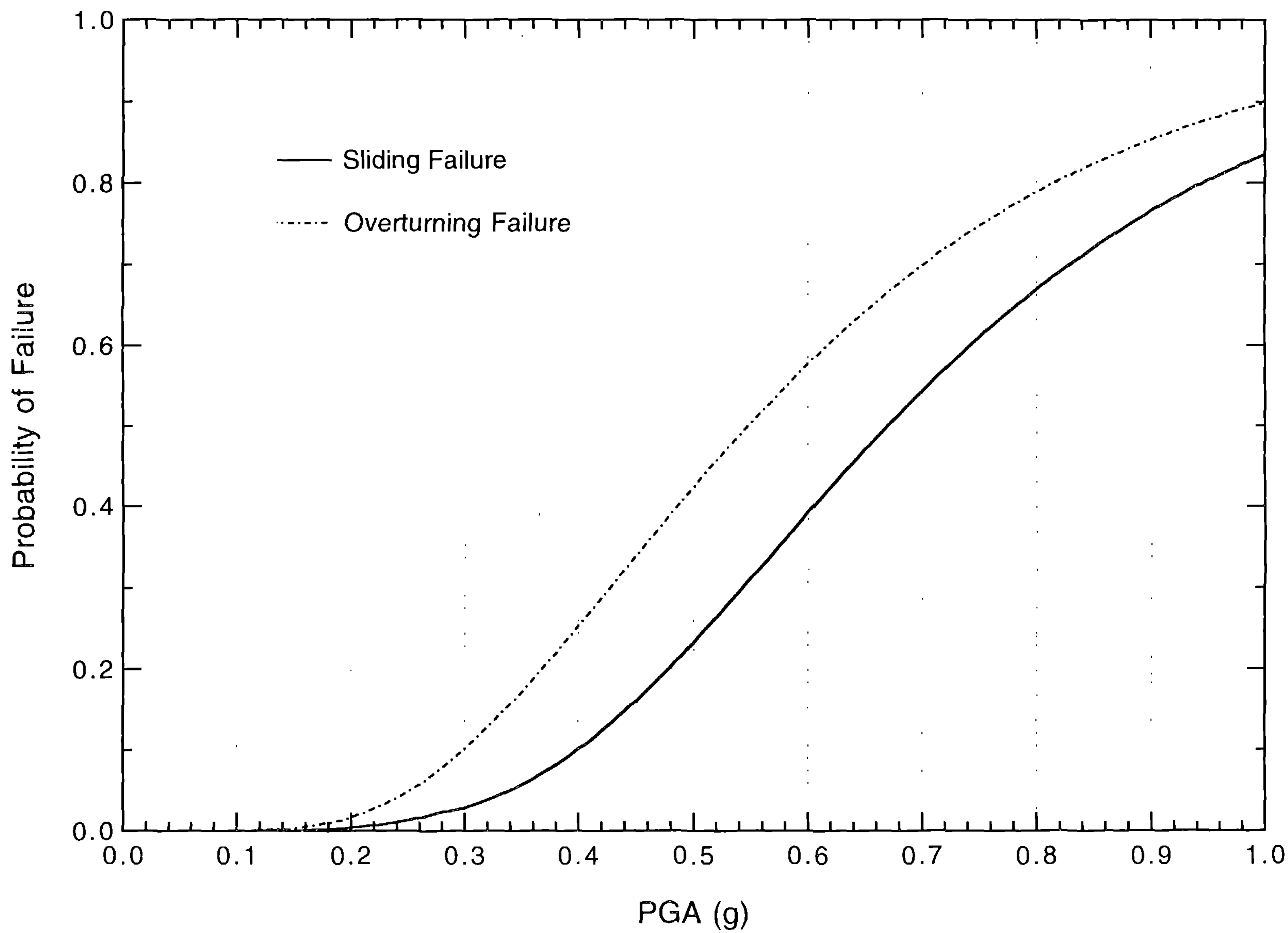

FIGURE 10-2 Fragility Curves of 12 kV Regulator

The failure of bolts in the wheel stop controls the sliding failure of the regulator. The total shear force of bolt A can be determined by substituting the weight W into Equation (9.15) as follows:

$$V = \sqrt{1565\ A^2 - 199894\ A + 12531228} \qquad (A > 0.26g) \qquad (10.2)$$

The shear force of the bolt is considered as a lognormal variable with the mean value taken from Equation (10.2) and the COV of 0.5. The shear yielding capacity of the bolt is also considered as a lognormal variable with the mean value of 7289.5 pounds and the COV of 0.11 as described in Section 9. The probabilities of failure in sliding corresponding to various PGA levels are computed from Equation (4.6) and summarized in Table 10-II, and the resulting fragility curve of sliding is shown in Figure 10-2. From the comparison of fragility curves of two failure modes, the 12 kV regulators will probably fail in overturning rather than in sliding.

SECTION 11
115 KV OIL CIRCUIT BREAKERS

11.1 Description of 115 kV OCBs

There are two 115 kV oil circuit breakers (OCB) used in Substation 21. One is a FK type OCB manufactured by General Electric, while the other is a GM-5 type OCB manufactured by Westinghouse. The information about these two OCBs is listed in Table 11-I.

Figure 11-1 shows a photograph of the FK type OCB located on the east side of the 115 kV switch structure. Figure 11-2 shows the plan and elevations. The OCB consists of three steel tanks containing switch devices and oil. There are two porcelain bushings on each tank (Figure 11-1). The cables connected to the bushings are flexible so that the tensile force in the cables is negligible in the event of an earthquake. The tank having four legs at the bottom is welded to two 8-inch "I" beams which are braced at three locations (Figure 11-2). The steel beam is anchored to a foundation with three 1×16 headed anchor bolts (Figure 11-3).

Figure 11-4 shows a photograph of the GM-5 type OCB, which is located at the west side of the 115 kV switch structure. The plan and elevation of the breaker are shown in Figures 11-5 and 11-6, respectively. This type of OCB also consists of three steel tanks. The bottom of the tank is mounted to two 10-inch "I" beams by four $\frac{1}{2}$ bolts. The steel beam is clamped at the bottom flange with 3 steel plates, and these steel plates are then anchored to a foundation by three $1\frac{1}{4}\times 18$ anchor bolts (Figure 11-7).

11.2 Fragility Analysis of FK Type 115 kV OCB

The failure of anchor bolts will cause overturning or excessive movement of tanks. In this study, the failure of anchor bolts is considered as the most probable failure mode of the FK type 115 kV OCB. The tensile yielding strength of the bolt controls the capacity of the anchor bolt because permanent stretch can occur in the anchor bolt when the anchor bolt yields.

TABLE 11-I Basic Information of 115 kV OCBs

Breaker Type	FK	GM-5
Manufacturer	General Electric	Westinghouse
Installed Date	1960s	1950s
Current (A)	1,200	1,200
Interrupting Rating (MVA)	5,000	3,500
Bushing Catalogue No.	DL-11B571	-
Diameter of Each Tank (in)	48	54
Height of Tank (in)	90	103
Total Weight (lb)	27,125	-

FIGURE 11-1 FK Type 115 kV OCB

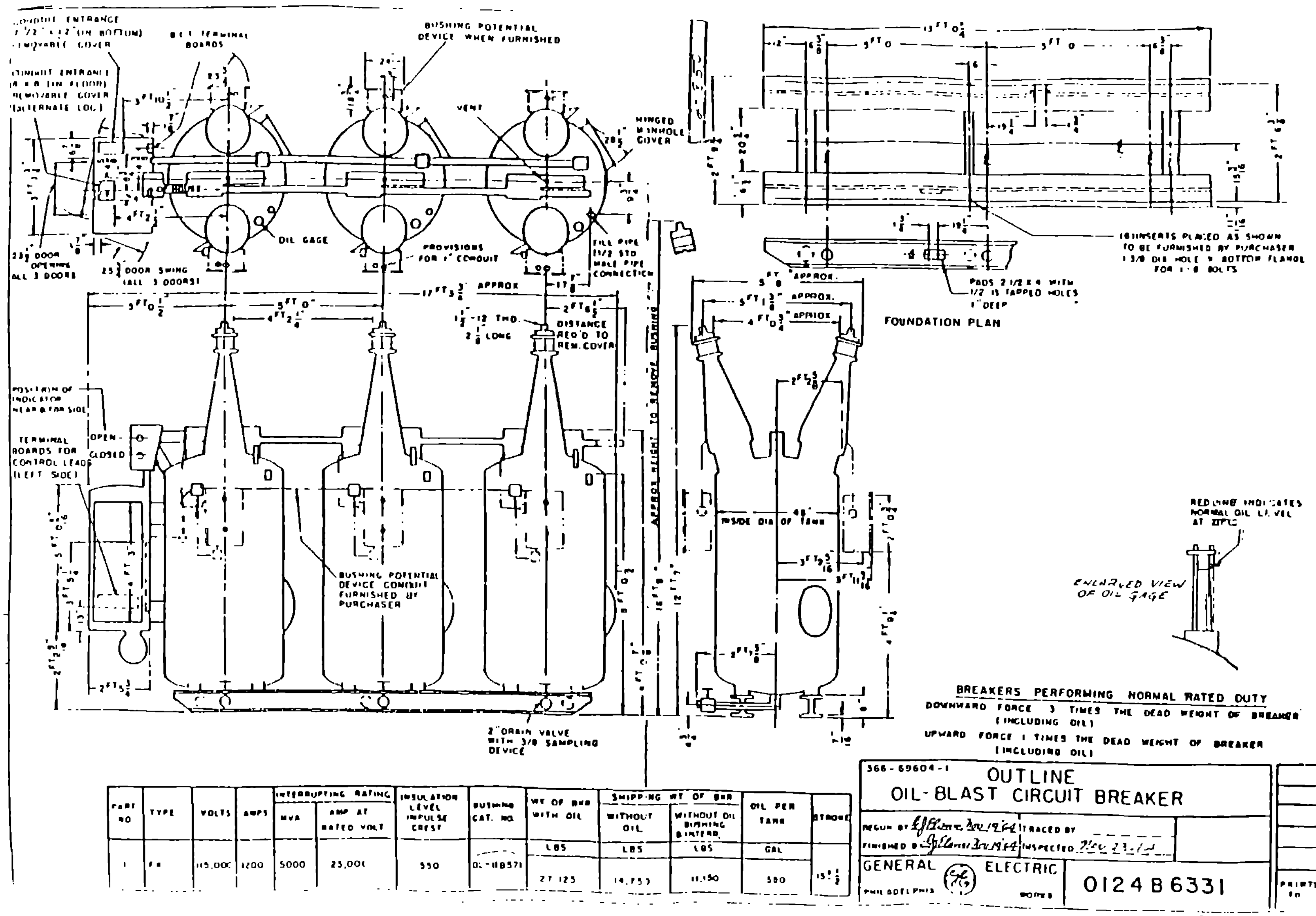

FIGURE 11-2 Plan and Elevations of FK Type 115 kV OCB

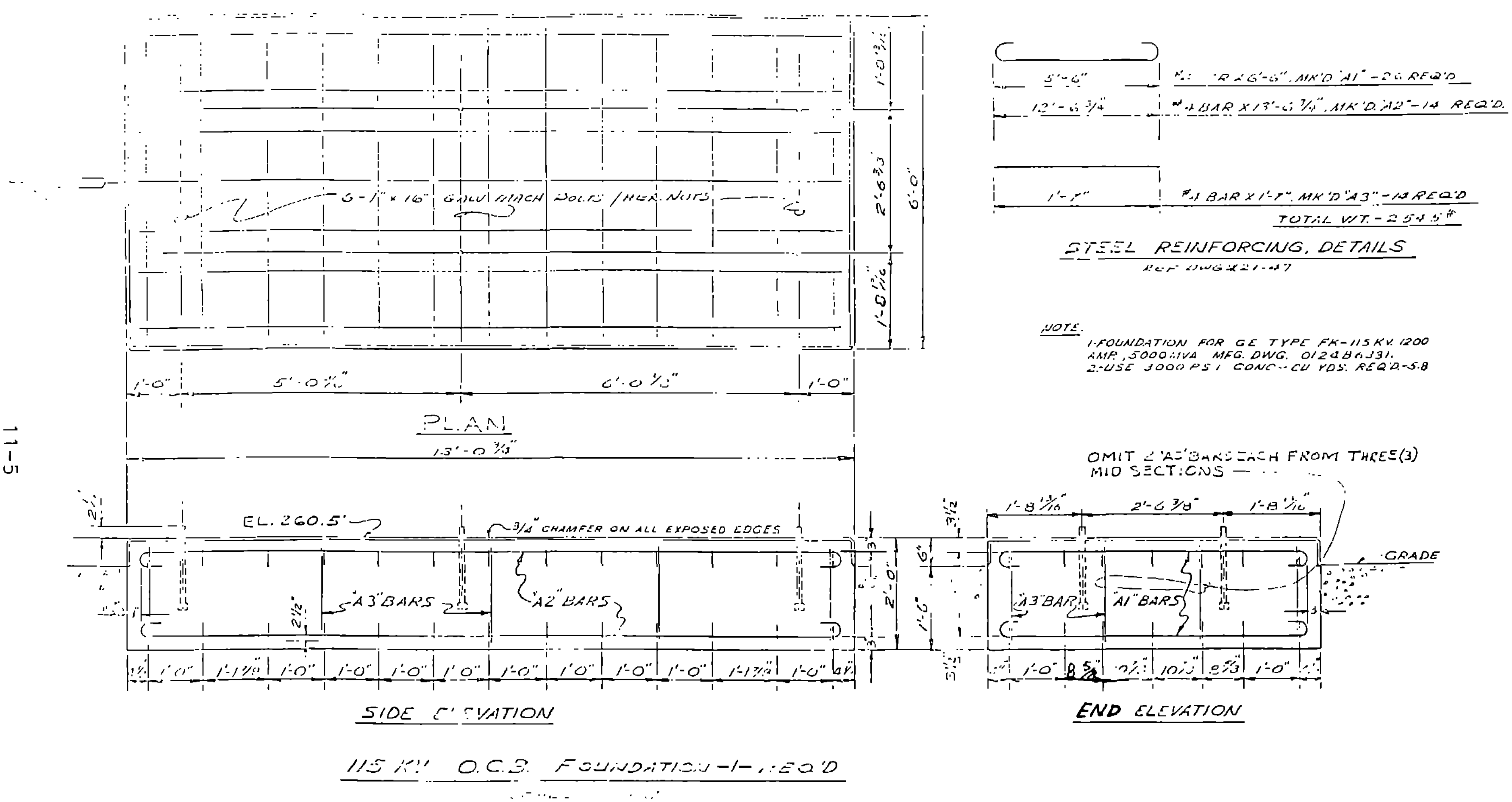

FIGURE 11-3 Detail of Foundation for FK Type 115 kV OCB

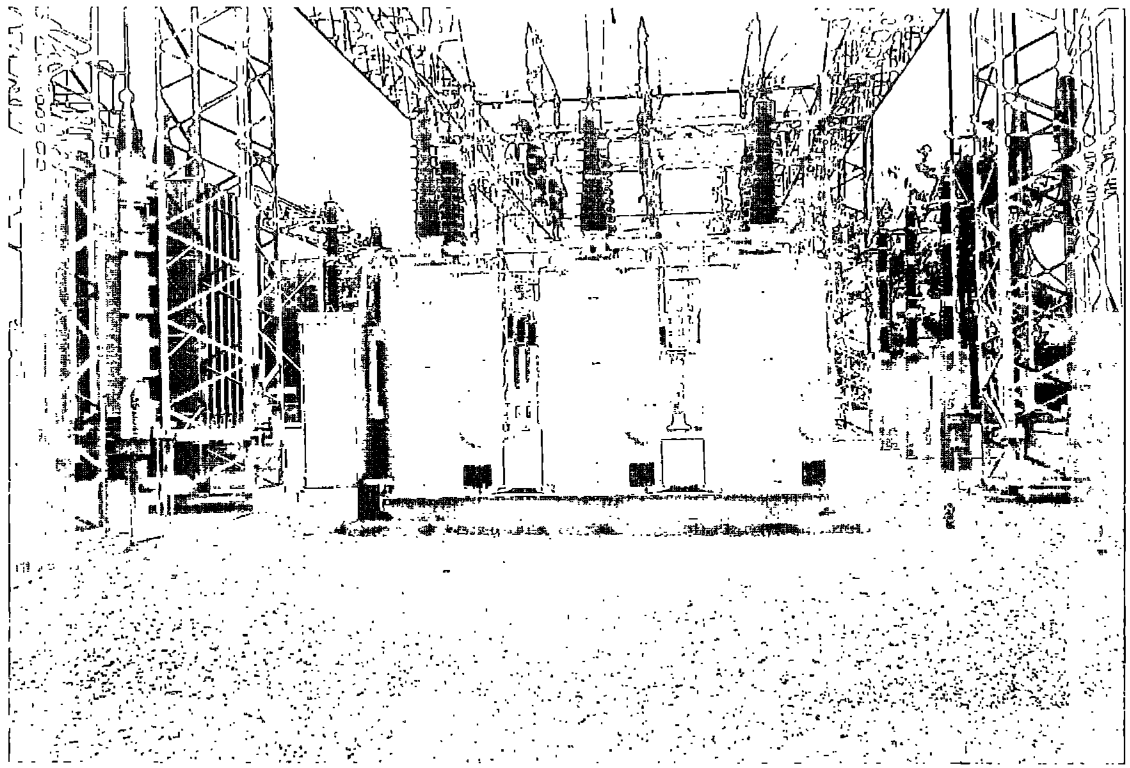

FIGURE 11-4 GM-5 Type 115 kV OCB

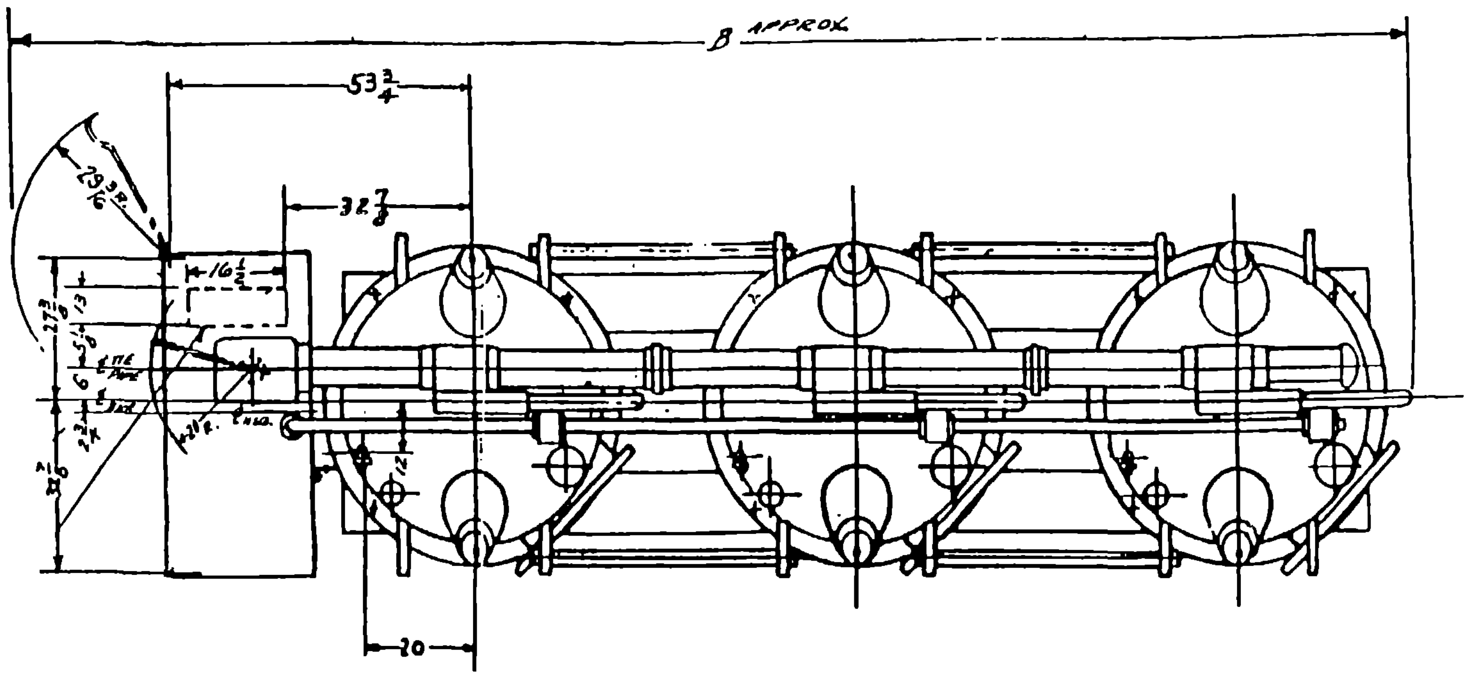

FIGURE 11-5 Plan of GM-5 Type 115 kV OCB

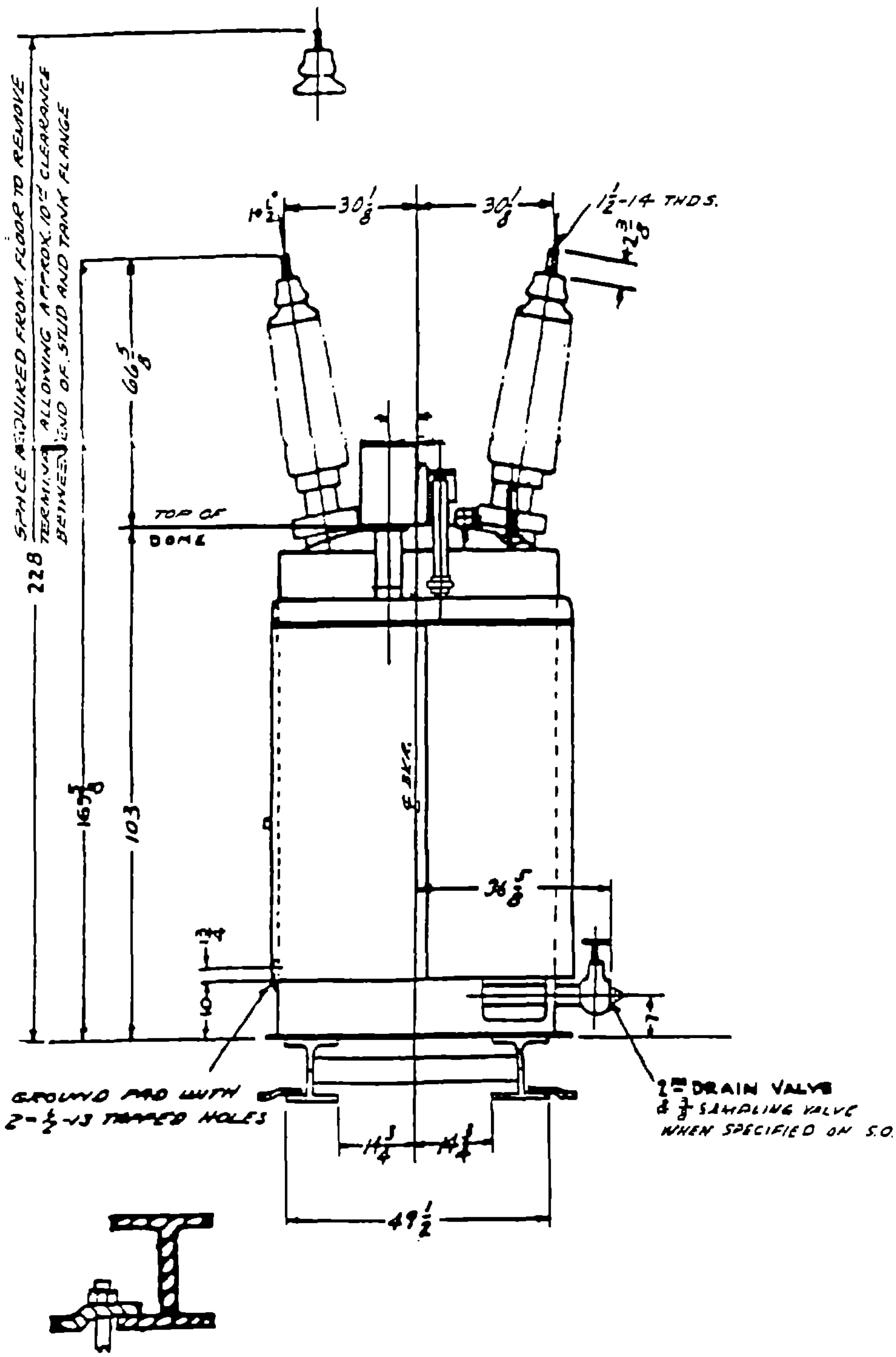

FIGURE 11-6 Elevation of GM-5 Type 115 kV OCB

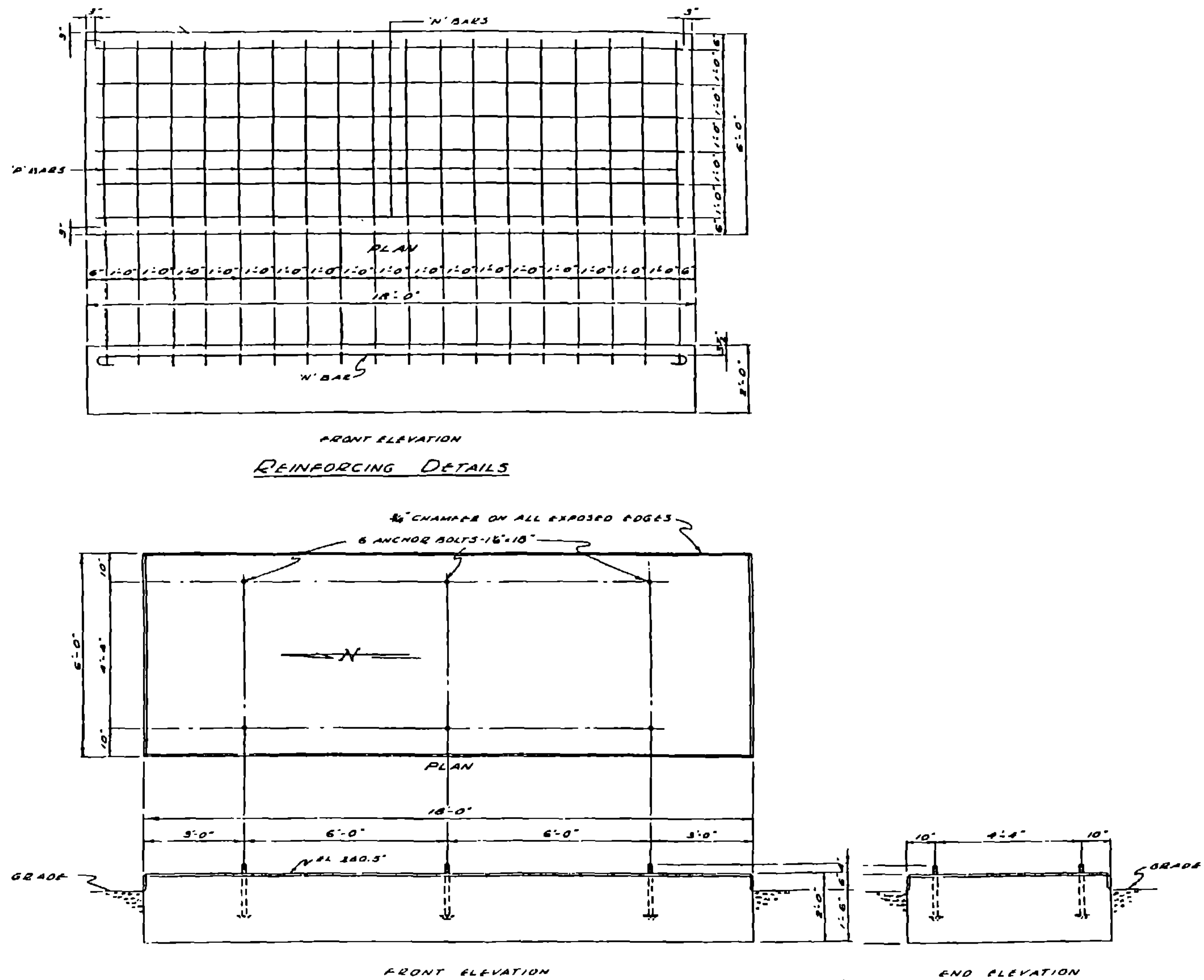

FIGURE 11-7 Detail of Foundation for GM-5 Type 115 kV OCB

As shown in Figure 11-3, the minimum anchor bolt spacing is $30\frac{3}{8}$ inches, embedment is $13\frac{3}{4}$ inches, and minimum edge distance is 12 inches. On the basis of these dimensions, the headed anchor bolts are classified as standard isolated anchor bolt, and the failure mechanism of the standard anchor bolt is controlled by the yielding of the anchor bolt steel, rather than by the brittle tensile failure of concrete (Shipp and Haninger, 1983). In the response analysis of OCB, the tanks are modeled as a rigid block (Figure 11-8). As shown in Figure 11-8a, force F_1 and F_2 are the axial forces and V_1 is the shear force of the bolts caused by the ground shaking in the transverse direction. Force F_2, caused by an earthquake (excluding the dead load), can be determined from the equilibrium of the moment about point A (Figure 11-8a)

$$F_2 \, B = \frac{W}{g} \, A \, h \qquad \text{or} \qquad F_2 = \frac{h}{B} \, \frac{W}{g} \, A \tag{11.1}$$

where B is the distance between the anchor bolts, h is the height of mass center of the OCB, W is the total weight of the OCB, and A is the horizontal PGA of the ground shaking. The value of B is 30.5 inches, h is 58 inches, and W is 27125 pounds. Three anchor bolts are used to hold each "I" beam at the base, the tensile force T_1 of one anchor bolt is

$$T_1 = \frac{F_2}{3} = \frac{h}{3B} \, \frac{W}{g} \, A \tag{11.2}$$

The shear force V_1 of one anchor bolt caused by the ground shaking in the transverse direction is

$$V_1 = \frac{1}{6} \, \frac{W}{g} \, A \tag{11.3}$$

The forces acting on the OCB caused by the ground shaking in the longitudinal direction are shown in Figure 11-8b. From the equilibrium of the moment about point C in Figure 11-8b, we have

$$F_4 \, L_1 + F_5 \, (L_1 + L_2) = \frac{W}{g} \, A \, h \tag{11.4}$$

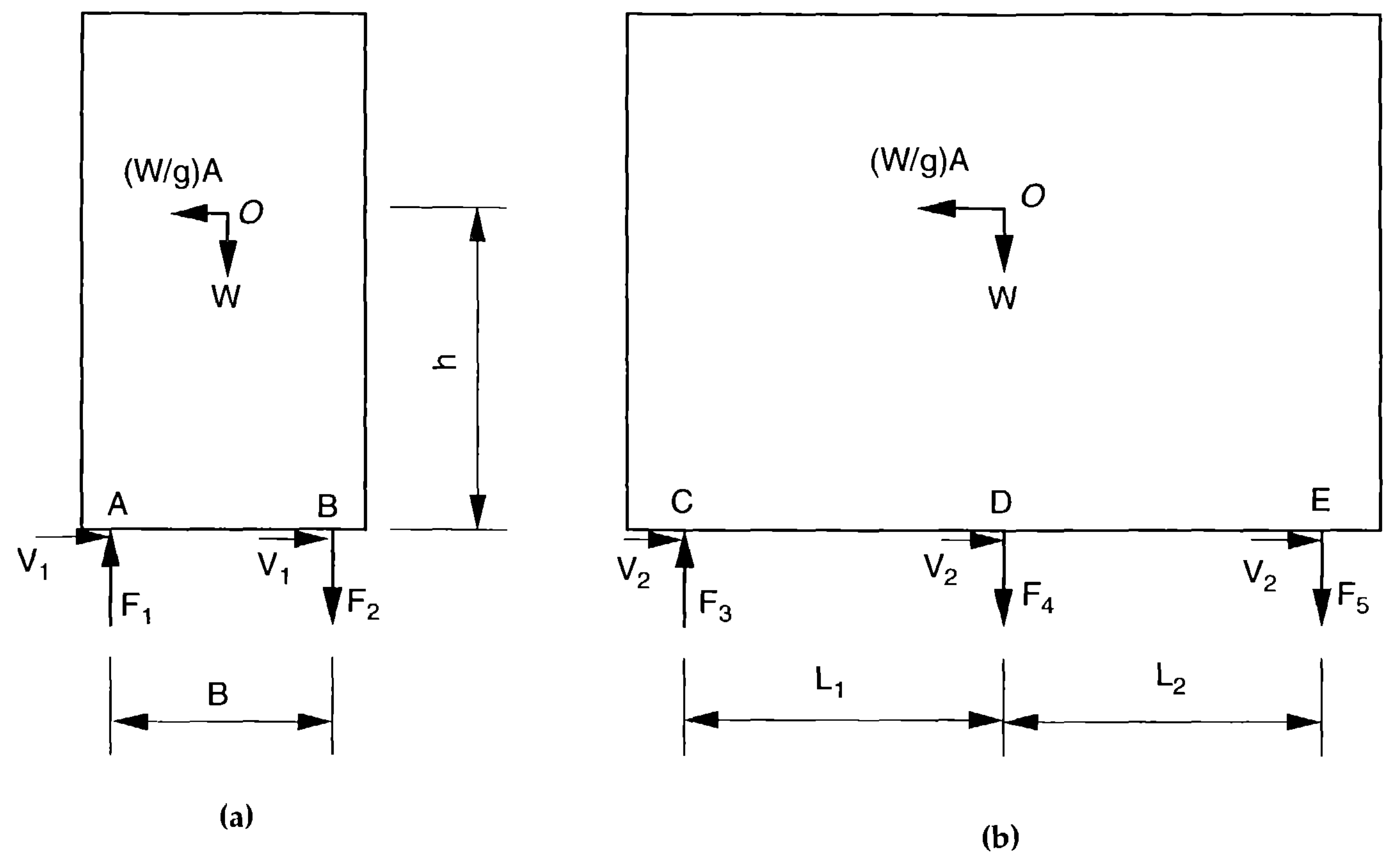

FIGURE 11-8 Model of FK Type 115 kV OCB

where L_1 and L_2 are the distances between the anchor bolts in the longitudinal direction, which are $60\frac{3}{8}$ and $72\frac{3}{8}$ inches, respectively. Assuming the stiffness of two "I" beams supporting the tanks of the OCB is great and the deformation of "I" beams is a straight line, F_4 and F_5 have the following relationship:

$$\frac{F_4}{F_5} = \frac{L_1}{L_1 + L_2} \tag{11.5}$$

Substituting Equation (11.5) into (11.4), the axial force T_2 in the anchor bolt at the corner of the foundation caused by the ground shaking in the longitudinal direction can be determined as follows:

$$T_2 = \frac{F_5}{2} = \frac{1}{2} \frac{h(L_1 + L_2)}{L_1^2 + (L_1 + L_2)^2} \frac{W}{g} A \tag{11.6}$$

The shear force V_2 of one bolt caused by the ground shaking in the longitudinal direction is,

$$V_2 = \frac{1}{6} \frac{W}{g} A \tag{11.7}$$

The tensile force T and shear force V of the most critical anchor bolt caused by the ground shaking in two horizontal directions can be obtained using the SRSS method.

$$T = \sqrt{T_1 + T_2} \tag{11.8}$$

$$V = \sqrt{V_1 + V_2} \tag{11.9}$$

The shear force on the anchor bolt will be transferred into effective tension by the shear friction between concrete and steel flange. The total effective tension force F of the anchor bolt from the combination of axial tension force and shear force can be determined as follows (Shipp and Haninger, 1983):

$$F = T + C \cdot V \tag{11.10}$$

where C is the shear coefficient which equals to the inverse of the shear friction. According to ACI 318 (1992), when as-rolled structural steel is anchored to concrete by headed studs or reinforced bars, the value of C is $\frac{1}{0.7}$ or 1.43.

The effect of dead load on the axial force of each anchor bolt is

$$F_D = -\frac{W}{6} \qquad (11.11)$$

The total tensile force of the most critical anchor bolt including the effect of dead load is then determined as

$$F_T = \sqrt{(\frac{h}{3B})^2 + [\frac{1}{2}\frac{h(L_1 + L_2)}{L_1^2 + (L_1 + L_2)^2}]^2}\ \frac{W}{g} A + \frac{C}{3\sqrt{2}}\frac{W}{g} A - \frac{W}{6} \qquad (11.12)$$

Substituting the values of h, B, L_1, L_2, C, and W into Equation (11.12), we have

$$F_T = 70.0\ A - 4520.8 \qquad (11.13)$$

where A is in the unit of in/sec^2. The total tensile force of the anchor bolt is considered as a lognormal variable with the mean value taken from Equation (11.13) and the COV of 0.5. For an A36 anchor bolt with a diameter of 1 inch and the thread stress area of 0.606 in^2, the specified tensile yielding strength is 21816 pounds. The mean value of the tensile yielding strength is then determined as (Ellingwood, 1983)

$$F_y = 1.1 \times 21816 = 23997.6 \text{ lb} \qquad (11.14)$$

The capacity of the anchor bolt is considered as a lognormal variable with the mean value computed in Equation (11.14) and the COV of 0.11. The failure probabilities of the FK type 115 kV OCB at various PGA levels are determined with Equation (4.6) and summarized in Table 11-II. The resulting fragility curve is displayed in Figure 11-9.

TABLE 11-II Fragility Data of 115 kV OCB

PGA (g)	Probability of Failure	
	FK Type	GM-5 Type
0.1	0.000	0.223×10^{-6}
0.2	0.112×10^{-11}	0.148×10^{-3}
0.3	0.178×10^{-4}	0.269×10^{-2}
0.4	0.145×10^{-2}	0.142×10^{-1}
0.5	0.125×10^{-1}	0.418×10^{-1}
0.6	0.447×10^{-1}	0.878×10^{-1}
0.7	0.102	0.150
0.8	0.180	0.223
0.9	0.270	0.302
1.0	0.363	0.382

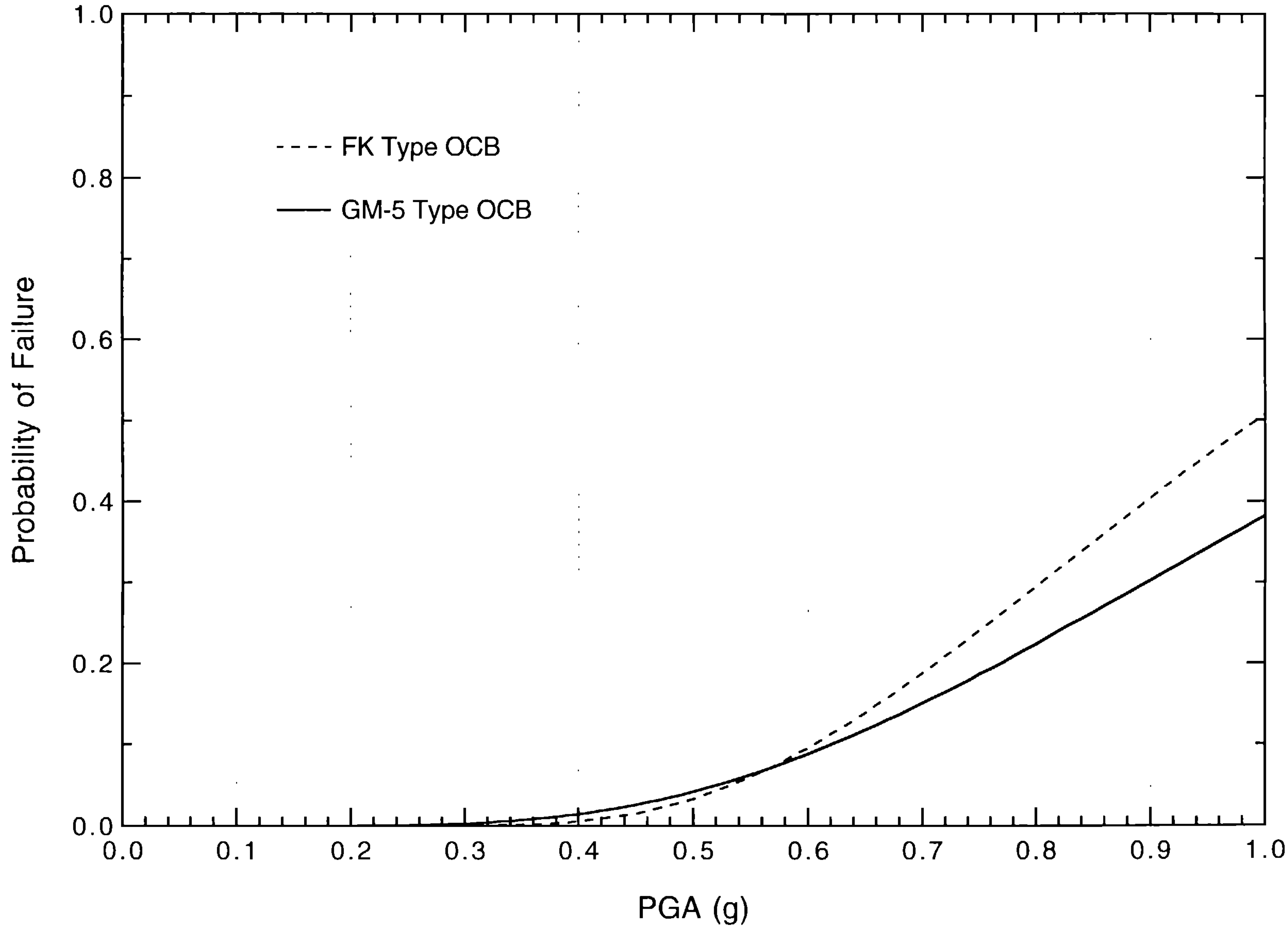

FIGURE 11-9 **Fragility Curves of 115 kV OCBs**

11.3 Fragility Analysis of GM-5 Type 115 kV OCB

Each tank of the GM-5 type 115 kV OCB is connected by four $\frac{1}{2}$ bolts to two "I" beams (Figure 11-6). The failure of the bolts in shear or in tension will cause the tank to move; thus, the failure of the bolts controls the failure mechanism of the GM-5 type 115 kV OCB. For the analysis of the bolts, the tank is considered as a rigid block (Figure 11-10). The bolts are in tension when the tank is uplifted, which occurs as the moment induced by the horizontal ground shaking exceeds the moment resulting from the weight of tank,

$$h \frac{W}{g} A_C > \frac{B}{2} W \tag{11.15}$$

or

$$A_C > \frac{B}{2h} g \tag{11.16}$$

where A_C is the value of horizontal PGA to cause the tank uplifting. The weight W of each tank is estimated as 12658 pounds and the height of the mass center h is 58 inches. The distance B between two adjacent bolts is 41.5 inches. Substituting the values of W, B, and h into Equation (11.16) shows the bolts are in tension only after PGA exceeds 0.36g. From the seismic hazard analysis for the study site, the bolts have little chance to fail in tension during the service period. In this study, the bolts are considered to be failed in shear.

The shear force V_1 of one bolt caused by ground shaking in each horizontal direction can be determined as follows:

$$V_1 = \frac{1}{4} \frac{W}{g} A \tag{11.17}$$

The total shear force V_T of one bolt caused by ground shaking in two horizontal directions is determined using the SRSS method.

$$V_T = \frac{1}{2\sqrt{2}} \frac{W}{g} A \tag{11.18}$$

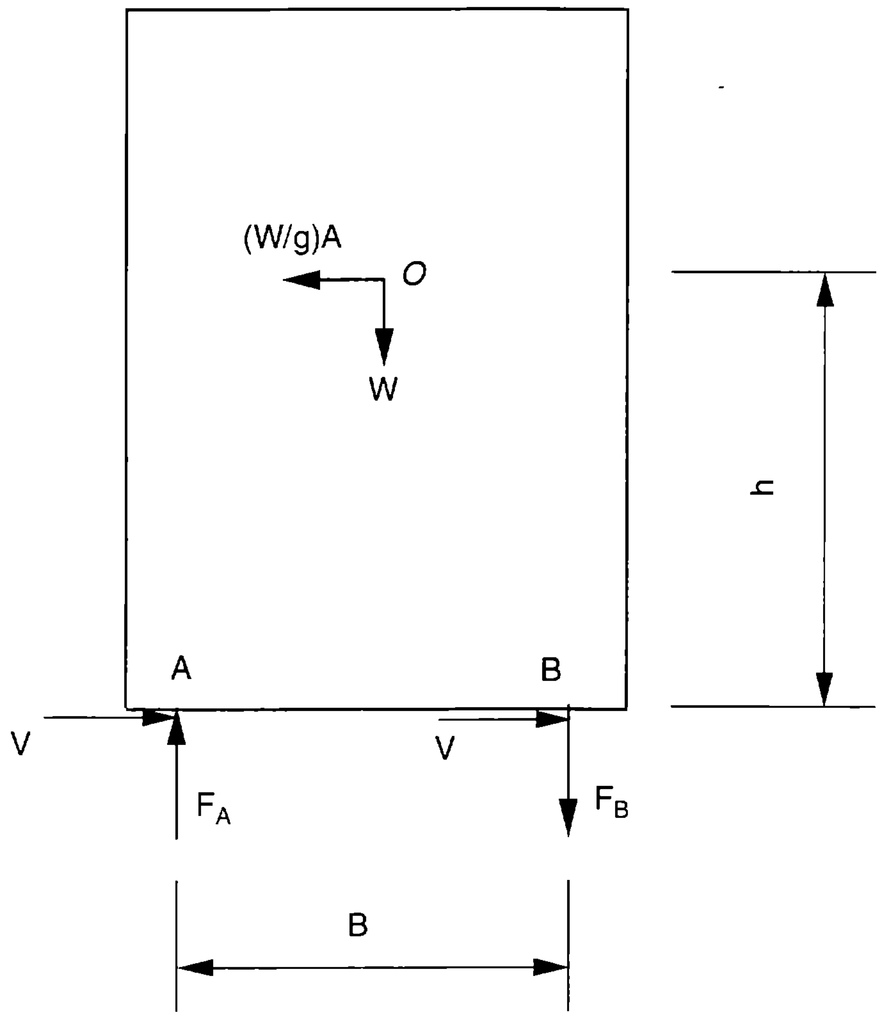

FIGURE 11-10 Model of GM-5 Type 115 kV OCB

Substituting the value of W into Equation (11.18), we have

$$V_T = 11.6\ A \tag{11.19}$$

The shear force of bolts is considered as a lognormal variable with the mean value taken from Equation (11.19) and the COV of 0.5. For an A36 bolt with a diameter of $\frac{1}{2}$ inch, the specified shear yielding strength through the body of the bolt is 4241.2 pounds, which is 60% of the tensile yielding strength (Segui, 1994). The capacity is also considered as a lognormal variable with the COV of 0.11 and the mean value taken as

$$F_y = 1.1 \times 4241.2 = 4665.3\ \text{lb} \tag{11.20}$$

The failure probabilities of the GM-5 type 115 kV OCB at various PGA levels are obtained with Equation (4.6) and listed in Table 11-II. The resulting fragility curve is shown in Figure 11-9.

SECTION 12
12 KV OIL CIRCUIT BREAKERS

12.1 Description of 12 kV OCBs

Five types of 12 kV oil circuit breakers (OCB) are installed in Substation 21. The one made by I-T-E consists of a single tank, while others made by General Electric and Westinghouse consist of three tanks. The basic information about these 12 kV OCBs is summarized in Table 12-I.

Figure 12-1 shows a photograph of the one-tank OCB, which has four arms at the top of the tank. Each arm is connected to a column by 3 bolts (Figure 12-1). The column made of $L4\times4\times\frac{1}{2}$ angle is welded to a rectangular steel plate, which in turn is anchored to a RC foundation with a $1\frac{1}{4}\times12$ headed anchor bolt (Figure 12-2). Figure 12-3 shows a photograph of a typical three-tank OCB. The plan and elevations of the OCB are shown in Figure 12-4. Four short arms on each tank of the OCB are connected by bolts to two C4×7.25 channel beams on the top of a steel frame structure (Figure 12-3). Four columns of the frame are made of $L4\times4\times\frac{1}{2}$ angles (Figures 12-3 and 12-4). The column of the supporting frame structure is anchored to a RC foundation by a $\frac{3}{4}\times12$ headed anchor bolt (Figure 12-5).

12.2 Structural Model

The three-tank OCB made by GE (FK-439 OCB) is taken as the representative of the 12 kV OCBs because this type of OCB is relative weak (smaller anchor bolts), and most 12 kV OCBs installed in Substation 21 belong to this type.

The supporting structure is modeled as a spatial steel frame (Figure 12-6). The arms on the tank are modeled as a beam element supporting the weight of the tank. The connection between the column of supporting structure and foundation is modeled as a hinge since only one anchor bolt is used. The thin bracing between columns is neglected.

TABLE 12-I Basic Information of 12 kV OCBs

OCB	I	II	III	IV	V
Manufacturer	I-T-E	General Electric	General Electric	Westing- house	Westing- house
Type	14.4KS 1000-128	FK-439- 14.4-1000	FK-339- 14.4-1500	144G1500- 3000A	144G1500- 1200A
Installed Date	1960s	1950s	1950s	1950s	1960s
Quantity	2	11	2	2	3
Tanks	1	3	3	3	3
Max. Voltage (kV)	14.4	14.4	14.4	14.4	14.4
Continuous Current (A)	1,200	1,200	2,000	3,000	1,200
Short Circuit Current (A)	35,000	40,000	60,000	-	-
Total Weight (lb)	6,075	8,050	9,115	8,800	6,400
Number of Anchor Bolts	4	4	8	4	4
Size of Anchor Bolts	$1\frac{1}{4}$	$\frac{3}{4}$	$\frac{3}{4}$	1	1

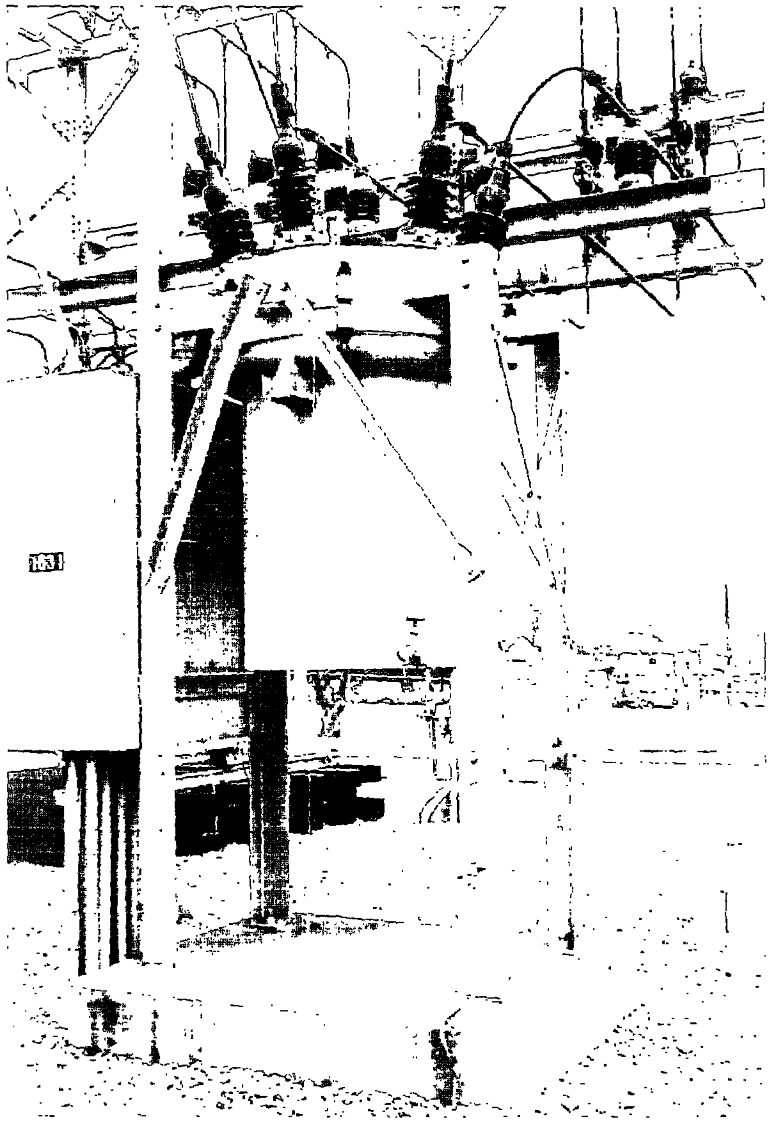

FIGURE 12-1 One-Tank 12 kV OCB

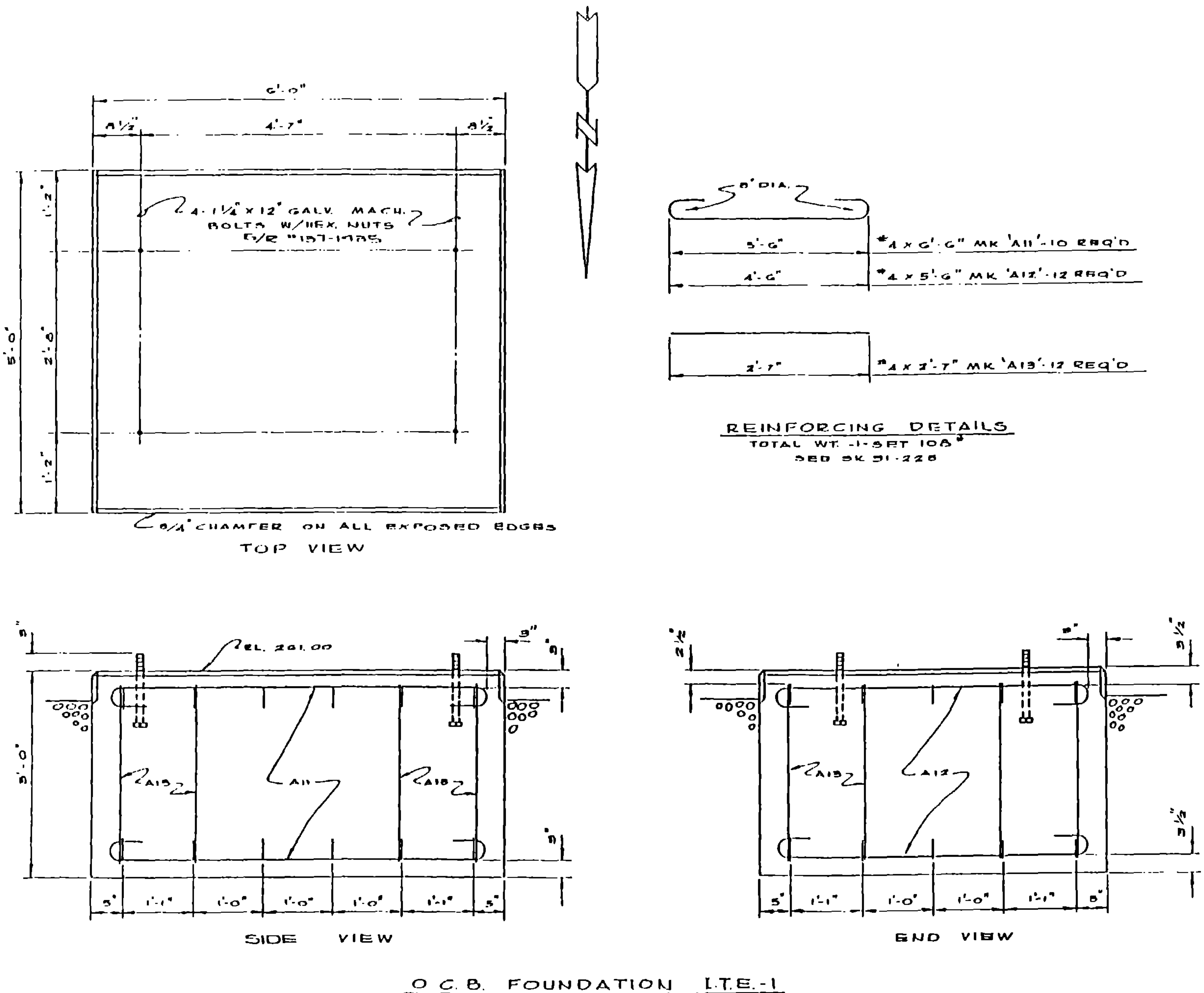

FIGURE 12-2 Detail of Foundation for One-Tank 12 kV OCB

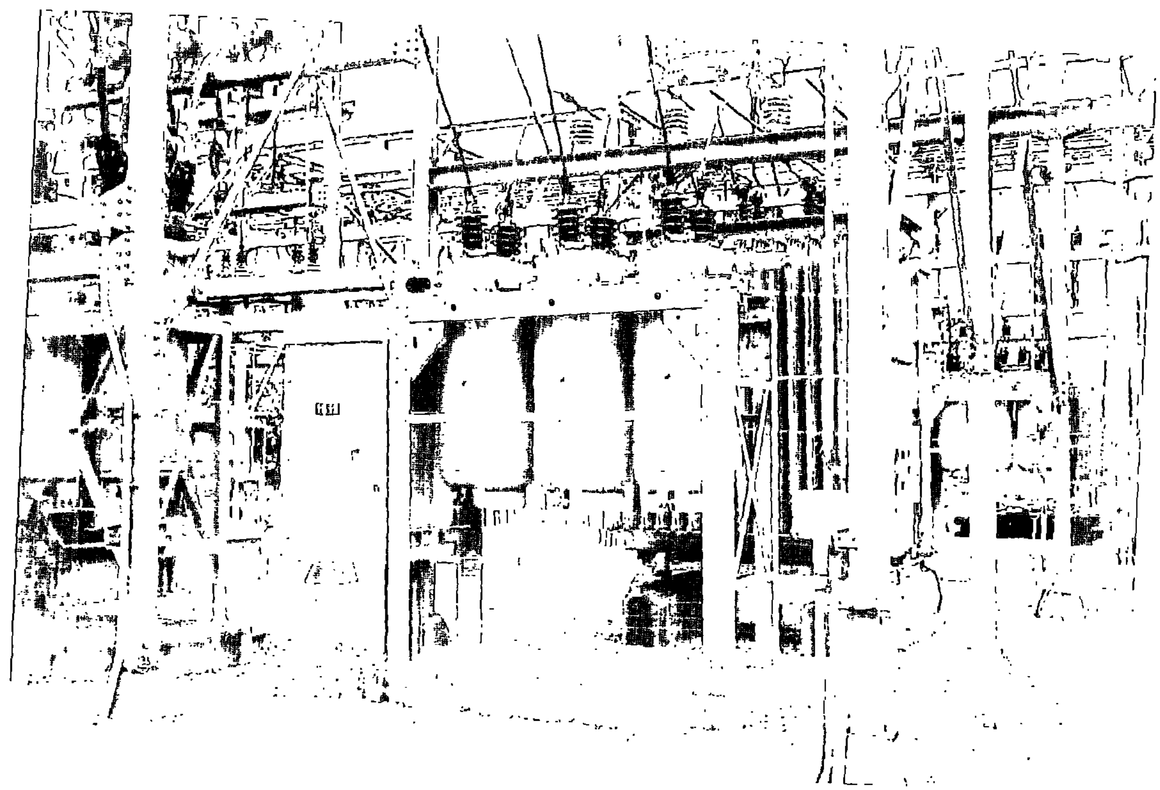

FIGURE 12-3 Three-Tank 12 kV OCB

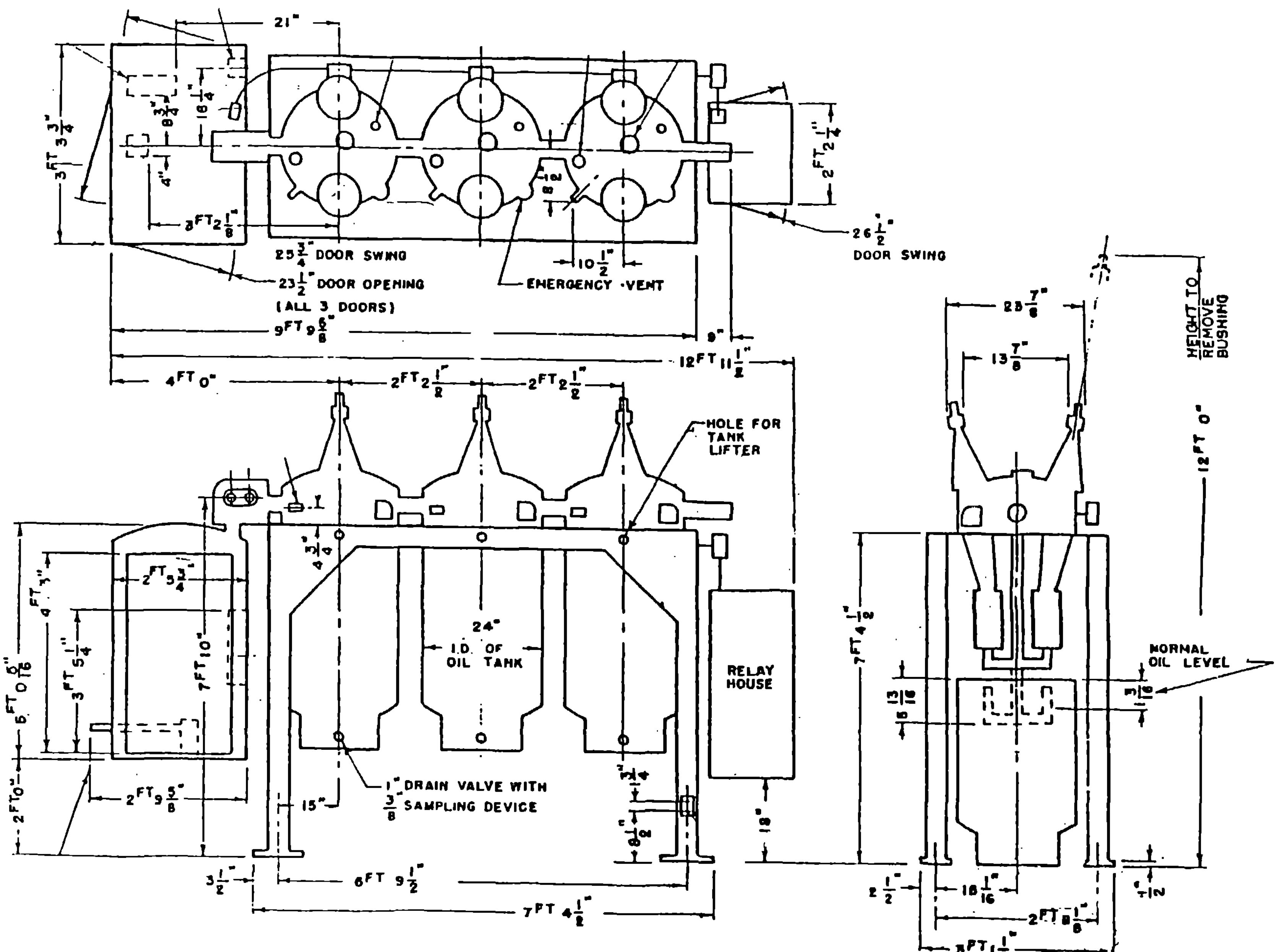

FIGURE 12-4 Plan and Elevations of Three-Tank 12 kV OCB

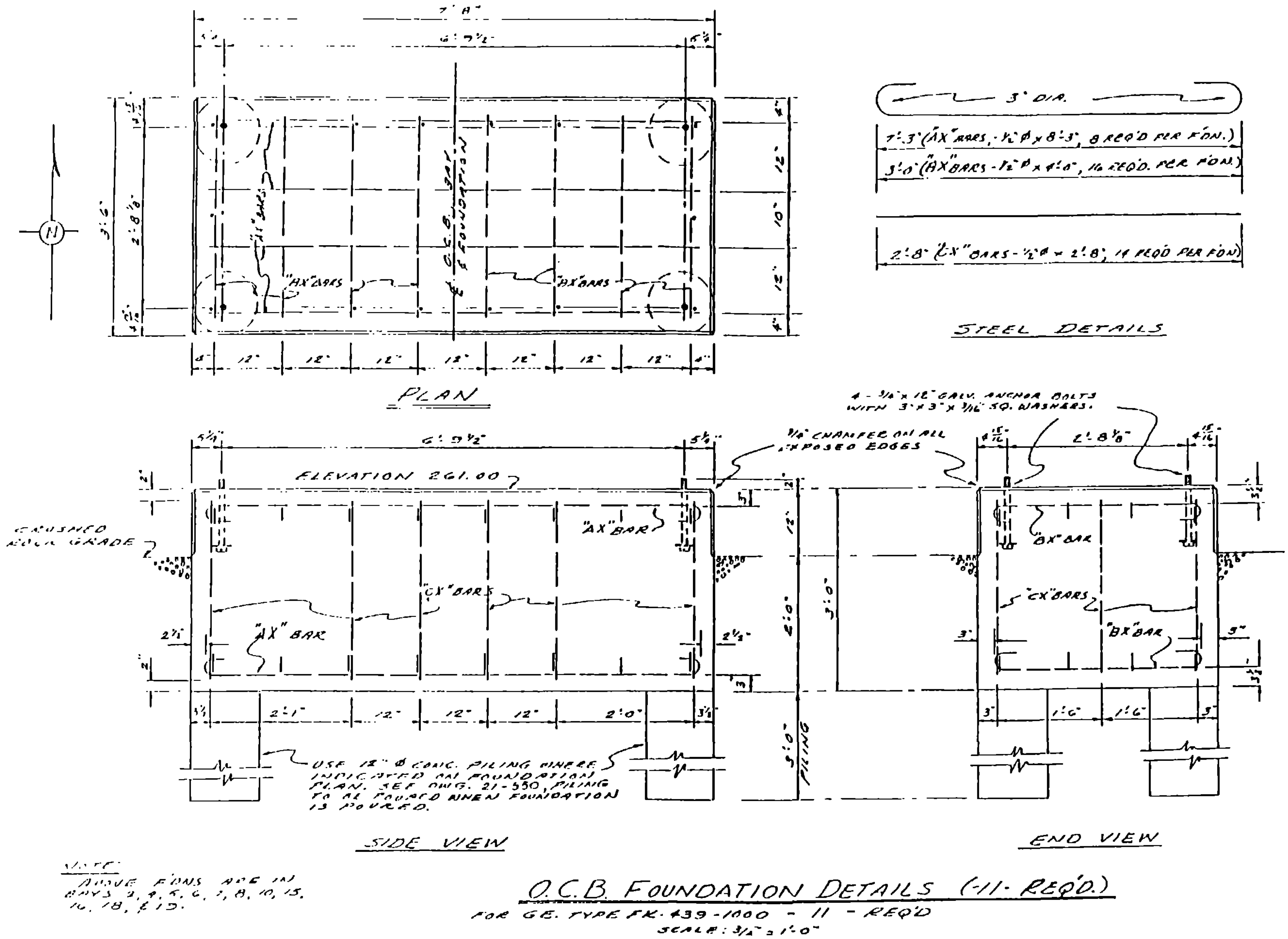

FIGURE 12-5 Detail of Foundation for Three-Tank 12 kV OCB

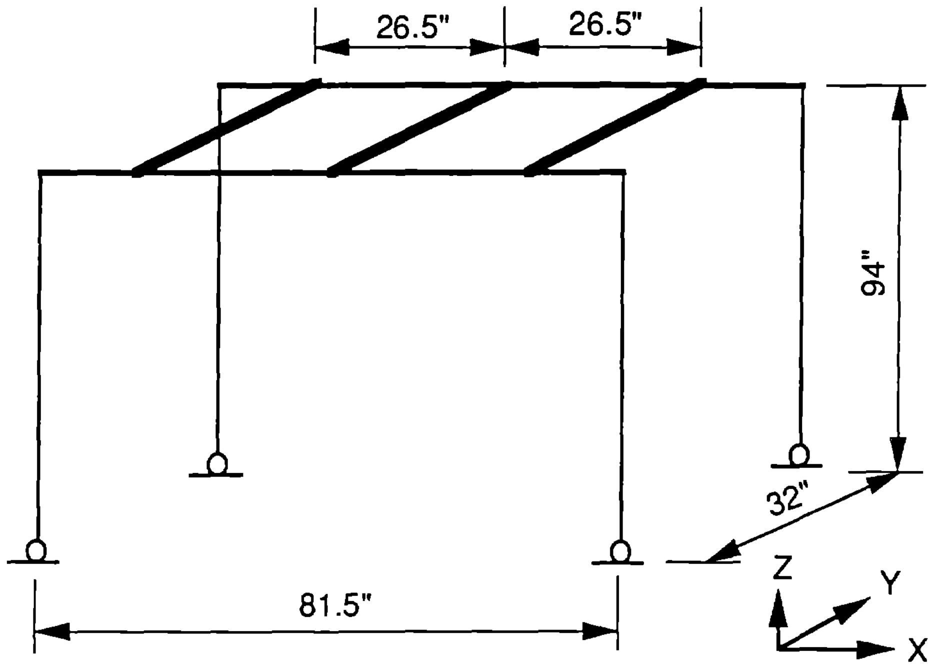

FIGURE 12-6 Model of 12 kV OCB

12.3 Fragility Analysis of 12 kV OCB

Each column of the supporting structure is anchored to the foundation by one anchor bolt. The yielding of the anchor bolt will cause an excessive deformation of the supporting structure and the failure of OCB. Thus, the yielding of the anchor bolt controls the failure mechanism of 12 kV OCB.

The 5% damped ground response spectra in both horizontal directions are used as the input to the structure. The forces of anchor bolts under the excitation of ground shaking in two horizontal directions are determined by the response spectrum analysis using the SAP program. The responses corresponding to various modes (Table 12-II) are combined with the CQC technique, while the responses caused by the ground motions in two horizontal directions are combined using the SRSS method. Thus, the tensile force T and shear force V of the anchor bolt caused by the ground shaking can be determined as

$$T = \sqrt{T_1 + T_2} \tag{12.1}$$

$$V = \sqrt{V_1 + V_2} \tag{12.2}$$

where subscripts "1" and "2" represent two horizontal directions.

TABLE 12-II Fundamental Periods of 12 kV OCB

Mode No.	Period (sec)	
	X-Direction	Y-Direction
1	0.806	0.662
2	0.019	0.016

Given the tensile force and shear force, the effective tensile force F of the anchor bolt can be determined as follows (Shipp and Haninger, 1983):

$$F = T + C \cdot V \tag{12.3}$$

where C is the shear coefficient, which is $\frac{1}{0.7}$ or 1.43 (ACI 318, 1992).

The compressive force of each anchor bolt caused by a dead load is

$$F_D = -\frac{W}{4} \tag{12.4}$$

The total tensile force of the anchor bolt F_T caused by earthquake and dead load is then obtained as follows:

$$F_T = F + F_D = T + C \cdot V - \frac{W}{4} \tag{12.5}$$

Table 12-III shows the forces of the anchor bolts corresponding to various PGA levels. The total tensile force of the anchor bolt is considered as a lognormal variable with the mean value taken from Equation (12.5) and the COV of 0.5.

For an A36 anchor bolt with a diameter of $\frac{3}{4}$ inches, the specified tensile yielding strength is 12020 pounds. The capacity of the anchor bolt is also considered as a lognormal variable with the mean value taken as

$$F_y = 1.1 \times 12020 = 13222 \text{ lb} \tag{12.6}$$

and the COV of 0.11 (Ellingwood, 1983). Using Equation (4.6), the failure probabilities of the 12 kV OCB corresponding to various PGA levels are computed and listed in Table 12-IV. The resulting fragility curve is shown in Figure 12-7.

TABLE 12-III Maximum Forces of 12 kV OCB Anchor Bolt

PGA (g)	Maximum Forces (lb)			
	Tension (Seismic)	Shear (Seismic)	Axial (Dead Load)	Total Effective Tension
0.05	1239	324	-2013	-311
0.10	2531	667	-2013	1473
0.15	3609	908	-2013	2894
0.20	4791	1169	-2013	4450
0.25	6088	1457	-2013	6159
0.30	7139	1696	-2013	7551
0.35	9060	2130	-2013	10093
0.40	10041	2341	-2013	11576
0.50	12176	2985	-2013	14431
0.60	14278	3359	-2013	17069
0.70	17100	4185	-2013	21071
0.80	19871	4676	-2013	24544
0.90	22170	5317	-2013	27760
1.00	24453	6036	-2013	31072

TABLE 12-IV Fragility Data of 12 kV OCB

PGA (g)	Probability of Failure
0.05	0
0.10	0.235×10^{-4}
0.15	0.215×10^{-2}
0.20	0.187×10^{-1}
0.25	0.672×10^{-1}
0.30	0.129
0.35	0.271
0.40	0.347
0.50	0.513
0.60	0.631
0.70	0.762
0.80	0.839
0.90	0.887
1.00	0.921

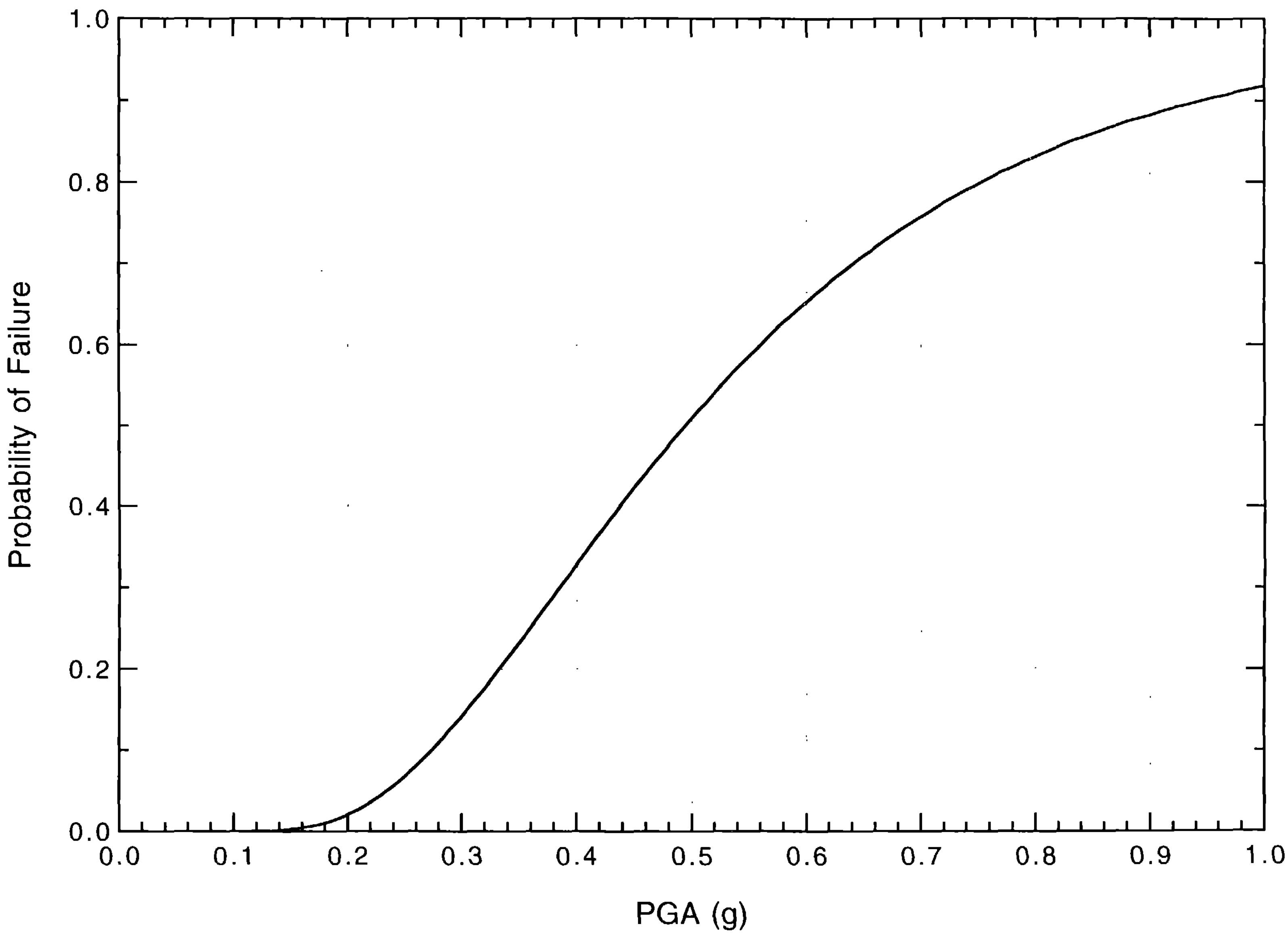

FIGURE 12-7 Fragility Curves of 12 kV OCB

SECTION 13
SUMMARY AND CONCLUSIONS

This report presents a seismic fragility analysis of equipment and structures in an electric substation in Memphis, Tennessee. The electric substation selected for this study is Substation 21, a key electricity supplier to several major hospitals in downtown Memphis. The performance of the substation is critical to the emergency operation of these hospitals in the event of a large New Madrid earthquake.

The fragility data of substation equipment and structures can be generated using actual earthquake damage data, experimental data, or analytical approaches. Even though the electric substations have been damaged in several earthquakes in California, seismic damage to electric facilities in the eastern United States is rare. In the practice of the power industry, the equipment with high voltage, for example, circuit breakers with voltage 169 kV and higher, is qualified by shake-table testing, while the equipment with low voltage is qualified by dynamic or static analysis. Thus, the information on the testing of low-voltage (115 kV) electric equipment similar to those installed in Substation 21 is not available. From these considerations, an analytical approach is used to carry out the fragility analysis of equipment and structures in Substation 21.

The failure modes of substation equipment and structures are usually controlled by the failure of porcelain insulators or the failure of anchor bolts of supporting structures. For each equipment or structure, the failure is defined as the state at which the component fails to perform its function. The capacity corresponding to this damage state is then established. The seismic response of structures and equipment is determined by either a response spectral analysis or a static analysis. The input site-specific ground motions are generated using the approach proposed by Hwang and Huo (1994). The uncertainties in seismic response and capacity are quantified and then the probability of failure is determined. The fragility curve is established from the probabilities of failure corresponding to various levels of ground shaking. Figure 13-1 shows the resulting fragility curves for the most critical structures and equipment in Substation 21.

It is noted that only the dominant failure modes of substation structures and equipment are identified for the reliability analysis using an analytical approach.

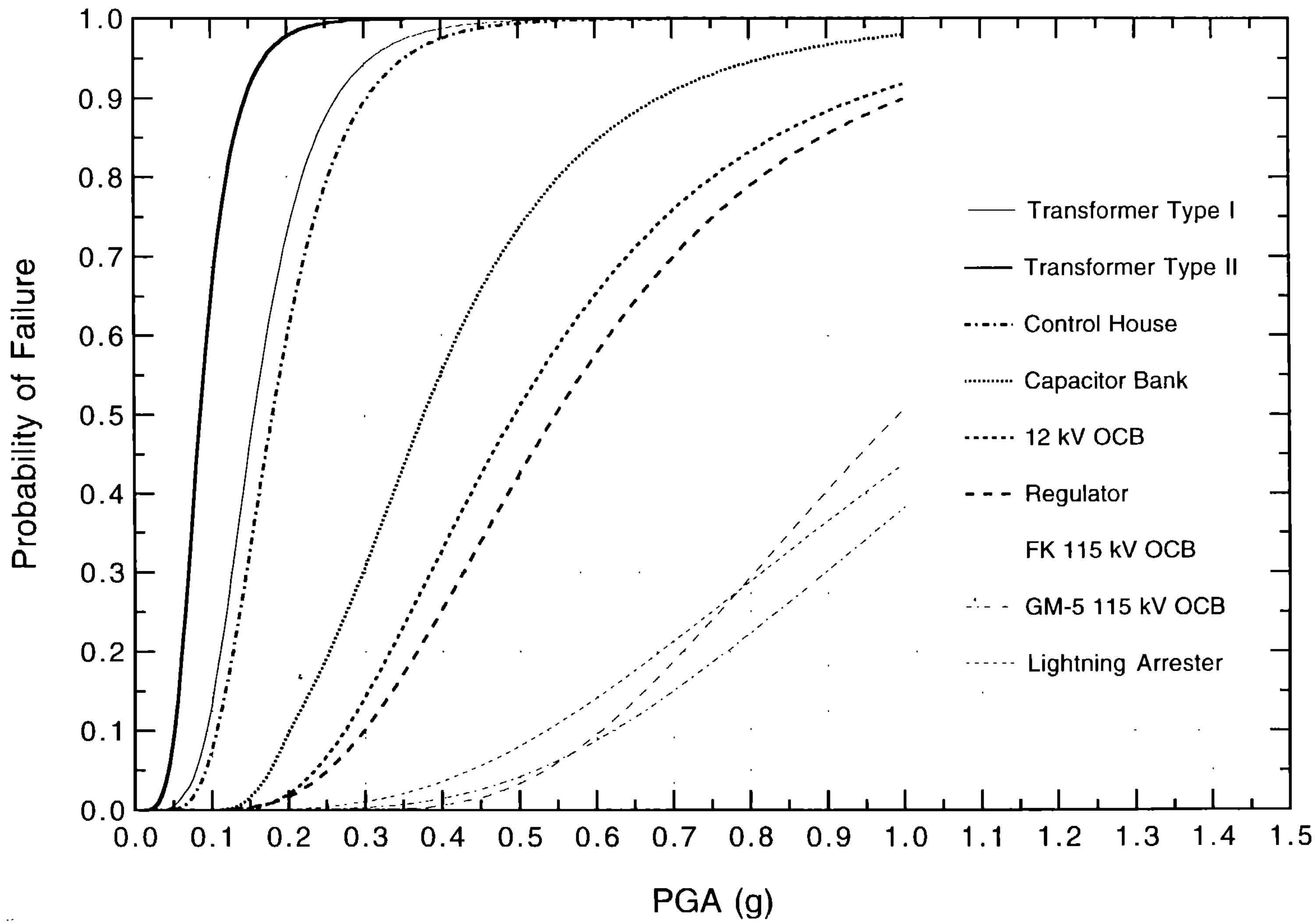

FIGURE 13-1 Fragility Curves for Various Component in MLGW Substation 21

Thus, not all the possible failure modes are covered in the analysis. For example, the gasket between the bushing and the tank of a 115 kV oil circuit breaker may loosen and cause the leaking of oil in the event of an earthquake. When possible, the fragility curves determined using an analytical method need to be verified with the earthquake damage data.

From the fragility analysis results, the expected performance of equipment and structures in a substation in the event of an earthquake can be revealed. For example, 115/12 kV transformers in Substation 21 are vulnerable to earthquakes even with moderate magnitude. The fragility analysis results can also provide the necessary data for evaluating the seismic performance of the entire electric substation and for performing the system reliability analysis of the electric transmission system.

SECTION 14
REFERENCES

ACI (1992). *Building Code Requirement for Reinforced Concrete (318M-89).* American Concrete Institute, Detroit, MI.

Algermissen, S.T., Perkins, D.M., Thenhaus, P.C., Hanson, S.L., and Bender, B.L. (1982). "Probabilistic Estimations of maximum acceleration and velocity in Rock in the Contiguous United States." *U.S.G.S. Open-File Report* 82-1033.

Ang, A. H-S., Pires, J., and Villaverde, R. (1993). "Probabilistic Seismic Reliability Assessment of Electric Power Transmission Systems." *Proceedings of the 6th International Conference on Structural Safety and Reliability,* Innsbruck, Austria, August 9-13, Vol. 2, 1207-1214.

ASCE (1991). *Design of Latticed Steel Transmission Structures.* ANSI/ASCE 10-90, American Society of Civil Engineers, New York, NY.

ATC (1985). "Earthquake Damage Evaluation Data for California." Applied Technology Council, ATC-13, Redwood City, California.

Buchanan, R.C. (1986). *Ceramic Materials for Electronics, Processing, Properties, and Applications.* Marcel Dekker, Inc., NY.

Ellingwood, B.R., and Hwang, H. (1985). "Probabilistic Descriptions of Resistance of Safety-Related Structures in Nuclear Power Plant." *Nuclear Engineering and Design,* Vol. 88, 167-178.

EPRI (1986). "Seismic Hazard Methodology for the Central and Eastern U.S." Technical Report NP-4726A (10 Volumes), Electric Power Research Institute, Polo Alto, CA.

FEMA (1985). "An Assessment of Damage and Casualties for Six Cities in the Central United States Resulting from Earthquakes in the New Madrid Seismic Zone." Report for Central United States Earthquake Preparedness Project, Federal Emergency Management Agency, Washington, D.C.

FEMA (1990). "Estimated Future Earthquake Losses for St. Louis City and County, Missouri." Federal Emergency Management Agency, FEMA 192, Washington, D.C.

Gutenberg, B., and Richter, C.F. (1944). "Frequency of Earthquakes in California." *Bulletin of the Seismological Society of America,* Vol. 34, 185-188.

Hwang, H. (1992). "Seismic Hazard along a Central U.S. Oil Pipeline." in *Lifeline Earthquake Engineering in the Central and Eastern U.S.*, Ballantyne, D.B. (ed.), Monograph No. 5, ASCE Technical Council on Lifeline Earthquake Engineering, American Society of Civil Engineers, New York, NY, 110-124.

Hwang, H., Ch'ng, A.L., and Hsu, H.-M. (1994). "Seismic Fragility Analysis of Sheahan Pumping Building." *Proceedings of ASCE Structures Congress XII,* Atlanta, GA, April 24-28, Vol. 2, 1006-1011.

Hwang, H. and Huo, J.-R. (1994), "Attenuation of Ground Motion in Hard Rock in the Central United State." Submitted to *Earthquake Spectrum.*

Hwang, H. and Huo, J.-R. (1994), "Generation of Hazard-Consistent Ground Motions." *International Journal of Soil Dynamics and Earthquake Engineering,* Vol. 13, No.6, 377-386.

Ishikawa, Y., and Kameda, H. (1991). "Probability-Based Determination of Specific Scenario Earthquakes." *Proceedings of the Fourth International Conference on Seismic Zonation,* Earthquake Engineering Research Institute, Oakland, California, Vol. II, 3-10.

Ishiyama, Y. (1982). "Motions of Rigid Bodies and Criteria for Overturning by Earthquake Excitations." *Earthquake Engineering and Structural Dynamics,* Vol. 10, 635-645.

Johnston, A.C. (1988). "Seismic Ground Motions in Shelby County." Technical Report 88-1, Center for Earthquake Research and Information, The University of Memphis, Memphis, TN.

Johnston, A.C. (1989). "Moment Magnitude Estimation for Stable Continental Earthquakes." *Seismological Research Letters*, Vol. 60, No. 1, 13.

Johnston, A.C. and Nava, S.J. (1990). "Seismic-Hazard Assessment in the Central United States." in *Neotectonics in Earthquake Evaluation,* Krinitzsky, E.L. and Slemmons, D.B. (eds.), The Geological Society of America, Inc., Boulder, CO, 47-57.

LAPP (1969). *Engineering Standards and Technical Data, Catalog 9-E*. LAPP Insulator Corporation, Inc., Le Roy, NY.

Moore. D.F. (1975). *Principles and Applications of Tribology*. Pergamon Press, Inc., Elmsford, NY.

Navias, L. (1926). "Methods of Testing and the Physical Properties of Wet-Process Electrical Porcelain." *Journal of American Ceramic Society*, Vol. 9, 501-510.

Newmark, N.M. and Hall, W.J. (1982). *Earthquake Spectra and Design*. Earthquake Engineering Research Institute, Berkeley, CA.

Pansini, A.J. (1992). *Electrical Distribution Engineering (2nd edition)*. The Fairmont Press, Inc., Lilburn, GA.

Parmley, R.O. (1977). *Standard Handbook of Fastening and Jointing*. McGraw-Hill Book Company, New York, NY.

Seed, H.B. and Idriss, I.M. (1982). "Ground Motion and Soil Liquefaction During Earthquakes" Earthquake Engineering Research Institute (EERI), Pasadena, CA.

Segui, W.T. (1989). *Fundamentals of Structural Steel Design*. PWS-ENT Publishing Company, Boston, MA.

Segui, W.T. (1994). *LRFD Steel Design*. PWS Publishing Company, Boston, MA.

Shipp, J.G. and Haninger, E.R. (1983). "Design of Headed Anchor Bolts." *Engineering Journal, American Institute of Steel Construction*, 2nd Quarter, 58-69.

Toro, G.R., Silva, W.J., McGuire, R.K., and Herrmann, R.B. (1992). "Probabilistic Seismic Hazard Mapping of the Mississippi Embayment." *Seismological Research Letters*, Vol. 63, 449-475.

Tsai, Y.-B. (1993). "Impact of Earthquake Strong Ground Motion on Substations." Technical Report, Department of Research and Development, Pacific Gas and Electric Company, San Ramon, CA.

Wilson, E.L. and Button, M.R. (1982). "Three-Dimensional Dynamic Analysis for Multicomponent Earthquake Spectra." *Earthquake Engineering and Structural Dynamics*, Vol. 10, 471-476.

APPENDIX A

DETERMINATION OF SEISMICITY PARAMETERS IN SEISMIC SOURCE ZONES

Three seismic source zones, Zone A, B, and C (Figure 3-3), within a radius of 300 km around the study site have been established. Zone A is the central part of the Reelfoot Rift where seismicity is intensive, and includes the epicenters of the three great New Madrid Earthquakes which occurred in the winter of 1811-1812. Zone B covers part of the Reelfoot Rift Complex, Ozark Uplift, and part of Arkansas and Missouri. Zone B is bounded by the circular boundary in the north and the Ouachita Fold Belt in the south. Zone C is the area below the Reelfoot Rift and is bounded by the Ouachita Fold Belt and the circular boundary.

Hwang (1992) evaluated the coefficients a and b in Equation (3.1) for Zone A from a combination of historical data (1804-1974) and instrumental data (1974-1990). The resulting frequency-magnitude relationship for the entire Zone A is

$$\log N = 3.15 - 0.91\, m_b \qquad \text{(A.1)}$$

The seismicity data in Zone B are not sufficient to establish the frequency-magnitude relationship. The seismic source zones located in the same tectonic province usually have similar b-values but different a-values (Algermissen et al., 1982). Since part of Zone B and Zone A are located in the same tectonic province, the Reelfoot Rift Complex, the b-value for Zone B is the same as that for Zone A, that is, 0.91. The a-value for Zone B is determined using the data from the report by EPRI (1986). In the report, occurrence rates of earthquakes with magnitude m_b equal to 3.3 and larger per year and unit degree area ($1^\circ \times 1^\circ$) for the region covering Zone B are listed. The average of the occurrence rate is determined as 0.134. The total area for Zone B is about 11.02 times the unit degree area. Thus, the occurrence of earthquakes with magnitude equal to 3.3 and larger for the entire Zone B is

$$N_{3.3}^{B} = 0.134 \times 11.02 = 1.479 \qquad \text{(A.2)}$$

From the following relation,

$$\text{Log}\,(N_{3.3}^{B}) = a - 0.91 \times 3.3 \qquad \text{(A.3).}$$

the a-value is determined as 3.17. Thus, the frequency-magnitude relationship for the entire Zone B is established as follows:

$$\log N = 3.17 - 0.91\, m_b \tag{A.4}$$

For Zone C, the frequency-magnitude relationship is established directly on the basis of data from EPRI (1986). The b-value for Zone C is taken as 1.0, which is about the average of the b-value for all the seismic source zones in the south-central United States (EPRI 1986). The average of occurrence rates of earthquakes with magnitude m_b equal to 3.3 and larger per year and unit degree area is estimated as 0.017. Since the total area of Zone C is approximately 12.2 times the unit degree area, the frequency-magnitude relation for the entire Zone C can be determined as

$$\log N = 2.61 - 1.00\, m_b \tag{A.5}$$

For engineering applications, a lower-bound (minimum) magnitude m_{bo} and an upper-bound (maximum) magnitude m_{bu} need to be specified. The lower-bound and upper-bound magnitudes for Zone A are selected as m_b of 4.0 and 7.5, respectively (Johnston, 1988; Toro et al., 1992). The lower-bound magnitudes are also set as m_b of 4.0 for both Zone B and Zone C; however, the upper-bound magnitudes are approximately taken as 6.5 and 6.0 for Zone B and Zone C, respectively (EPRI, 1986). The seismic parameters of three seismic source zones considered for the study site are summarized in Table 3-I.

NATIONAL CENTER FOR EARTHQUAKE ENGINEERING RESEARCH
LIST OF TECHNICAL REPORTS

The National Center for Earthquake Engineering Research (NCEER) publishes technical reports on a variety of subjects related to earthquake engineering written by authors funded through NCEER. These reports are available from both NCEER's Publications Department and the National Technical Information Service (NTIS). Requests for reports should be directed to the Publications Department, National Center for Earthquake Engineering Research, State University of New York at Buffalo, Red Jacket Quadrangle, Buffalo, New York 14261. Reports can also be requested through NTIS, 5285 Port Royal Road, Springfield, Virginia 22161. NTIS accession numbers are shown in parenthesis, if available.

NCEER-87-0001 "First-Year Program in Research, Education and Technology Transfer," 3/5/87, (PB88-134275).

NCEER-87-0002 "Experimental Evaluation of Instantaneous Optimal Algorithms for Structural Control," by R.C. Lin, T.T. Soong and A.M. Reinhorn, 4/20/87, (PB88-134341).

NCEER-87-0003 "Experimentation Using the Earthquake Simulation Facilities at University at Buffalo," by A.M. Reinhorn and R.L. Ketter, to be published.

NCEER-87-0004 "The System Characteristics and Performance of a Shaking Table," by J.S. Hwang, K.C. Chang and G.C. Lee, 6/1/87, (PB88-134259). This report is available only through NTIS (see address given above).

NCEER-87-0005 "A Finite Element Formulation for Nonlinear Viscoplastic Material Using a Q Model," by O. Gyebi and G. Dasgupta, 11/2/87, (PB88-213764).

NCEER-87-0006 "Symbolic Manipulation Program (SMP) - Algebraic Codes for Two and Three Dimensional Finite Element Formulations," by X. Lee and G. Dasgupta, 11/9/87, (PB88-218522).

NCEER-87-0007 "Instantaneous Optimal Control Laws for Tall Buildings Under Seismic Excitations," by J.N. Yang, A. Akbarpour and P. Ghaemmaghami, 6/10/87, (PB88-134333). This report is only available through NTIS (see address given above).

NCEER-87-0008 "IDARC: Inelastic Damage Analysis of Reinforced Concrete Frame - Shear-Wall Structures," by Y.J. Park, A.M. Reinhorn and S.K. Kunnath, 7/20/87, (PB88-134325).

NCEER-87-0009 "Liquefaction Potential for New York State: A Preliminary Report on Sites in Manhattan and Buffalo," by M. Budhu, V. Vijayakumar, R.F. Giese and L. Baumgras, 8/31/87, (PB88-163704). This report is available only through NTIS (see address given above).

NCEER-87-0010 "Vertical and Torsional Vibration of Foundations in Inhomogeneous Media," by A.S. Veletsos and K.W. Dotson, 6/1/87, (PB88-134291).

NCEER-87-0011 "Seismic Probabilistic Risk Assessment and Seismic Margins Studies for Nuclear Power Plants," by Howard H.M. Hwang, 6/15/87, (PB88-134267).

NCEER-87-0012 "Parametric Studies of Frequency Response of Secondary Systems Under Ground-Acceleration Excitations," by Y. Yong and Y.K. Lin, 6/10/87, (PB88-134309).

NCEER-87-0013 "Frequency Response of Secondary Systems Under Seismic Excitation," by J.A. HoLung, J. Cai and Y.K. Lin, 7/31/87, (PB88-134317).

NCEER-87-0014 "Modelling Earthquake Ground Motions in Seismically Active Regions Using Parametric Time Series Methods," by G.W. Ellis and A.S. Cakmak, 8/25/87, (PB88-134283).

NCEER-87-0015 "Detection and Assessment of Seismic Structural Damage," by E. DiPasquale and A.S. Cakmak, 8/25/87, (PB88-163712).

NCEER-87-0016 "Pipeline Experiment at Parkfield, California," by J. Isenberg and E. Richardson, 9/15/87, (PB88-163720). This report is available only through NTIS (see address given above).

NCEER-87-0017 "Digital Simulation of Seismic Ground Motion," by M. Shinozuka, G. Deodatis and T. Harada, 8/31/87, (PB88-155197). This report is available only through NTIS (see address given above).

NCEER-87-0018 "Practical Considerations for Structural Control: System Uncertainty, System Time Delay and Truncation of Small Control Forces," J.N. Yang and A. Akbarpour, 8/10/87, (PB88-163738).

NCEER-87-0019 "Modal Analysis of Nonclassically Damped Structural Systems Using Canonical Transformation," by J.N. Yang, S. Sarkani and F.X. Long, 9/27/87, (PB88-187851).

NCEER-87-0020 "A Nonstationary Solution in Random Vibration Theory," by J.R. Red-Horse and P.D. Spanos, 11/3/87, (PB88-163746).

NCEER-87-0021 "Horizontal Impedances for Radially Inhomogeneous Viscoelastic Soil Layers," by A.S. Veletsos and K.W. Dotson, 10/15/87, (PB88-150859).

NCEER-87-0022 "Seismic Damage Assessment of Reinforced Concrete Members," by Y.S. Chung, C. Meyer and M. Shinozuka, 10/9/87, (PB88-150867). This report is available only through NTIS (see address given above).

NCEER-87-0023 "Active Structural Control in Civil Engineering," by T.T. Soong, 11/11/87, (PB88-187778).

NCEER-87-0024 "Vertical and Torsional Impedances for Radially Inhomogeneous Viscoelastic Soil Layers," by K.W. Dotson and A.S. Veletsos, 12/87, (PB88-187786).

NCEER-87-0025 "Proceedings from the Symposium on Seismic Hazards, Ground Motions, Soil-Liquefaction and Engineering Practice in Eastern North America," October 20-22, 1987, edited by K.H. Jacob, 12/87, (PB88-188115).

NCEER-87-0026 "Report on the Whittier-Narrows, California, Earthquake of October 1, 1987," by J. Pantelic and A. Reinhorn, 11/87, (PB88-187752). This report is available only through NTIS (see address given above).

NCEER-87-0027 "Design of a Modular Program for Transient Nonlinear Analysis of Large 3-D Building Structures," by S. Srivastav and J.F. Abel, 12/30/87, (PB88-187950).

NCEER-87-0028 "Second-Year Program in Research, Education and Technology Transfer," 3/8/88, (PB88-219480).

NCEER-88-0001 "Workshop on Seismic Computer Analysis and Design of Buildings With Interactive Graphics," by W. McGuire, J.F. Abel and C.H. Conley, 1/18/88, (PB88-187760).

NCEER-88-0002 "Optimal Control of Nonlinear Flexible Structures," by J.N. Yang, F.X. Long and D. Wong, 1/22/88, (PB88-213772).

NCEER-88-0003 "Substructuring Techniques in the Time Domain for Primary-Secondary Structural Systems," by G.D. Manolis and G. Juhn, 2/10/88, (PB88-213780).

NCEER-88-0004 "Iterative Seismic Analysis of Primary-Secondary Systems," by A. Singhal, L.D. Lutes and P.D. Spanos, 2/23/88, (PB88-213798).

NCEER-88-0005 "Stochastic Finite Element Expansion for Random Media," by P.D. Spanos and R. Ghanem, 3/14/88, (PB88-213806).

NCEER-88-0006 "Combining Structural Optimization and Structural Control," by F.Y. Cheng and C.P. Pantelides, 1/10/88, (PB88-213814).

NCEER-88-0007 "Seismic Performance Assessment of Code-Designed Structures," by H.H-M. Hwang, J-W. Jaw and H-J. Shau, 3/20/88, (PB88-219423).

NCEER-88-0008 "Reliability Analysis of Code-Designed Structures Under Natural Hazards," by H.H-M. Hwang, H. Ushiba and M. Shinozuka, 2/29/88, (PB88-229471).

NCEER-88-0009 "Seismic Fragility Analysis of Shear Wall Structures," by J-W Jaw and H.H-M. Hwang, 4/30/88, (PB89-102867).

NCEER-88-0010 "Base Isolation of a Multi-Story Building Under a Harmonic Ground Motion - A Comparison of Performances of Various Systems," by F-G Fan, G. Ahmadi and I.G. Tadjbakhsh, 5/18/88, (PB89-122238).

NCEER-88-0011 "Seismic Floor Response Spectra for a Combined System by Green's Functions," by F.M. Lavelle, L.A. Bergman and P.D. Spanos, 5/1/88, (PB89-102875).

NCEER-88-0012 "A New Solution Technique for Randomly Excited Hysteretic Structures," by G.Q. Cai and Y.K. Lin, 5/16/88, (PB89-102883).

NCEER-88-0013 "A Study of Radiation Damping and Soil-Structure Interaction Effects in the Centrifuge," by K. Weissman, supervised by J.H. Prevost, 5/24/88, (PB89-144703).

NCEER-88-0014 "Parameter Identification and Implementation of a Kinematic Plasticity Model for Frictional Soils," by J.H. Prevost and D.V. Griffiths, to be published.

NCEER-88-0015 "Two- and Three- Dimensional Dynamic Finite Element Analyses of the Long Valley Dam," by D.V. Griffiths and J.H. Prevost, 6/17/88, (PB89-144711).

NCEER-88-0016 "Damage Assessment of Reinforced Concrete Structures in Eastern United States," by A.M. Reinhorn, M.J. Seidel, S.K. Kunnath and Y.J. Park, 6/15/88, (PB89-122220).

NCEER-88-0017 "Dynamic Compliance of Vertically Loaded Strip Foundations in Multilayered Viscoelastic Soils," by S. Ahmad and A.S.M. Israil, 6/17/88, (PB89-102891).

NCEER-88-0018 "An Experimental Study of Seismic Structural Response With Added Viscoelastic Dampers," by R.C. Lin, Z. Liang, T.T. Soong and R.H. Zhang, 6/30/88, (PB89-122212). This report is available only through NTIS (see address given above).

NCEER-88-0019 "Experimental Investigation of Primary - Secondary System Interaction," by G.D. Manolis, G. Juhn and A.M. Reinhorn, 5/27/88, (PB89-122204).

NCEER-88-0020 "A Response Spectrum Approach For Analysis of Nonclassically Damped Structures," by J.N. Yang, S. Sarkani and F.X. Long, 4/22/88, (PB89-102909).

NCEER-88-0021 "Seismic Interaction of Structures and Soils: Stochastic Approach," by A.S. Veletsos and A.M. Prasad, 7/21/88, (PB89-122196).

NCEER-88-0022 "Identification of the Serviceability Limit State and Detection of Seismic Structural Damage," by E. DiPasquale and A.S. Cakmak, 6/15/88, (PB89-122188). This report is available only through NTIS (see address given above).

NCEER-88-0023 "Multi-Hazard Risk Analysis: Case of a Simple Offshore Structure," by B.K. Bhartia and E.H. Vanmarcke, 7/21/88, (PB89-145213).

NCEER-88-0024 "Automated Seismic Design of Reinforced Concrete Buildings," by Y.S. Chung, C. Meyer and M. Shinozuka, 7/5/88, (PB89-122170). This report is available only through NTIS (see address given above).

NCEER-88-0025 "Experimental Study of Active Control of MDOF Structures Under Seismic Excitations," by L.L. Chung, R.C. Lin, T.T. Soong and A.M. Reinhorn, 7/10/88, (PB89-122600).

NCEER-88-0026 "Earthquake Simulation Tests of a Low-Rise Metal Structure," by J.S. Hwang, K.C. Chang, G.C. Lee and R.L. Ketter, 8/1/88, (PB89-102917).

NCEER-88-0027 "Systems Study of Urban Response and Reconstruction Due to Catastrophic Earthquakes," by F. Kozin and H.K. Zhou, 9/22/88, (PB90-162348).

NCEER-88-0028 "Seismic Fragility Analysis of Plane Frame Structures," by H.H-M. Hwang and Y.K. Low, 7/31/88, (PB89-131445).

NCEER-88-0029 "Response Analysis of Stochastic Structures," by A. Kardara, C. Bucher and M. Shinozuka, 9/22/88, (PB89-174429).

NCEER-88-0030 "Nonnormal Accelerations Due to Yielding in a Primary Structure," by D.C.K. Chen and L.D. Lutes, 9/19/88, (PB89-131437).

NCEER-88-0031 "Design Approaches for Soil-Structure Interaction," by A.S. Veletsos, A.M. Prasad and Y. Tang, 12/30/88, (PB89-174437). This report is available only through NTIS (see address given above).

NCEER-88-0032 "A Re-evaluation of Design Spectra for Seismic Damage Control," by C.J. Turkstra and A.G. Tallin, 11/7/88, (PB89-145221).

NCEER-88-0033 "The Behavior and Design of Noncontact Lap Splices Subjected to Repeated Inelastic Tensile Loading," by V.E. Sagan, P. Gergely and R.N. White, 12/8/88, (PB89-163737).

NCEER-88-0034 "Seismic Response of Pile Foundations," by S.M. Mamoon, P.K. Banerjee and S. Ahmad, 11/1/88, (PB89-145239).

NCEER-88-0035 "Modeling of R/C Building Structures With Flexible Floor Diaphragms (IDARC2)," by A.M. Reinhorn, S.K. Kunnath and N. Panahshahi, 9/7/88, (PB89-207153).

NCEER-88-0036 "Solution of the Dam-Reservoir Interaction Problem Using a Combination of FEM, BEM with Particular Integrals, Modal Analysis, and Substructuring," by C-S. Tsai, G.C. Lee and R.L. Ketter, 12/31/88, (PB89-207146).

NCEER-88-0037 "Optimal Placement of Actuators for Structural Control," by F.Y. Cheng and C.P. Pantelides, 8/15/88, (PB89-162846).

NCEER-88-0038 "Teflon Bearings in Aseismic Base Isolation: Experimental Studies and Mathematical Modeling," by A. Mokha, M.C. Constantinou and A.M. Reinhorn, 12/5/88, (PB89-218457). This report is available only through NTIS (see address given above).

NCEER-88-0039 "Seismic Behavior of Flat Slab High-Rise Buildings in the New York City Area," by P. Weidlinger and M. Ettouney, 10/15/88, (PB90-145681).

NCEER-88-0040 "Evaluation of the Earthquake Resistance of Existing Buildings in New York City," by P. Weidlinger and M. Ettouney, 10/15/88, to be published.

NCEER-88-0041 "Small-Scale Modeling Techniques for Reinforced Concrete Structures Subjected to Seismic Loads," by W. Kim, A. El-Attar and R.N. White, 11/22/88, (PB89-189625).

NCEER-88-0042 "Modeling Strong Ground Motion from Multiple Event Earthquakes," by G.W. Ellis and A.S. Cakmak, 10/15/88, (PB89-174445).

NCEER-88-0043 "Nonstationary Models of Seismic Ground Acceleration," by M. Grigoriu, S.E. Ruiz and E. Rosenblueth, 7/15/88, (PB89-189617).

NCEER-88-0044 "SARCF User's Guide: Seismic Analysis of Reinforced Concrete Frames," by Y.S. Chung, C. Meyer and M. Shinozuka, 11/9/88, (PB89-174452).

NCEER-88-0045 "First Expert Panel Meeting on Disaster Research and Planning," edited by J. Pantelic and J. Stoyle, 9/15/88, (PB89-174460).

NCEER-88-0046 "Preliminary Studies of the Effect of Degrading Infill Walls on the Nonlinear Seismic Response of Steel Frames," by C.Z. Chrysostomou, P. Gergely and J.F. Abel, 12/19/88, (PB89-208383).

NCEER-88-0047 "Reinforced Concrete Frame Component Testing Facility - Design, Construction, Instrumentation and Operation," by S.P. Pessiki, C. Conley, T. Bond, P. Gergely and R.N. White, 12/16/88, (PB89-174478).

NCEER-89-0001 "Effects of Protective Cushion and Soil Compliancy on the Response of Equipment Within a Seismically Excited Building," by J.A. HoLung, 2/16/89, (PB89-207179).

NCEER-89-0002 "Statistical Evaluation of Response Modification Factors for Reinforced Concrete Structures," by H.H-M. Hwang and J-W. Jaw, 2/17/89, (PB89-207187).

NCEER-89-0003 "Hysteretic Columns Under Random Excitation," by G-Q. Cai and Y.K. Lin, 1/9/89, (PB89-196513).

NCEER-89-0004 "Experimental Study of 'Elephant Foot Bulge' Instability of Thin-Walled Metal Tanks," by Z-H. Jia and R.L. Ketter, 2/22/89, (PB89-207195).

NCEER-89-0005 "Experiment on Performance of Buried Pipelines Across San Andreas Fault," by J. Isenberg, E. Richardson and T.D. O'Rourke, 3/10/89, (PB89-218440). This report is available only through NTIS (see address given above).

NCEER-89-0006 "A Knowledge-Based Approach to Structural Design of Earthquake-Resistant Buildings," by M. Subramani, P. Gergely, C.H. Conley, J.F. Abel and A.H. Zaghw, 1/15/89, (PB89-218465).

NCEER-89-0007 "Liquefaction Hazards and Their Effects on Buried Pipelines," by T.D. O'Rourke and P.A. Lane, 2/1/89, (PB89-218481).

NCEER-89-0008 "Fundamentals of System Identification in Structural Dynamics," by H. Imai, C-B. Yun, O. Maruyama and M. Shinozuka, 1/26/89, (PB89-207211).

NCEER-89-0009 "Effects of the 1985 Michoacan Earthquake on Water Systems and Other Buried Lifelines in Mexico," by A.G. Ayala and M.J. O'Rourke, 3/8/89, (PB89-207229).

NCEER-89-R010 "NCEER Bibliography of Earthquake Education Materials," by K.E.K. Ross, Second Revision, 9/1/89, (PB90-125352).

NCEER-89-0011 "Inelastic Three-Dimensional Response Analysis of Reinforced Concrete Building Structures (IDARC-3D), Part I - Modeling," by S.K. Kunnath and A.M. Reinhorn, 4/17/89, (PB90-114612).

NCEER-89-0012 "Recommended Modifications to ATC-14," by C.D. Poland and J.O. Malley, 4/12/89, (PB90-108648).

NCEER-89-0013 "Repair and Strengthening of Beam-to-Column Connections Subjected to Earthquake Loading," by M. Corazao and A.J. Durrani, 2/28/89, (PB90-109885).

NCEER-89-0014 "Program EXKAL2 for Identification of Structural Dynamic Systems," by O. Maruyama, C-B. Yun, M. Hoshiya and M. Shinozuka, 5/19/89, (PB90-109877).

NCEER-89-0015 "Response of Frames With Bolted Semi-Rigid Connections, Part I - Experimental Study and Analytical Predictions," by P.J. DiCorso, A.M. Reinhorn, J.R. Dickerson, J.B. Radziminski and W.L. Harper, 6/1/89, to be published.

NCEER-89-0016 "ARMA Monte Carlo Simulation in Probabilistic Structural Analysis," by P.D. Spanos and M.P. Mignolet, 7/10/89, (PB90-109893).

NCEER-89-P017 "Preliminary Proceedings from the Conference on Disaster Preparedness - The Place of Earthquake Education in Our Schools," Edited by K.E.K. Ross, 6/23/89, (PB90-108606).

NCEER-89-0017 "Proceedings from the Conference on Disaster Preparedness - The Place of Earthquake Education in Our Schools," Edited by K.E.K. Ross, 12/31/89, (PB90-207895). This report is available only through NTIS (see address given above).

NCEER-89-0018 "Multidimensional Models of Hysteretic Material Behavior for Vibration Analysis of Shape Memory Energy Absorbing Devices, by E.J. Graesser and F.A. Cozzarelli, 6/7/89, (PB90-164146).

NCEER-89-0019 "Nonlinear Dynamic Analysis of Three-Dimensional Base Isolated Structures (3D-BASIS)," by S. Nagarajaiah, A.M. Reinhorn and M.C. Constantinou, 8/3/89, (PB90-161936). This report is available only through NTIS (see address given above).

NCEER-89-0020 "Structural Control Considering Time-Rate of Control Forces and Control Rate Constraints," by F.Y. Cheng and C.P. Pantelides, 8/3/89, (PB90-120445).

NCEER-89-0021 "Subsurface Conditions of Memphis and Shelby County," by K.W. Ng, T-S. Chang and H-H.M. Hwang, 7/26/89, (PB90-120437).

NCEER-89-0022 "Seismic Wave Propagation Effects on Straight Jointed Buried Pipelines," by K. Elhmadi and M.J. O'Rourke, 8/24/89, (PB90-162322).

NCEER-89-0023 "Workshop on Serviceability Analysis of Water Delivery Systems," edited by M. Grigoriu, 3/6/89, (PB90-127424).

NCEER-89-0024 "Shaking Table Study of a 1/5 Scale Steel Frame Composed of Tapered Members," by K.C. Chang, J.S. Hwang and G.C. Lee, 9/18/89, (PB90-160169).

NCEER-89-0025 "DYNA1D: A Computer Program for Nonlinear Seismic Site Response Analysis - Technical Documentation," by Jean H. Prevost, 9/14/89, (PB90-161944). This report is available only through NTIS (see address given above).

NCEER-89-0026 "1:4 Scale Model Studies of Active Tendon Systems and Active Mass Dampers for Aseismic Protection," by A.M. Reinhorn, T.T. Soong, R.C. Lin, Y.P. Yang, Y. Fukao, H. Abe and M. Nakai, 9/15/89, (PB90-173246).

NCEER-89-0027 "Scattering of Waves by Inclusions in a Nonhomogeneous Elastic Half Space Solved by Boundary Element Methods," by P.K. Hadley, A. Askar and A.S. Cakmak, 6/15/89, (PB90-145699).

NCEER-89-0028 "Statistical Evaluation of Deflection Amplification Factors for Reinforced Concrete Structures," by H.H.M. Hwang, J-W. Jaw and A.L. Ch'ng, 8/31/89, (PB90-164633).

NCEER-89-0029 "Bedrock Accelerations in Memphis Area Due to Large New Madrid Earthquakes," by H.H.M. Hwang, C.H.S. Chen and G. Yu, 11/7/89, (PB90-162330).

NCEER-89-0030 "Seismic Behavior and Response Sensitivity of Secondary Structural Systems," by Y.Q. Chen and T.T. Soong, 10/23/89, (PB90-164658).

NCEER-89-0031 "Random Vibration and Reliability Analysis of Primary-Secondary Structural Systems," by Y. Ibrahim, M. Grigoriu and T.T. Soong, 11/10/89, (PB90-161951).

NCEER-89-0032 "Proceedings from the Second U.S. - Japan Workshop on Liquefaction, Large Ground Deformation and Their Effects on Lifelines, September 26-29, 1989," Edited by T.D. O'Rourke and M. Hamada, 12/1/89, (PB90-209388).

NCEER-89-0033 "Deterministic Model for Seismic Damage Evaluation of Reinforced Concrete Structures," by J.M. Bracci, A.M. Reinhorn, J.B. Mander and S.K. Kunnath, 9/27/89.

NCEER-89-0034 "On the Relation Between Local and Global Damage Indices," by E. DiPasquale and A.S. Cakmak, 8/15/89, (PB90-173865).

NCEER-89-0035 "Cyclic Undrained Behavior of Nonplastic and Low Plasticity Silts," by A.J. Walker and H.E. Stewart, 7/26/89, (PB90-183518).

NCEER-89-0036 "Liquefaction Potential of Surficial Deposits in the City of Buffalo, New York," by M. Budhu, R. Giese and L. Baumgrass, 1/17/89, (PB90-208455).

NCEER-89-0037 "A Deterministic Assessment of Effects of Ground Motion Incoherence," by A.S. Veletsos and Y. Tang, 7/15/89, (PB90-164294).

NCEER-89-0038 "Workshop on Ground Motion Parameters for Seismic Hazard Mapping," July 17-18, 1989, edited by R.V. Whitman, 12/1/89, (PB90-173923).

NCEER-89-0039 "Seismic Effects on Elevated Transit Lines of the New York City Transit Authority," by C.J. Costantino, C.A. Miller and E. Heymsfield, 12/26/89, (PB90-207887).

NCEER-89-0040 "Centrifugal Modeling of Dynamic Soil-Structure Interaction," by K. Weissman, Supervised by J.H. Prevost, 5/10/89, (PB90-207879).

NCEER-89-0041 "Linearized Identification of Buildings With Cores for Seismic Vulnerability Assessment," by I-K. Ho and A.E. Aktan, 11/1/89, (PB90-251943).

NCEER-90-0001 "Geotechnical and Lifeline Aspects of the October 17, 1989 Loma Prieta Earthquake in San Francisco," by T.D. O'Rourke, H.E. Stewart, F.T. Blackburn and T.S. Dickerman, 1/90, (PB90-208596).

NCEER-90-0002 "Nonnormal Secondary Response Due to Yielding in a Primary Structure," by D.C.K. Chen and L.D. Lutes, 2/28/90, (PB90-251976).

NCEER-90-0003 "Earthquake Education Materials for Grades K-12," by K.E.K. Ross, 4/16/90, (PB91-251984).

NCEER-90-0004 "Catalog of Strong Motion Stations in Eastern North America," by R.W. Busby, 4/3/90, (PB90-251984).

NCEER-90-0005 "NCEER Strong-Motion Data Base: A User Manual for the GeoBase Release (Version 1.0 for the Sun3)," by P. Friberg and K. Jacob, 3/31/90 (PB90-258062).

NCEER-90-0006 "Seismic Hazard Along a Crude Oil Pipeline in the Event of an 1811-1812 Type New Madrid Earthquake," by H.H.M. Hwang and C-H.S. Chen, 4/16/90(PB90-258054).

NCEER-90-0007 "Site-Specific Response Spectra for Memphis Sheahan Pumping Station," by H.H.M. Hwang and C.S. Lee, 5/15/90, (PB91-108811).

NCEER-90-0008 "Pilot Study on Seismic Vulnerability of Crude Oil Transmission Systems," by T. Ariman, R. Dobry, M. Grigoriu, F. Kozin, M. O'Rourke, T. O'Rourke and M. Shinozuka, 5/25/90, (PB91-108837).

NCEER-90-0009 "A Program to Generate Site Dependent Time Histories: EQGEN," by G.W. Ellis, M. Srinivasan and A.S. Cakmak, 1/30/90, (PB91-108829).

NCEER-90-0010 "Active Isolation for Seismic Protection of Operating Rooms," by M.E. Talbott, Supervised by M. Shinozuka, 6/8/9, (PB91-110205).

NCEER-90-0011 "Program LINEARID for Identification of Linear Structural Dynamic Systems," by C-B. Yun and M. Shinozuka, 6/25/90, (PB91-110312).

NCEER-90-0012 "Two-Dimensional Two-Phase Elasto-Plastic Seismic Response of Earth Dams," by A.N. Yiagos, Supervised by J.H. Prevost, 6/20/90, (PB91-110197).

NCEER-90-0013 "Secondary Systems in Base-Isolated Structures: Experimental Investigation, Stochastic Response and Stochastic Sensitivity," by G.D. Manolis, G. Juhn, M.C. Constantinou and A.M. Reinhorn, 7/1/90, (PB91-110320).

NCEER-90-0014 "Seismic Behavior of Lightly-Reinforced Concrete Column and Beam-Column Joint Details," by S.P. Pessiki, C.H. Conley, P. Gergely and R.N. White, 8/22/90, (PB91-108795).

NCEER-90-0015 "Two Hybrid Control Systems for Building Structures Under Strong Earthquakes," by J.N. Yang and A. Danielians, 6/29/90, (PB91-125393).

NCEER-90-0016 "Instantaneous Optimal Control with Acceleration and Velocity Feedback," by J.N. Yang and Z. Li, 6/29/90, (PB91-125401).

NCEER-90-0017 "Reconnaissance Report on the Northern Iran Earthquake of June 21, 1990," by M. Mehrain, 10/4/90, (PB91-125377).

NCEER-90-0018 "Evaluation of Liquefaction Potential in Memphis and Shelby County," by T.S. Chang, P.S. Tang, C.S. Lee and H. Hwang, 8/10/90, (PB91-125427).

NCEER-90-0019 "Experimental and Analytical Study of a Combined Sliding Disc Bearing and Helical Steel Spring Isolation System," by M.C. Constantinou, A.S. Mokha and A.M. Reinhorn, 10/4/90, (PB91-125385).

NCEER-90-0020 "Experimental Study and Analytical Prediction of Earthquake Response of a Sliding Isolation System with a Spherical Surface," by A.S. Mokha, M.C. Constantinou and A.M. Reinhorn, 10/11/90, (PB91-125419).

NCEER-90-0021 "Dynamic Interaction Factors for Floating Pile Groups," by G. Gazetas, K. Fan, A. Kaynia and E. Kausel, 9/10/90, (PB91-170381).

NCEER-90-0022 "Evaluation of Seismic Damage Indices for Reinforced Concrete Structures," by S. Rodriguez-Gomez and A.S. Cakmak, 9/30/90, PB91-171322).

NCEER-90-0023 "Study of Site Response at a Selected Memphis Site," by H. Desai, S. Ahmad, E.S. Gazetas and M.R. Oh, 10/11/90, (PB91-196857).

NCEER-90-0024 "A User's Guide to Strongmo: Version 1.0 of NCEER's Strong-Motion Data Access Tool for PCs and Terminals," by P.A. Friberg and C.A.T. Susch, 11/15/90, (PB91-171272).

NCEER-90-0025 "A Three-Dimensional Analytical Study of Spatial Variability of Seismic Ground Motions," by L-L. Hong and A.H.-S. Ang, 10/30/90, (PB91-170399).

NCEER-90-0026 "MUMOID User's Guide - A Program for the Identification of Modal Parameters," by S. Rodriguez-Gomez and E. DiPasquale, 9/30/90, (PB91-171298).

NCEER-90-0027 "SARCF-II User's Guide - Seismic Analysis of Reinforced Concrete Frames," by S. Rodriguez-Gomez, Y.S. Chung and C. Meyer, 9/30/90, (PB91-171280).

NCEER-90-0028 "Viscous Dampers: Testing, Modeling and Application in Vibration and Seismic Isolation," by N. Makris and M.C. Constantinou, 12/20/90 (PB91-190561).

NCEER-90-0029 "Soil Effects on Earthquake Ground Motions in the Memphis Area," by H. Hwang, C.S. Lee, K.W. Ng and T.S. Chang, 8/2/90, (PB91-190751).

NCEER-91-0001 "Proceedings from the Third Japan-U.S. Workshop on Earthquake Resistant Design of Lifeline Facilities and Countermeasures for Soil Liquefaction, December 17-19, 1990," edited by T.D. O'Rourke and M. Hamada, 2/1/91, (PB91-179259).

NCEER-91-0002 "Physical Space Solutions of Non-Proportionally Damped Systems," by M. Tong, Z. Liang and G.C. Lee, 1/15/91, (PB91-179242).

NCEER-91-0003 "Seismic Response of Single Piles and Pile Groups," by K. Fan and G. Gazetas, 1/10/91, (PB92-174994).

NCEER-91-0004 "Damping of Structures: Part 1 - Theory of Complex Damping," by Z. Liang and G. Lee, 10/10/91, (PB92-197235).

NCEER-91-0005 "3D-BASIS - Nonlinear Dynamic Analysis of Three Dimensional Base Isolated Structures: Part II," by S. Nagarajaiah, A.M. Reinhorn and M.C. Constantinou, 2/28/91, (PB91-190553).

NCEER-91-0006 "A Multidimensional Hysteretic Model for Plasticity Deforming Metals in Energy Absorbing Devices," by E.J. Graesser and F.A. Cozzarelli, 4/9/91, (PB92-108364).

NCEER-91-0007 "A Framework for Customizable Knowledge-Based Expert Systems with an Application to a KBES for Evaluating the Seismic Resistance of Existing Buildings," by E.G. Ibarra-Anaya and S.J. Fenves, 4/9/91, (PB91-210930).

NCEER-91-0008 "Nonlinear Analysis of Steel Frames with Semi-Rigid Connections Using the Capacity Spectrum Method," by G.G. Deierlein, S-H. Hsieh, Y-J. Shen and J.F. Abel, 7/2/91, (PB92-113828).

NCEER-91-0009 "Earthquake Education Materials for Grades K-12," by K.E.K. Ross, 4/30/91, (PB91-212142).

NCEER-91-0010 "Phase Wave Velocities and Displacement Phase Differences in a Harmonically Oscillating Pile," by N. Makris and G. Gazetas, 7/8/91, (PB92-108356).

NCEER-91-0011 "Dynamic Characteristics of a Full-Size Five-Story Steel Structure and a 2/5 Scale Model," by K.C. Chang, G.C. Yao, G.C. Lee, D.S. Hao and Y.C. Yeh," 7/2/91, (PB93-116648).

NCEER-91-0012 "Seismic Response of a 2/5 Scale Steel Structure with Added Viscoelastic Dampers," by K.C. Chang, T.T. Soong, S-T. Oh and M.L. Lai, 5/17/91, (PB92-110816).

NCEER-91-0013 "Earthquake Response of Retaining Walls; Full-Scale Testing and Computational Modeling," by S. Alampalli and A-W.M. Elgamal, 6/20/91, to be published.

NCEER-91-0014 "3D-BASIS-M: Nonlinear Dynamic Analysis of Multiple Building Base Isolated Structures," by P.C. Tsopelas, S. Nagarajaiah, M.C. Constantinou and A.M. Reinhorn, 5/28/91, (PB92-113885).

NCEER-91-0015 "Evaluation of SEAOC Design Requirements for Sliding Isolated Structures," by D. Theodossiou and M.C. Constantinou, 6/10/91, (PB92-114602).

NCEER-91-0016 "Closed-Loop Modal Testing of a 27-Story Reinforced Concrete Flat Plate-Core Building," by H.R. Somaprasad, T. Toksoy, H. Yoshiyuki and A.E. Aktan, 7/15/91, (PB92-129980).

NCEER-91-0017 "Shake Table Test of a 1/6 Scale Two-Story Lightly Reinforced Concrete Building," by A.G. El-Attar, R.N. White and P. Gergely, 2/28/91, (PB92-222447).

NCEER-91-0018 "Shake Table Test of a 1/8 Scale Three-Story Lightly Reinforced Concrete Building," by A.G. El-Attar, R.N. White and P. Gergely, 2/28/91, (PB93-116630).

NCEER-91-0019 "Transfer Functions for Rigid Rectangular Foundations," by A.S. Veletsos, A.M. Prasad and W.H. Wu, 7/31/91.

NCEER-91-0020 "Hybrid Control of Seismic-Excited Nonlinear and Inelastic Structural Systems," by J.N. Yang, Z. Li and A. Danielians, 8/1/91, (PB92-143171).

NCEER-91-0021 "The NCEER-91 Earthquake Catalog: Improved Intensity-Based Magnitudes and Recurrence Relations for U.S. Earthquakes East of New Madrid," by L. Seeber and J.G. Armbruster, 8/28/91, (PB92-176742).

NCEER-91-0022 "Proceedings from the Implementation of Earthquake Planning and Education in Schools: The Need for Change - The Roles of the Changemakers," by K.E.K. Ross and F. Winslow, 7/23/91, (PB92-129998).

NCEER-91-0023 "A Study of Reliability-Based Criteria for Seismic Design of Reinforced Concrete Frame Buildings," by H.H.M. Hwang and H-M. Hsu, 8/10/91, (PB92-140235).

NCEER-91-0024 "Experimental Verification of a Number of Structural System Identification Algorithms," by R.G. Ghanem, H. Gavin and M. Shinozuka, 9/18/91, (PB92-176577).

NCEER-91-0025 "Probabilistic Evaluation of Liquefaction Potential," by H.H.M. Hwang and C.S. Lee," 11/25/91, (PB92-143429).

NCEER-91-0026 "Instantaneous Optimal Control for Linear, Nonlinear and Hysteretic Structures - Stable Controllers," by J.N. Yang and Z. Li, 11/15/91, (PB92-163807).

NCEER-91-0027 "Experimental and Theoretical Study of a Sliding Isolation System for Bridges," by M.C. Constantinou, A. Kartoum, A.M. Reinhorn and P. Bradford, 11/15/91, (PB92-176973).

NCEER-92-0001 "Case Studies of Liquefaction and Lifeline Performance During Past Earthquakes, Volume 1: Japanese Case Studies," Edited by M. Hamada and T. O'Rourke, 2/17/92, (PB92-197243).

NCEER-92-0002 "Case Studies of Liquefaction and Lifeline Performance During Past Earthquakes, Volume 2: United States Case Studies," Edited by T. O'Rourke and M. Hamada, 2/17/92, (PB92-197250).

NCEER-92-0003 "Issues in Earthquake Education," Edited by K. Ross, 2/3/92, (PB92-222389).

NCEER-92-0004 "Proceedings from the First U.S. - Japan Workshop on Earthquake Protective Systems for Bridges," Edited by I.G. Buckle, 2/4/92, (PB94-142239, A99, MF-A06).

NCEER-92-0005 "Seismic Ground Motion from a Haskell-Type Source in a Multiple-Layered Half-Space," A.P. Theoharis, G. Deodatis and M. Shinozuka, 1/2/92, to be published.

NCEER-92-0006 "Proceedings from the Site Effects Workshop," Edited by R. Whitman, 2/29/92, (PB92-197201).

NCEER-92-0007 "Engineering Evaluation of Permanent Ground Deformations Due to Seismically-Induced Liquefaction," by M.H. Baziar, R. Dobry and A-W.M. Elgamal, 3/24/92, (PB92-222421).

NCEER-92-0008 "A Procedure for the Seismic Evaluation of Buildings in the Central and Eastern United States," by C.D. Poland and J.O. Malley, 4/2/92, (PB92-222439).

NCEER-92-0009 "Experimental and Analytical Study of a Hybrid Isolation System Using Friction Controllable Sliding Bearings," by M.Q. Feng, S. Fujii and M. Shinozuka, 5/15/92, (PB93-150282).

NCEER-92-0010 "Seismic Resistance of Slab-Column Connections in Existing Non-Ductile Flat-Plate Buildings," by A.J. Durrani and Y. Du, 5/18/92.

NCEER-92-0011 "The Hysteretic and Dynamic Behavior of Brick Masonry Walls Upgraded by Ferrocement Coatings Under Cyclic Loading and Strong Simulated Ground Motion," by H. Lee and S.P. Prawel, 5/11/92, to be published.

NCEER-92-0012 "Study of Wire Rope Systems for Seismic Protection of Equipment in Buildings," by G.F. Demetriades, M.C. Constantinou and A.M. Reinhorn, 5/20/92.

NCEER-92-0013 "Shape Memory Structural Dampers: Material Properties, Design and Seismic Testing," by P.R. Witting and F.A. Cozzarelli, 5/26/92.

NCEER-92-0014 "Longitudinal Permanent Ground Deformation Effects on Buried Continuous Pipelines," by M.J. O'Rourke, and C. Nordberg, 6/15/92.

NCEER-92-0015 "A Simulation Method for Stationary Gaussian Random Functions Based on the Sampling Theorem," by M. Grigoriu and S. Balopoulou, 6/11/92, (PB93-127496).

NCEER-92-0016 "Gravity-Load-Designed Reinforced Concrete Buildings: Seismic Evaluation of Existing Construction and Detailing Strategies for Improved Seismic Resistance," by G.W. Hoffmann, S.K. Kunnath, A.M. Reinhorn and J.B. Mander, 7/15/92, (PB94-142007, A08, MF-A02).

NCEER-92-0017 "Observations on Water System and Pipeline Performance in the Limón Area of Costa Rica Due to the April 22, 1991 Earthquake," by M. O'Rourke and D. Ballantyne, 6/30/92, (PB93-126811).

NCEER-92-0018 "Fourth Edition of Earthquake Education Materials for Grades K-12," Edited by K.E.K. Ross, 8/10/92.

NCEER-92-0019 "Proceedings from the Fourth Japan-U.S. Workshop on Earthquake Resistant Design of Lifeline Facilities and Countermeasures for Soil Liquefaction," Edited by M. Hamada and T.D. O'Rourke, 8/12/92, (PB93-163939).

NCEER-92-0020 "Active Bracing System: A Full Scale Implementation of Active Control," by A.M. Reinhorn, T.T. Soong, R.C. Lin, M.A. Riley, Y.P. Wang, S. Aizawa and M. Higashino, 8/14/92, (PB93-127512).

NCEER-92-0021 "Empirical Analysis of Horizontal Ground Displacement Generated by Liquefaction-Induced Lateral Spreads," by S.F. Bartlett and T.L. Youd, 8/17/92, (PB93-188241).

NCEER-92-0022 "IDARC Version 3.0: Inelastic Damage Analysis of Reinforced Concrete Structures," by S.K. Kunnath, A.M. Reinhorn and R.F. Lobo, 8/31/92, (PB93-227502, A07, MF-A02).

NCEER-92-0023 "A Semi-Empirical Analysis of Strong-Motion Peaks in Terms of Seismic Source, Propagation Path and Local Site Conditions, by M. Kamiyama, M.J. O'Rourke and R. Flores-Berrones, 9/9/92, (PB93-150266).

NCEER-92-0024 "Seismic Behavior of Reinforced Concrete Frame Structures with Nonductile Details, Part I: Summary of Experimental Findings of Full Scale Beam-Column Joint Tests," by A. Beres, R.N. White and P. Gergely, 9/30/92, (PB93-227783, A05, MF-A01).

NCEER-92-0025 "Experimental Results of Repaired and Retrofitted Beam-Column Joint Tests in Lightly Reinforced Concrete Frame Buildings," by A. Beres, S. El-Borgi, R.N. White and P. Gergely, 10/29/92, (PB93-227791, A05, MF-A01).

NCEER-92-0026 "A Generalization of Optimal Control Theory: Linear and Nonlinear Structures," by J.N. Yang, Z. Li and S. Vongchavalitkul, 11/2/92, (PB93-188621).

NCEER-92-0027 "Seismic Resistance of Reinforced Concrete Frame Structures Designed Only for Gravity Loads: Part I - Design and Properties of a One-Third Scale Model Structure," by J.M. Bracci, A.M. Reinhorn and J.B. Mander, 12/1/92, (PB94-104502, A08, MF-A02).

NCEER-92-0028 "Seismic Resistance of Reinforced Concrete Frame Structures Designed Only for Gravity Loads: Part II - Experimental Performance of Subassemblages," by L.E. Aycardi, J.B. Mander and A.M. Reinhorn, 12/1/92, (PB94-104510, A08, MF-A02).

NCEER-92-0029 "Seismic Resistance of Reinforced Concrete Frame Structures Designed Only for Gravity Loads: Part III - Experimental Performance and Analytical Study of a Structural Model," by J.M. Bracci, A.M. Reinhorn and J.B. Mander, 12/1/92, (PB93-227528, A09, MF-A01).

NCEER-92-0030 "Evaluation of Seismic Retrofit of Reinforced Concrete Frame Structures: Part I - Experimental Performance of Retrofitted Subassemblages," by D. Choudhuri, J.B. Mander and A.M. Reinhorn, 12/8/92, (PB93-198307, A07, MF-A02).

NCEER-92-0031 "Evaluation of Seismic Retrofit of Reinforced Concrete Frame Structures: Part II - Experimental Performance and Analytical Study of a Retrofitted Structural Model," by J.M. Bracci, A.M. Reinhorn and J.B. Mander, 12/8/92, (PB93-198315, A09, MF-A03).

NCEER-92-0032 "Experimental and Analytical Investigation of Seismic Response of Structures with Supplemental Fluid Viscous Dampers," by M.C. Constantinou and M.D. Symans, 12/21/92, (PB93-191435).

NCEER-92-0033 "Reconnaissance Report on the Cairo, Egypt Earthquake of October 12, 1992," by M. Khater, 12/23/92, (PB93-188621).

NCEER-92-0034 "Low-Level Dynamic Characteristics of Four Tall Flat-Plate Buildings in New York City," by H. Gavin, S. Yuan, J. Grossman, E. Pekelis and K. Jacob, 12/28/92, (PB93-188217).

NCEER-93-0001 "An Experimental Study on the Seismic Performance of Brick-Infilled Steel Frames With and Without Retrofit," by J.B. Mander, B. Nair, K. Wojtkowski and J. Ma, 1/29/93, (PB93-227510, A07, MF-A02).

NCEER-93-0002 "Social Accounting for Disaster Preparedness and Recovery Planning," by S. Cole, E. Pantoja and V. Razak, 2/22/93, (PB94-142114, A12, MF-A03).

NCEER-93-0003 "Assessment of 1991 NEHRP Provisions for Nonstructural Components and Recommended Revisions," by T.T. Soong, G. Chen, Z. Wu, R-H. Zhang and M. Grigoriu, 3/1/93, (PB93-188639).

NCEER-93-0004 "Evaluation of Static and Response Spectrum Analysis Procedures of SEAOC/UBC for Seismic Isolated Structures," by C.W. Winters and M.C. Constantinou, 3/23/93, (PB93-198299).

NCEER-93-0005 "Earthquakes in the Northeast - Are We Ignoring the Hazard? A Workshop on Earthquake Science and Safety for Educators," edited by K.E.K. Ross, 4/2/93, (PB94-103066, A09, MF-A02).

NCEER-93-0006 "Inelastic Response of Reinforced Concrete Structures with Viscoelastic Braces," by R.F. Lobo, J.M. Bracci, K.L. Shen, A.M. Reinhorn and T.T. Soong, 4/5/93, (PB93-227486, A05, MF-A02).

NCEER-93-0007 "Seismic Testing of Installation Methods for Computers and Data Processing Equipment," by K. Kosar, T.T. Soong, K.L. Shen, J.A. HoLung and Y.K. Lin, 4/12/93, (PB93-198299).

NCEER-93-0008 "Retrofit of Reinforced Concrete Frames Using Added Dampers," by A. Reinhorn, M. Constantinou and C. Li, to be published.

NCEER-93-0009 "Seismic Behavior and Design Guidelines for Steel Frame Structures with Added Viscoelastic Dampers," by K.C. Chang, M.L. Lai, T.T. Soong, D.S. Hao and Y.C. Yeh, 5/1/93, (PB94-141959, A07, MF-A02).

NCEER-93-0010 "Seismic Performance of Shear-Critical Reinforced Concrete Bridge Piers," by J.B. Mander, S.M. Waheed, M.T.A. Chaudhary and S.S. Chen, 5/12/93, (PB93-227494, A08, MF-A02).

NCEER-93-0011 "3D-BASIS-TABS: Computer Program for Nonlinear Dynamic Analysis of Three Dimensional Base Isolated Structures," by S. Nagarajaiah, C. Li, A.M. Reinhorn and M.C. Constantinou, 8/2/93, (PB94-141819, A09, MF-A02).

NCEER-93-0012 "Effects of Hydrocarbon Spills from an Oil Pipeline Break on Ground Water," by O.J. Helweg and H.H.M. Hwang, 8/3/93, (PB94-141942, A06, MF-A02).

NCEER-93-0013 "Simplified Procedures for Seismic Design of Nonstructural Components and Assessment of Current Code Provisions," by M.P. Singh, L.E. Suarez, E.E. Matheu and G.O. Maldonado, 8/4/93, (PB94-141827, A09, MF-A02).

NCEER-93-0014 "An Energy Approach to Seismic Analysis and Design of Secondary Systems," by G. Chen and T.T. Soong, 8/6/93, (PB94-142767, A11, MF-A03).

NCEER-93-0015 "Proceedings from School Sites: Becoming Prepared for Earthquakes - Commemorating the Third Anniversary of the Loma Prieta Earthquake," Edited by F.E. Winslow and K.E.K. Ross, 8/16/93.

NCEER-93-0016 "Reconnaissance Report of Damage to Historic Monuments in Cairo, Egypt Following the October 12, 1992 Dahshur Earthquake," by D. Sykora, D. Look, G. Croci, E. Karaesmen and E. Karaesmen, 8/19/93, (PB94-142221, A08, MF-A02).

NCEER-93-0017 "The Island of Guam Earthquake of August 8, 1993," by S.W. Swan and S.K. Harris, 9/30/93, (PB94-141843, A04, MF-A01).

NCEER-93-0018 "Engineering Aspects of the October 12, 1992 Egyptian Earthquake," by A.W. Elgamal, M. Amer, K. Adalier and A. Abul-Fadl, 10/7/93, (PB94-141983, A05, MF-A01).

NCEER-93-0019 "Development of an Earthquake Motion Simulator and its Application in Dynamic Centrifuge Testing," by I. Krstelj, Supervised by J.H. Prevost, 10/23/93, (PB94-181773, A-10, MF-A03).

NCEER-93-0020 "NCEER-Taisei Corporation Research Program on Sliding Seismic Isolation Systems for Bridges: Experimental and Analytical Study of a Friction Pendulum System (FPS)," by M.C. Constantinou, P. Tsopelas, Y-S. Kim and S. Okamoto, 11/1/93, (PB94-142775, A08, MF-A02).

NCEER-93-0021 "Finite Element Modeling of Elastomeric Seismic Isolation Bearings," by L.J. Billings, Supervised by R. Shepherd, 11/8/93, to be published.

NCEER-93-0022 "Seismic Vulnerability of Equipment in Critical Facilities: Life-Safety and Operational Consequences," by K. Porter, G.S. Johnson, M.M. Zadeh, C. Scawthorn and S. Eder, 11/24/93, (PB94-181765, A16, MF-A03).

NCEER-93-0023 "Hokkaido Nansei-oki, Japan Earthquake of July 12, 1993, by P.I. Yanev and C.R. Scawthorn, 12/23/93, (PB94-181500, A07, MF-A01).

NCEER-94-0001 "An Evaluation of Seismic Serviceability of Water Supply Networks with Application to the San Francisco Auxiliary Water Supply System," by I. Markov, Supervised by M. Grigoriu and T. O'Rourke, 1/21/94.

NCEER-94-0002 "NCEER-Taisei Corporation Research Program on Sliding Seismic Isolation Systems for Bridges: Experimental and Analytical Study of Systems Consisting of Sliding Bearings, Rubber Restoring Force Devices and Fluid Dampers," Volumes I and II, by P. Tsopelas, S. Okamoto, M.C. Constantinou, D. Ozaki and S. Fujii, 2/4/94, (PB94-181740, A09, MF-A02 and PB94-181757, A12, MF-A03).

NCEER-94-0003 "A Markov Model for Local and Global Damage Indices in Seismic Analysis," by S. Rahman and M. Grigoriu, 2/18/94.

NCEER-94-0004 "Proceedings from the NCEER Workshop on Seismic Response of Masonry Infills," edited by D.P. Abrams, 3/1/94, (PB94-180783, A07, MF-A02).

NCEER-94-0005 "The Northridge, California Earthquake of January 17, 1994: General Reconnaissance Report," edited by J.D. Goltz, 3/11/94, (PB193943, A10, MF-A03).

NCEER-94-0006 "Seismic Energy Based Fatigue Damage Analysis of Bridge Columns: Part I - Evaluation of Seismic Capacity," by G.A. Chang and J.B. Mander, 3/14/94, (PB94-219185, A11, MF-A03).

NCEER-94-0007 "Seismic Isolation of Multi-Story Frame Structures Using Spherical Sliding Isolation Systems," by T.M. Al-Hussaini, V.A. Zayas and M.C. Constantinou, 3/17/94, (PB193745, A09, MF-A02).

NCEER-94-0008 "The Northridge, California Earthquake of January 17, 1994: Performance of Highway Bridges," edited by I.G. Buckle, 3/24/94, (PB94-193851, A06, MF-A02).

NCEER-94-0009 "Proceedings of the Third U.S.-Japan Workshop on Earthquake Protective Systems for Bridges," edited by I.G. Buckle and I. Friedland, 3/31/94, (PB94-195815, A99, MF-MF).

NCEER-94-0010 "3D-BASIS-ME: Computer Program for Nonlinear Dynamic Analysis of Seismically Isolated Single and Multiple Structures and Liquid Storage Tanks," by P.C. Tsopelas, M.C. Constantinou and A.M. Reinhorn, 4/12/94.

NCEER-94-0011 "The Northridge, California Earthquake of January 17, 1994: Performance of Gas Transmission Pipelines," by T.D. O'Rourke and M.C. Palmer, 5/16/94.

NCEER-94-0012 "Feasibility Study of Replacement Procedures and Earthquake Performance Related to Gas Transmission Pipelines," by T.D. O'Rourke and M.C. Palmer, 5/25/94, (PB94-206638, A09, MF-A02).

NCEER-94-0013 "Seismic Energy Based Fatigue Damage Analysis of Bridge Columns: Part II - Evaluation of Seismic Demand," by G.A. Chang and J.B. Mander, 6/1/94, (PB95-18106, A08, MF-A02).

NCEER-94-0014 "NCEER-Taisei Corporation Research Program on Sliding Seismic Isolation Systems for Bridges: Experimental and Analytical Study of a System Consisting of Sliding Bearings and Fluid Restoring Force/Damping Devices," by P. Tsopelas and M.C. Constantinou, 6/13/94, (PB94-219144, A10, MF-A03).

NCEER-94-0015 "Generation of Hazard-Consistent Fragility Curves for Seismic Loss Estimation Studies," by H. Hwang and J-R. Huo, 6/14/94, (PB95-181996, A09, MF-A02).

NCEER-94-0016 "Seismic Study of Building Frames with Added Energy-Absorbing Devices," by W.S. Pong, C.S. Tsai and G.C. Lee, 6/20/94, (PB94-219136, A10, A03).

NCEER-94-0017 "Sliding Mode Control for Seismic-Excited Linear and Nonlinear Civil Engineering Structures," by J. Yang, J. Wu, A. Agrawal and Z. Li, 6/21/94, (PB95-138483, A06, MF-A02).

NCEER-94-0018 "3D-BASIS-TABS Version 2.0: Computer Program for Nonlinear Dynamic Analysis of Three Dimensional Base Isolated Structures," by A.M. Reinhorn, S. Nagarajaiah, M.C. Constantinou, P. Tsopelas and R. Li, 6/22/94, (PB95-182176, A08, MF-A02).

NCEER-94-0019 "Proceedings of the International Workshop on Civil Infrastructure Systems: Application of Intelligent Systems and Advanced Materials on Bridge Systems," Edited by G.C. Lee and K.C. Chang, 7/18/94, (PB95-252474, A20, MF-A04).

NCEER-94-0020 "Study of Seismic Isolation Systems for Computer Floors," by V. Lambrou and M.C. Constantinou, 7/19/94, (PB95-138533, A10, MF-A03).

NCEER-94-0021 "Proceedings of the U.S.-Italian Workshop on Guidelines for Seismic Evaluation and Rehabilitation of Unreinforced Masonry Buildings," Edited by D.P. Abrams and G.M. Calvi, 7/20/94, (PB95-138749, A13, MF-A03).

NCEER-94-0022 "NCEER-Taisei Corporation Research Program on Sliding Seismic Isolation Systems for Bridges: Experimental and Analytical Study of a System Consisting of Lubricated PTFE Sliding Bearings and Mild Steel Dampers," by P. Tsopelas and M.C. Constantinou, 7/22/94, (PB95-182184, A08, MF-A02).

NCEER-94-0023 "Development of Reliability-Based Design Criteria for Buildings Under Seismic Load," by Y.K. Wen, H. Hwang and M. Shinozuka, 8/1/94, (PB95-211934, A08, MF-A02).

NCEER-94-0024 "Experimental Verification of Acceleration Feedback Control Strategies for an Active Tendon System," by S.J. Dyke, B.F. Spencer, Jr., P. Quast, M.K. Sain, D.C. Kaspari, Jr. and T.T. Soong, 8/29/94, (PB95-212320, A05, MF-A01).

NCEER-94-0025 "Seismic Retrofitting Manual for Highway Bridges," Edited by I.G. Buckle and I.F. Friedland, to be published.

NCEER-94-0026 "Proceedings from the Fifth U.S.-Japan Workshop on Earthquake Resistant Design of Lifeline Facilities and Countermeasures Against Soil Liquefaction," Edited by T.D. O'Rourke and M. Hamada, 11/7/94, (PB95-220802, A99, MF-E08).

NCEER-95-0001 "Experimental and Analytical Investigation of Seismic Retrofit of Structures with Supplemental Damping: Part 1 - Fluid Viscous Damping Devices," by A.M. Reinhorn, C. Li and M.C. Constantinou, 1/3/95, (PB95-266599, A09, MF-A02).

NCEER-95-0002 "Experimental and Analytical Study of Low-Cycle Fatigue Behavior of Semi-Rigid Top-And-Seat Angle Connections," by G. Pekcan, J.B. Mander and S.S. Chen, 1/5/95.

NCEER-95-0003 "NCEER-ATC Joint Study on Fragility of Buildings," by T. Anagnos, C. Rojahn and A.S. Kiremidjian, 1/20/95, (PB95-220026, A06, MF-A02).

NCEER-95-0004 "Nonlinear Control Algorithms for Peak Response Reduction," by Z. Wu, T.T. Soong, V. Gattulli and R.C. Lin, 2/16/95.

NCEER-95-0005 "Pipeline Replacement Feasibility Study: A Methodology for Minimizing Seismic and Corrosion Risks to Underground Natural Gas Pipelines," by R.T. Eguchi, H.A. Seligson and D.G. Honegger, 3/2/95, (PB95-252326, A06, MF-A02).

NCEER-95-0006 "Evaluation of Seismic Performance of an 11-Story Frame Building During the 1994 Northridge Earthquake," by F. Naeim, R. DiSulio, K. Benuska, A. Reinhorn and C. Li, to be published.

NCEER-95-0007 "Prioritization of Bridges for Seismic Retrofitting," by N. Basöz and A.S. Kiremidjian, 4/24/95, (PB95-252300, A08, MF-A02).

NCEER-95-0008 "Method for Developing Motion Damage Relationships for Reinforced Concrete Frames," by A. Singhal and A.S. Kiremidjian, 5/11/95, (PB95-266607, A06, MF-A02).

NCEER-95-0009 "Experimental and Analytical Investigation of Seismic Retrofit of Structures with Supplemental Damping: Part II - Friction Devices," by C. Li and A.M. Reinhorn, 7/6/95.

NCEER-95-0010 "Experimental Performance and Analytical Study of a Non-Ductile Reinforced Concrete Frame Structure Retrofitted with Elastomeric Spring Dampers," by G. Pekcan, J.B. Mander and S.S. Chen, 7/14/95.

NCEER-95-0011 "Development and Experimental Study of Semi-Active Fluid Damping Devices for Seismic Protection of Structures," by M.D. Symans and M.C. Constantinou, 8/3/95.

NCEER-95-0012 "Real-Time Structural Parameter Modification (RSPM): Development of Innervated Structures," by Z. Liang, M. Tong and G.C. Lee, 4/11/95.

NCEER-95-0013 "Experimental and Analytical Investigation of Seismic Retrofit of Structures with Supplemental Damping: Part III - Viscous Damping Walls," by A.M. Reinhorn and C. Lin, 10/1/95, to be published.

NCEER-95-0014 "Seismic Fragility Analysis of Equipment and Structures in a Memphis Electric Substation," by J-R. Huo and H.H.M. Hwang, 8/10/95.